Fall 2010

A Peptide-Based Platform for Displaying Antibodies to Engage T Cells

Ying Zheng

A PEPTIDE-BASED PLATFORM FOR DISPLAYING ANTIBODIES TO ENGAGE T CELLS

A Dissertation

Submitted to the Graduate School of Pharmaceutical Sciences

Duquesne University

In partial fulfillment of the requirements for

the degree of Doctor of Philosophy in Pharmaceutics

By

Ying Zheng

December 2010

A PEPTIDE-BASED PLATFORM FOR DISPLAYING ANTIBODIES

TO ENGAGE T CELLS

By

Ying Zheng

Approved October 14, 2010

Wilson S. Meng, Ph.D. Associate Professor of Pharmaceutical Sciences (Committee Chair)	James K. Drennen, III, Ph.D. Associate Professor of Pharmaceutics Associate Dean for Graduate Programs and Research (Committee Member)
Philip E. Auron, Ph.D Professor and Chair of Biological Sciences (Committee Member)	Ellen Gawalt, Ph.D Associate Professor of Chemistry and Biochemistry (Committee Member)
Peter Wildfong, Ph.D Associate Professor of Pharmaceutics (Committee Member)	J. Douglas Bricker, Ph.D Professor of Pharmacology-Toxicology Dean of the Mylan School of Pharmacy

ABSTRACT

A PEPTIDE-BASED PLATFORM FOR DISPLAYING ANTIBODIES

TO ENGAGE T CELLS

By

Ying Zheng

December 2010

Dissertation supervised by Wilson S. Meng, Ph.D.

This study investigated a strategy by which antibodies were displayed on a gel-like substance to engage T cells. The substance, a peptidic composite, was characterized *in vitro* and explored as an injectable system *in vivo*. The composite consists of two amphiphilic peptides, AEAEAKAKAEAEAKAK (referred to as "EAK") and AEAEAKAKAEAEAKAKHHHHHH ("EAKH6"). Spectroscopic analysis showed the two peptides integrated into a single structure. Prior to combination, conformational analysis revealed that EAKH6 adopts a mixed α-helix/β-strand conformation. In the presence of EAK, EAKH6 exists predominantly in a β-strand conformation. Using nickel-bound horseradish peroxidase as a probe, the composite of EAK-EAKH6 was found to display His-tags. T-cell-specific antibodies were found stably displayed on the

EAK-EAKH6 assembly using recombinant protein A/G and anti-hexahistidine antibody as an adaptor. When mounted with an anti-CD4 antibody, the system was shown to capture CD4 T cells in a mixed population of lymphocytes. Antibodies were concentrated in the subcutaneous space in mice when co-administered with EAK and EAKH6 along with protein A/G and anti-hexahistidine antibody as an aqueous (deionized water) solution. Taken together, these results indicate that the design can be used as a platform for engaging specific subsets of leukocytes for purpose of immune modulation.

ACKNOWLEDGEMENTS

I would like to gratefully acknowledge my advisor, Dr. Wilson Meng, for his unlimited support, valuable advisory and continued guidance throughout my graduate study. His sincere dedication and tireless devotion to research has provided me with the courage to strive at difficult times and will continue to be indispensable for my professional development. I would also like to thank Dr. Philip E. Auron and Dr. Ellen Gawalt for their encouragement and tremendous technical guidance in confocal microscopy and FTIR spectroscopy. I also would like to extend my sincere appreciation to Dr. James K. Drennen III and Dr. Peter Wildfong for their contributions and commitment to this project. In addition, expertise and helpful discussions with Dr. Rita Mihaelescu, Dr. Hongmei Shen and Dr. Nick Giannoukakis have been extremely instrumental for circular dichroism and flow cytometry studies.

I also want to extend my special thanks to our current and previous group members as well as undergraduate research assistants for all their help: Jeffery R. Kovacs, Liang Jia, Yi Wen, Megan Mitchell, Amanda George and Alison Steinbach. Their friendship, both professionally and personally, has been a wonderful source of support. I am grateful to Denise Butler-Bucchilli for her help in the animal studies.

I am also greatly indebted to other faculty members: Dr. Carl A. Anderson, Dr. Laurence H. Block, Dr. Riccardo L. Boni for the high-quality training and education they have provided during my graduate studies in Pharmaceutical Sciences.

Lastly, I would like to thank my family: my father and my brother, for their endless support and understanding in my graduate study. Even from afar, they have been my constant source of strength to achieve my academic and personal goals.

TABLE OF CONTENTS

LIST OF FIGURES

ABBREVIATIONS

Ab:	Antibody
ADCC:	Antibody-dependent cell-mediated cytotoxicity
Ag:	Antigen
APCs:	Antigen-presenting cells
CD4:	Cluster of differentiation 4
CD:	Circular dichroism
CDC:	Complement-dependent cytotoxicity
CTLA4:	Cytotoxic T-lymphocyte-associated antigen 4
DCs:	Dendrtic cells
EAK:	The peptide with the sequence: AEAEAKAKAEAEAKAK
EAKH6:	The peptide with the sequence: AEAEAKAKAEAEAKAKHHHHHH
Foxp3:	Forkhead box P3
FTIR:	Fourier transform infrared spectroscopy
GITR:	Glucocorticoid-induced tumor-necrosis factor (TNF)-receptor related protein
GM-CSF:	Granulocyte-macrophage colony-stimulating factor
HRP-Ni:	Nickel conjugated horseradish peroxidase
IgG:	Immunoglobulin G
IL:	Interleukin
INF-γ:	Interferon-γ
$K_{d:}$	Dissociation constant

mAb:	Monoclonal antibody
MHC:	Major histocompatibility complex
ODN:	Decoy oligodeoxynucleotides
PLGA:	Poly (lactic-co-glycolic acid)
PVA:	Polyvinyl alcohol
RT-PCR	Reverse transcription polymerase chain reaction
rpAG:	Recombinant protein A/G
siRNA:	Small interfering RNA
TCR:	T cell receptor
Tregs:	Regulatory T cells
T_H cells:	Helper T cells

Single letter code of amino acids

G:	glycine	M:	methionine	T:	threonine	D:	aspartate
A:	alanine	F:	phenylalanine	C:	cysteine	E:	glutamate
V:	valine	W:	tryptophan	Y:	tyrosine	K:	lysine
L:	leucine	P:	proline	N:	asparagine	R:	arginine
I:	isoleucine	S:	serine	Q:	glutamine	H:	histidine

CHAPTER 1

INTRODUCTION

Monoclonal antibodies (mAb) represent an important class of therapeutics. In the United States alone, more than 20 antibody and similar molecules are currently approved for a variety of diseases, including cancer, autoimmune and inflammatory diseases. [1, 2] Of the 26 new drugs approved in 2009 by the U.S. Food and Drug Administration, four are mAb. Currently, more than 200 Abs are presently in various stages of clinical development.[1] Among these are several that aim to modulate functions of T cells through blocking or activating cell surface molecules, including CD3, CD4, CD25, and cytotoxic T lymphocyte antigen-4 (CTLA4).[2, 3] These modes of action preserve the overall T cell populations but alter a subset of cells in order to modify the course of the disease.

Normally, T cells accumulate and recirculate within secondary lymphoid organs (spleen and lymph nodes). In pathological conditions, these lymphocytes flux robustly to diseased locales to release cytokines and factors that, in most instances, sustain or accelerate the condition. For example, T cells reactive against antigens expressed by islets of Langerhans infiltrate into pancreas of patients with insulin-dependent diabetes mellitus. [4] In malignant cancers, regulatory T (Treg) cells populate tumors and promote tumorigenesis by suppressing the functions of other immune cells.[5] The rationale for using antibodies is that the high specificity and binding strength of antibodies allow them to bind to the target cells or block the signal pathway, leading to the depletion or

deactivation of the bound T cells. In pre-clinical and clinical settings of cancer or autoimmunity, T cell-specific antibodies are typically administered systemically. [3, 6, 7] Consequently, all T cells (and sometimes other leukocytes that express the target epitope) are affected, leading to non-specific immune modulation, which can result in adverse events in patients.[8] Thus, the intrinsic specificity of an anti-T cell mAb is lost when delivered systemically. Proposed here is a strategy by which disease-driving T cells operating locally can be selectively engaged (and altered phenotypically) as a means to induce specific immune modulation.

The peptide AEAEAKAKAEAEAKAK (single amino acid code; hereafter "EAK") self-assembles into high-molecular-weight structures.[9] The EAK sequence encompasses periodic repeats of alternating polar and nonpolar residues. In pure water, the peptide adopts a β−strand conformation in which the polar and non-polar side chains orient toward opposite sides. In the presence of monovalent metal ions, the β−strands self-associate into nano-scaled fibers through inter-sheet ionic pairing between charged residues (glutamate and lysine) and hydrophobic interaction between alanines.[9-11] Subsequent spontaneous cross-linking of the fibers yields quaternary β-sheet structures resistant to acids and proteases.[11] These networks of interwoven peptidic fibers have been explored as scaffolds for tissue growth or regeneration through cell attachments.[12] Such matrices have the potential to provide molecular cues for a variety of cells to grow and differentiate. An area of application that has not been explored is to use the fibrillar structures to enhance the therapeutic functions of Abs. The objective is to use mAb to intercept migratory leukocytes participating in cancer pathogenesis. The central

hypothesis of this research is that an injectable EAK-based system can be developed to engage specific T cells via monoclonal antibodies.

To transform EAK matrices into a structure that will engage specific cells, a versatile recognition mechanism is needed. To this end, a modified EAK peptide with six consecutive histidines (H6) appended at the C−terminus was used to introduce binding sites. The H6 domain is recognized by anti-polyhistidine antibodies and metal ions such as nickel through coordination bonds, making this a multifunctional platform. The modified peptide, referred hereafter as "EAKH6", was designed on the basis that the amphiphilic domain $(AEAEAKAK)_2$ would intercalate into the crossed β−sheets of EAK to form a composite in which H6 domains extend from the peptide assembly. We envisaged that the histidine appendage would not hinder the ability of the amphiphilic domain in EAKH6 to engage the same as in EAK. In the meantime, it is hypothesized that the incorporation of EAKH6 does not interfere with the self-association of EAK.

This work was motivated by the need for new strategies to localize anti-T cell Ab to the site of action. Described herein are characteristics of a peptide-based system developed as an Ab displaying platform, made possible by the use of a bi-functional peptide containing a β-strand domain and a H6 domain. Integration of EAKH6 into EAK β-sheets was confirmed in that a composite of the two contained imidazole, the side chain of histidine. EAKH6 appeared to transit from a mixed α-helix/β-strand conformation to a predominately β-strand conformation in the presence of EAK. Display of functional H6 domains in the EAK-EAKH6 composite was evidenced in the experiments showing that HRP-Ni and IgG were captured through coordination bonds or via the adaptor protein A/G complexed with anti-H6 Ab, respectively. EAK-EAKH6 but not EAK capture cells

when mounted with anti-CD4 IgG; a subset of CD4+ T cells expressing CD25 and Foxp3 was depleted form cell suspensions containing different lymphocytes. Thus, the EAK structure was transformed from a non-specific matrix to a cell-selective structure in EAK-EAKH6 construct. The system proved to be amenable as an injectable material. *In vivo*, a solution of EAK, EAKH6, protein A/G, anti-H6 Ab and IgG-PE injected subcutaneously associated to concentrate the fluorescent Ab at the injection site for at least 24 h. The EAK-EAKH6 composite thus serves to cluster antibody molecules. Such clustering reduces the entropic loss upon antigen binding, thereby increasing the collective avidity of the Ab. This should in theory result in superior efficacy of EAK-EAKH6 associated Ab compared to free Ab.

This dissertation consists of nine chapters. *Chapter 1* provides an overview of the work that includes a brief introduction to mAb, the design of EAK-EAKH6 composite, and the main experimental results and conclusions. Within the chapter an elaboration of the central hypothesis and the scope of the work can be found. In *Chapter 2* the significance of the research is discussed. The advantage of using EAK-EAKH6 assembly to cluster antibodies with increased avidity is addressed. *Chapter 3* provides a review of literatures concerning the background information as well as relevant recent studies and discoveries. The first part concerns T cell differentiation and activation in health and diseases. In particular, the change of Treg cells in cancer patients. Secondly, the mechanisms and factors governing assembly of amphiphilic peptides are addressed. Applications of peptide scaffolds in drug delivery and 3-D cell cultures are also reviewed. *Chapter 4* presents analytical data supporting the formation of EAK-EAKH6 composite. Spectroscopic data confirming the presence of EAKH6 in the composite are provided.

The mechanism of EAKH6 integration into EAK is also addressed. The function and stability of H6 domains were evaluated. *Chapter 5* reports the feasibility of using protein A/G as an adapter to load the EAK-EAKH6 composite with antibodies. Evidence of formation of the antibody-mounted peptide assembly *in vivo* is also presented. *Chapter 6* details the investigation of the capability of anti-CD4 EAK-EAKH6 assembly to capture Treg cells. *Chapter 7* describes the development and characterization of submicron PLGA particles used to deliver nucleic acids, particularly, the encapsulated oligodeoxynucleotide (ODN) and the surface adsorbed siRNA. The improved *in vitro* uptake efficiency to primary mouse leukocytes is reported. The investigation of *in vivo* function of siRNA carried by PLGA particles in mouse melanoma model is also described. These particles may be loaded onto the EAK-EAKH6 as a drug delivery module. *Chapter 8* is a narration of the overall conclusions of the studies and contributions of this research to the biomaterial community. The last chapter is included as chapter 9, for it contains data generated outside the scope of the work towards testing of the main hypothesis.

CHAPTER 2

SIGNIFICANCE OF THE RESEARCH

First introduced by Köhler and Milstein in 1975, mAb represent a mainstay in biological therapeutics and biotechnology.[1, 13] The mechanisms by which mAb modulate the functions of their target antigens are diverse. These include binding and neutralizing soluble cytokines and growth factors to prevent them from activating their cognate receptors. An example for this is the first therapeutic antibody, infliximab (Remicade; Centocor/Merck), which binds tumor necrosis factor (TNF). Binding of ligands to receptors can also be blocked by mAb directed to their cognate receptors and inhibit receptor activation or function, for example, tocilizumab (Actemra/RoActemra; Chugai/Roche) targeting the IL-6 receptor. Another class of mAb binds to cell surface antigens and depletes antigen-bearing cells through complement-mediated lysis and opsonization, as well as Fc receptor for IgG mediated clearance. Rituximab (Rituxan/Mabthera; Genetech/Roche/Biogen Idec), which is a chimeric CD20-specific antibody, succeeded in achieving B cell depletion in lymphoma patients. Therapeutic mAb can also induce active signals that alter cellular fates. Binding of the T cell receptor (TCR)-CD3 complex by teplizumab (MGA031; MacroGenics/Eli Lilly) can induce an altered pattern of cytokine production favoring IL-10 rather than interferon-γ (IFN-γ) expression. Hence, this mAb modulate T cell function by altering T cells from an activating phenotype to potentially a tolerizing phenotype.[1, 2, 14] Besides CD20 and CD3, there are hundreds of surface molecules identified for leukocytes, numbered to 350 for humans most recently.[15] These molecules are not merely markers on the cell surface to

define leukocytes; they also play an important role in cell activities, such as acting as receptors. Therefore, these molecules are critical because both innate immunity and adaptive immune responses depend upon the activity of leukocytes. Currently, half of the 24 therapeutic antibodies on the market target surface molecules of leukocytes. [1, 2] It remains to be a huge pool of new targets to generate mAb as effective treatments for diseases.

The prowess of mAb lies in their specificity and high affinity towards cognate target molecules. When given intravenously (i.v.), however, these two features are inevitably diluted. Specificity is diminished when all leukocytes are affected when the drug is intended in only a subset T cells participating in the disease. Affinity is overshadowed when only a small concentration of the i.v.-infused mAb reached the target cells. New strategies overcoming these limitations would make possible the full realization of mAb's therapeutic potential.

A simple way to enhance the binding strength of antibodies is the strategy of multivalency. An antibody's affinity is defined as the strength of the binding to its cognate antigen. Affinity is typically quantified by the dissociation constant, K_d, of an individual epitope (of the antigen) from an individual antibody-binding site. [4, 16, 17]

$$Ag + Ab \leftrightarrow Ag - Ab$$

$$K_d = \frac{[Ag] \times [Ab]}{[Ag - Ab]} \qquad \text{Equation. 2-1}$$

This specific energetic relationship between one antibody binding-site and its complementary antigenic determinant is described by the "intrinsic" affinity. This is the

affinity that is displayed by a monovalent fragment, and it also describes any binding of either monovalent or multivalent immunoglobulin to soluble, identical, monomeric antigens.[16-18] In case of polymeric antigens or surface antigens, such as receptors distributed on a cell surface, the measured affinity can be considerably enhanced by the formation of multiple binding interactions. The term "avidity", or "functional affinity" was then introduced to describe the enhancement of binding strength by multivalency.[16-18] Although avidity is the accumulated strength of multiple affinities summed up from multiple binding interactions, it is usually more than the sum of the individual affinities quantitatively. Single-chain antibody fragments (scFv) are comprised of individual antigen-recognition sites from a mAb and have proven to be a very useful tool for investigating the role of affinity and avidity. Through phage display, an anti-human Her2 (also designated as CD340, overexpressed on the surface of breast cancer cells) scFv, G98A, was generated and the binding affinity was determined as $K_d=3.2\times10^{-7}$ M. G98A was also successfully expressed as IgG variants, which containing two antigen binding sites. The K_d (now is avidity for the IgG molecules) was found increased to 5.0×10^{-10} M.[19] It thus appears that avidity can be modulated exponentially by changing the valence of the mAb in a given system. A number of quantitative approaches for multivalency have been developed. Diabodies, triabodies, and even tetrabodies were designed from examples of scFv molecules and applied in virus and cancer targeting.[19-21] However, the gain contributed by the second binding site is only observed if the antigen is on a surface or is polymeric.[18] Hence multivalent design is not an applicable strategy for mAb targeting to soluble cytokines. While the multi-expression of surface

molecules on T cells make it possible to improve the functional affinity of corresponding mAb through multivalency.

Based on the theory described above, the conceptual innovation of this research is to exploit antibody clustering to capture T cells. A composite material consisting of two peptides, EAK and EAKH6, was developed for this purpose. EAK is an amphiphilic peptide, which self-assembles to form a β-strand-based macroscopic structure upon injection.[10] EAKH6 is designed to provide H6 domains extending out as mounting sites when the rest of the peptide is intercalated into the β-strands. With this design, mAb can be immobilized onto the EAK-EAKH6 composite using an adaptor (protein A/G complexed withanti-H6 antibody). In contrast to soluble antibodies operating independently from one another, this composite serves to congregate a collection of antibody molecules displayed in the same orientation. Once the first antigen has reached the binding site, the whole cell experiences a reduction in mobility, the other antigens being restricted to the neighborhood for a second antibody to establish an additional connection.[18, 22] In these multiple interactions, rebinding can occur when one antigen dissociates.[20] After complete adsorption has occurred, several surface antigens have to leave simultaneously before the whole cell is desorbed, thereby make the process irreversible.[23] The increased in avidity makes it extremely difficult for the target cell to dissociate (figure 2-1), unless the composite disintegrate. Cells interacting with the antibodies cannot digest the structure when the size of the peptide assembly (mm) exceeds the limit of endocytosis.[24] The theoretical justification for this is that when soluble antibodies bind to cell surface antigens, the decrease in disorderness (-ΔS) in the system must compensate by enthalpic changes (ΔH), namely electrostatic interactions at

the antigen-antibody interface (figure 2-1 a). However, if multiple antibody molecules were immobilized on a surface in a defined area, there should be small or no net change in entropy upon binding to antigens. In this scenario the enthalpic change would dominate Ab-Ag association. Thus the design is underpinned by thermodynamic considerations.

Additionally, the injectable and self-assembling properties of EAK render the system described above a local delivery strategy at the pathological sites for mAb. Intravenous injection is often incapable of delivering functional mAb or their fragments to the target tissue, as many mAb are degraded in the blood, are captured by receptors and non-specific binding sites. Furthermore, systemic administration of mAb is always accompanied with severe adverse effects, especially for those leukocytes-targeted mAb. Examples include teplizumab (anti-CD3 mAb), which inhibits acute allograft rejection by T-cell depletion, increases the risk of infection and cancer.[25] Inhibition of CTLA-4 in patients using ipilimumab represents a new and promising strategy to induce tumor regression. However, immune-related adverse events (IRAEs) such as rash, colitis and hepatitis are also observed.[26] Collectively, local rather than systemic delivery may be the preferred route of mAb delivery to modulate the immunity of host.

Our long-term goal is to modulate immunity locally at the pathological sites. The studies presented justify the utility of self-assembling peptides as a platform to display a collection of mAb. The concept of enhanced binding strength through multivalency (avidity) is applicable by placing multiple antigen-binding moieties in a close physical proximity (“clustering”). The described experiments suggest the possibility to engage

specific subset T cells via immobilized surface molecule-targeted mAb. This prospect might lead to new treatments using mAb with higher specificity and binding strength.

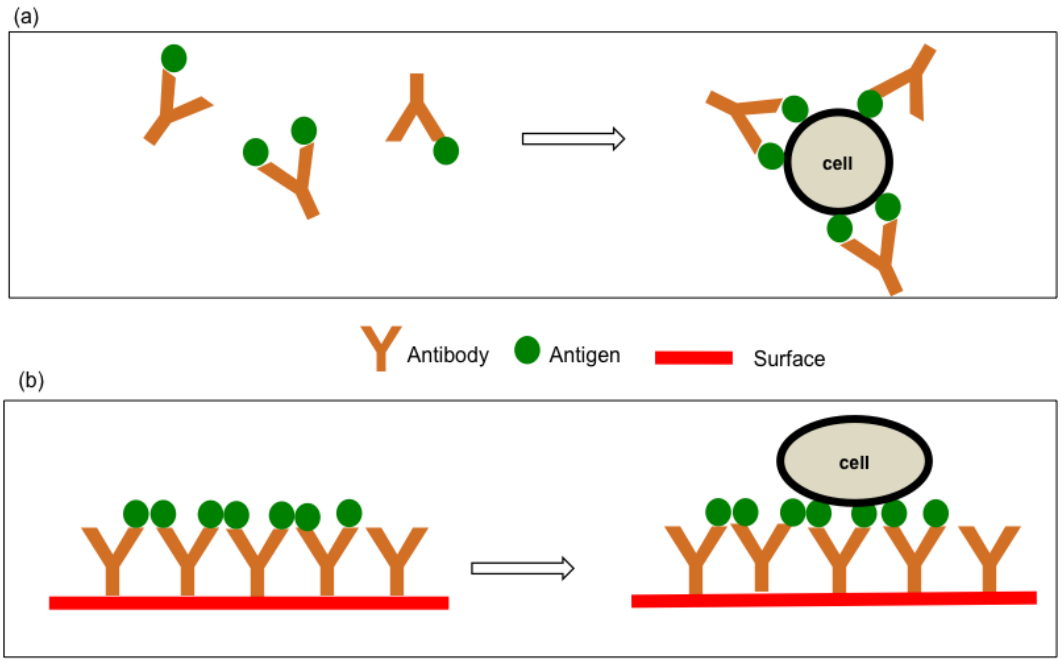

Figure 2-1: Schematic of affinity and avidity of antigen-antibody binding. (a) individual antibodies, (b) a collection of antibodies immobilized on a surface.

CHAPTER 3

LITERATURE REIVEW

T CELLS IN HEALTH AND DISEASES

Cells in immune system

The immune system in vertebrates encompasses components and processes that collectively mitigate and limit harmful effects of pathogens through elimination or neutralization. Macrophages and neutrophils of the innate immune system provide a first line of defense against many common microorganisms and are essential for the control of common infections. However, this defense depends on invariant receptors recognizing common features of pathogens, which can be overcome by mutational structural changes. Lymphocytes in the adaptive immune system have provided a more versatile means of defense with the capability of memory by which subsequent infection by the same pathogens can be arrested early on.

Adaptive immune responses depend upon lymphocytes, of which there are two major types: B cells and T cells. Both B and T lymphocytes originate in the bone marrow, but only the B lymphocytes mature there; the precursor T lymphocytes migrate to the thymus to undergo their maturation. The sole effector function of B cells is to produce immunoglobulin as defense against pathogens in the extracellular fluids. This antibody-mediated response, also known as humoral immunity, is not effective against intracellular pathogens such as parasites and viruses, or genetically transformed cells like tumors. Coordination of T and B cells responses are required to mount effective immunity.

T cell activation and differentiation

Once matured in the thymus, T cells leave and remain recirculating between blood and peripheral lymphoid tissue. Naive T cells, those that have not yet encountered their cognate antigens, remain resting until being stimulated by antigen-presenting cells (APCs). APCs engage naive T cells' antigen recognition receptor (or T-cell receptor; TCR) through major histocompatibility complex (MHC) molecules in which antigen fragments (peptides) are presented. This specific interaction requires augmentation by a second signal, or co-stimulation, figure 3-1. Effector T cells fall into two major functional classes distinguished by the expression of the cell-surface proteins CD4 and CD8. Peptides from intracellular pathogens that multiply in the cytoplasm are carried to the cell surface by MHC class I molecules and presented to CD8 T cells. They then differentiate into cytotoxic T cells that kill infected target cells. Peptide antigens from pathogens multiplying in intracellular vesicles and those derived from ingested extracellular bacteria and toxins, are carried to the cell surface by MHC class II molecules and presented to CD4 T cells. They then differentiate into helper T cells that activate other cells such as B cells and macrophages.

Only dendrtic cells (DCs), macrophages, and B cells are able to express MHC molecules as well as the co-stimulatory cell-surface molecules (B7 molecules). The receptor for B7 molecules on the T cell is CD28. Ligation of CD28 by B7 molecules is absolutely required for the clonal expansion of naive T cells and their differentiation into armed effector T cells. The most potent activators of naive T cells are DCs, and they are thought to maintain T cell homeostasis *in vivo*. Precursor or immature DCs take up

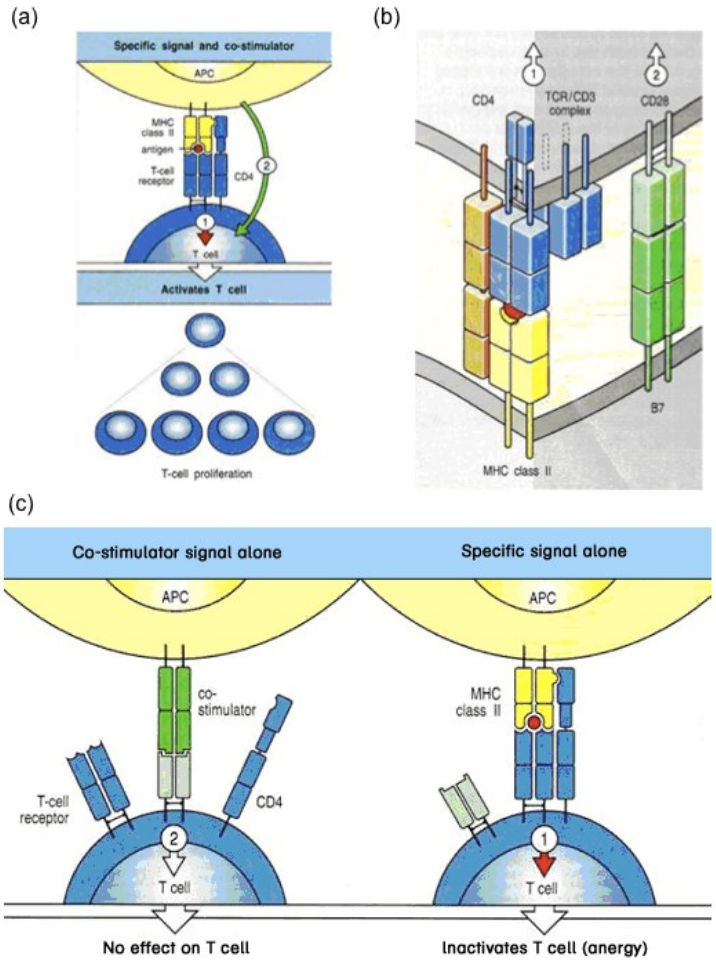

Figure 3-1: Activation of naive T cells requires two independent signals. (a) The binding of the peptide: MHC-II complex of APCs to the TCR:CD4 complex of T cells results in a signal (signal 1) to the T cell that antigen has been recognized. Activation of naive T cells requires a second "co-stimulatory" signal (signal 2) that is provided by (b) the binding of the T cell CD28 receptor to the APC B7 molecule. (c) An APC will neither activate nor inactivate a T cell if the appropriate antigen is nor present on the APC surface, even if it expresses a co-stimulatory molecule and can deliver signal 2. However, when a T cell recognizes antigen in the absence of co-stimulatory molecules, it receives signal 1 alone and is inactivated.[4] Reprinted with permission from ©2005 Garlan Science Publishing: [Immunobiology] (6th edition, page 328,339).

antigens by phagocytosis and macropinocytosis at inflammatory locales and subsequently migrate to draining lymph nodes. Therein DCs engage T cells flux from tissues continually. Dual fulfilment of MHC-TCR and co-stimulation leads to activation of T cells. This stringent requirement serves to minimize T cells from responding to self-antigens expressed in normal tissues, which lack co-stimulatory activities. Antigen recognition in the absence of co-stimulation inactivates naïve T cells, inducing a state known as anergy, in which proliferation and differentiation are prevented, figure 3-1 c.

Subsets of helper T cells

CD4+ helper T cells regulate immune responses via the production of soluble factors that instruct other cellular elements of the immune system. The first well-defined helper T cell subsets are T_H1 and T_H2 by Mosmann and Coffman in 1986.[27] T_H1 effector cells are characterized by production of IFN-γ, and are thought to be responsible for activating macrophages and enabling them to kill intracellular and ingested pathogens. T_H1 cells also produce IL-2, which is required for the proliferation of CD8 T cells. T_H2 cells are defined by production of IL-4 as well as the related cytokine, IL-13. T_H2 cells are considered the classical helper T cells providing help to B cells to generate class-switched antibodies. Indeed, when T_H2 cells are preferentially induced, the main response is humoral immunity. Generally speaking, exposure to IL-4, IL-5, IL-9, IL-10, and IL-13 favors the development of T_H2, whereas IL-12 and IFN-γ favor T_H1 cell development.[28-30] In 2005, the IL-17 producing cells, named T_H17, were classified as a new subset of CD4+ helper T cells.[31, 32] Activation of precursor T helper cells in the presence of TGF-β and IL-6 is thought to drive differentiation of T_H17 cells. T_H17 cells are thought to be particularly important in maintaining barrier immunity at mucosal surfaces, such as the

gut and lungs, as well as the skin. Consistent with this, T_H17 cells are highly prevalent in the mucosal tissues of healthy individuals. The fourth main subset of CD4+ T cells is regulatory T cells (Treg cells), characterized by expression of the transcription factor Foxp3. Treg cells can emerge directly from the thymus or induced in the periphery from naive CD4+ T cells through TGF-β.[29, 33]

Many diseases can be characterized as an abnormal change in the polarization of T cells. For example, in AIDS patients, HIV infection initiates a rapid and substantial decline in CD4+ T cells. [34] In inflammatory allergic reactions, for example, asthma, are associated with the production of IgE antibodies against common, innocuous antigens. IgE antibody production requires T_H2 cells that produce IL-4 and IL-13, and it can be inhibited by T_H1 cells. The presentation of low does of antigen can favor the activation of T_H2 cells over T_H1 cells, and many common allergens are delivered to the respiratory mucosa by the inhalation of a low dose. On the other hand, delayed-type hypersensitivity reactions, e.g., insect venom caused local skin swelling and erythema, are mediated by T_H1 cells and CD8 cytotoxic T cells.[4, 35] Beyond the T_H1 and T_H2 subsets, T_H17 cell have recently been identified as important in the response to pulmonary and colonic bacterial infections.[36, 37] Commensal gut floras contribute to the expansion of T_H17 cells, leading to inflammatory bowl diseases (IBD). IL-17 mRNA has been also found to be highly expressed in inflamed mucosa from IBD patients. More recently, it has been shown that T_H17 cells present in tumors.[38] While the cause-effect relationship between T_H17 cells operating in tumors has been controversial. Evidence is accumulating to suggest that T_H17 cells can promote protective antitumor immune response.

Regulatory T cells

Deficiency of Treg cells (in frequency or functions) can result in severe autoimmune syndromes, such as massive lymphatic proliferation, diabetes and enteropathy.[39] Conversely, an increased level of Tregs often occurs in malignancies, allowing the tumors to circumvent host immune attacks.[40, 41] First described in the 1970s as "suppressive T cells", this elusive subset is now named "regulatory T cells" with much renewed interest.[39, 40, 42, 43] In 1995, Sakaguchi and coworkers showed that the interleukin-2 (IL-2) receptor α-chain, CD25, is constitutively overexpressed on CD4+ regulatory T cells. These CD4+CD25+ cells constitute approximately 10% of the total peripheral CD4+ T cells. It is now generally accepted that this subset contributes to the maintenance of self-tolerance by down-regulating immune responses to both self and non-self antigens in an antigen specific and non-specific manner. [44]

Treg cells have been extensively studied in a variety of physiological and pathological conditions in mouse and man. The data support the fact that Treg cells suppress responder (CD8+) T cells and myeloid cells by secreting suppressive cytokines (e.g., IL-10, TGF-β), competitively consuming IL-2, and inducing cytolysis. It has also been found that Treg cells can suppress the function APCs and thus indirectly block the activation of T cells.[45] This latter mode of action has been attributed to the action of cytotoxic T lymphocyte-4 (CTLA-4), a membrane-bound competitor of CD28 for B7 molecules on APC. CTLA-4 binds B7 molecules about 20 times more avidly than does CD28 and delivers an inhibitory signal to the activated T cell.[46] Efficacy of mAb blocking this negative co-stimulator has been demonstrated in mouse models of various tumors and are being evaluated in phase III clinical trials. .[47]

It has been postulated that Treg cell-mediated immunosuppression promotes tumor growth by changing the functions of CD8+ cytotoxic T cells and NK cells operating in tumors. [40, 42, 48, 49] It has been suggested as a factor to explain the sub-optimal clinical responses of active tumor immunotherapy, including various formats of vaccines.[48] Data from Valzasina et al.'s work demonstrate that the number of CD4+CD25+ T cells has been increased in draining lymph nodes and the spleen of tumor-bearing mice. In that study, about 10-15% of CD4+ T cells were found bearing the CD25 marker in draining lymph nodes and the spleen of tumor-free mice. Whereas this level increased to 22-30%, even to 40% as the highest in tumor-bearing mice.[41] Thereafter, a higher frequency of Treg cells in peripheral blood was reported in patients with various cancers including non-small-cell lung cancer, breast cancer, ovarian cancer, pancreatic cancer, etc. These studies demonstrated that peripheral Treg cells possess suppressive activities thereby comprise anti-tumor immunity in cancer patients.[40, 49-52]

Based on these results, it was predicted that removal of Treg cells from tumors and tumor-draining lymph nodes would unveil a strong antitumor immunity. Monoclonal antibodies targeting to the surface molecules of Tregs have been found, in some cases, to reverse Treg-dependent tumor immune-tolerance.[40, 42] *In vivo* administration of CD4 or CD25-specific antibodies have been found to induce effective tumor rejection in murine tumor models. Concomitantly, dramatic increases of CD8+ T cells and INF-γ production were detected inside the tumor after CD4+ T cell depletion. [6, 53] In the study done by Coe et al. demonstrated that Treg cells constitutively expressed higher level of glucocorticoid-induced tumor necrosis factor receptor (GITR), a member of the TNF receptor family, than conventional T cells. A single injection of DTA-1 (anti-GITR mAb)

resulted in the regression of established solid tumors. It was also showed that the regression of tumor by anti-GITR mAb therapy was correlated with increased accumulation of tumor-infiltrating CD4+ (17% compared to 3% in untreated group) and CD8+ (22% compared to 4% in untreated group), but decreased accumulation of Treg cells (0.4% compared to 1.2% in untreated group).[54]

Several of the mAb are on the market, for example daclizumab (Roche), a CD25-specific agent, and tremelimumab (Pfizer) and ipilimumab (Bristol-Myers Squibb), CTLA4-specific agents.[2] These antibody-based treatments have been proved to be effective to enhance adaptive immunity and promote tumor regression. However, clinical outcomes are limited by nonspecific depletion of effector T cells, and in many cases, systemic autoimmune side effects. Thus these antibody-based approaches are limited. Moreover, the tumor mass is not amenable to the penetration, distribution and accumulation of antibodies. It is acidic (pH~6), increasing the likelihood of antibody denaturation. The elevated pressure (due to microvascular hypertension) resulting from extravasated fluids causes an outward convective current, moving macromolecules out of the tumor.[55] Collectively these factors call for new strategies in using anti-T cell antibodies. The ability to capture CD4+ T cells and alter their phenotypes in vivo could be developed into a new type of immunotherapy.

BETA STRUCTURE-BASED SELF-ASSEMBLING PEPTIDE SCAFFOLDS

In the past decade, many studies have focused on the design and use of self-assembling peptides as biological scaffolds. These peptides share a common feature of self-association in aqueous solutions. They are either fragments of natural proteins or derived by de novo biomolecular design. Within the biomaterials community, molecular self-assembly is, defined as spontaneous organization of molecules under near thermodynamic equilibrium conditions into structurally well-defined and stable arrangements through noncovalent interactions.[56] Such interactions typically include hydrogen bonding, electrostatic and van der Waals interactions. The first member of the family which has the sequence Ac-$(AEAEAKAK)_2$-NH_2, commonly referred to as "EAK16" or "EAK-II", (now termed "EAK" here), was discovered in the yeast Z-DNA binding protein Zuotin.[9, 10] EAK contains repeats of alternating polar and nonpolar residues and repetitive pattern of positive and negative charges (figure 3-2 a). These physical properties provide the mechanisms for intermolecular complementarities of hydrophobic and ionic interactions.

Proposed self-assembly mechanism

EAK contains tandem repeats of alternating hydrophilic and hydrophobic residues, in which every other residue in the peptide is alanine. At neutral pH, the four glutamic acids and four lysines are negatively and positively charged, respectively. In deionized or low ionic water, EAK forms stable β-sheets in which the polar and non-polar side chains orient to opposite sides (figure 3-2 b). Resulting is a structure in which the charged side chains lie on the same side and all alanine side chains are oriented on the opposite side. Upon exposure to salt solution, these amphiphilic β-sheets spontaneously stack up by

inter-strand pairing of charged residues (glutamate and lysine) and hydrophobic interactions of alanines (figure 3-2 c).[10, 57-59] Stacks of fibrous oligomers (7-20 in diameter) interweave to form macroscopic membrane-like structures (figure 3-2 d and e).[10, 57] Once formed, these macroscopic structures acid and protease-resistant, and remains intact at temperature up to 90°C.[11]

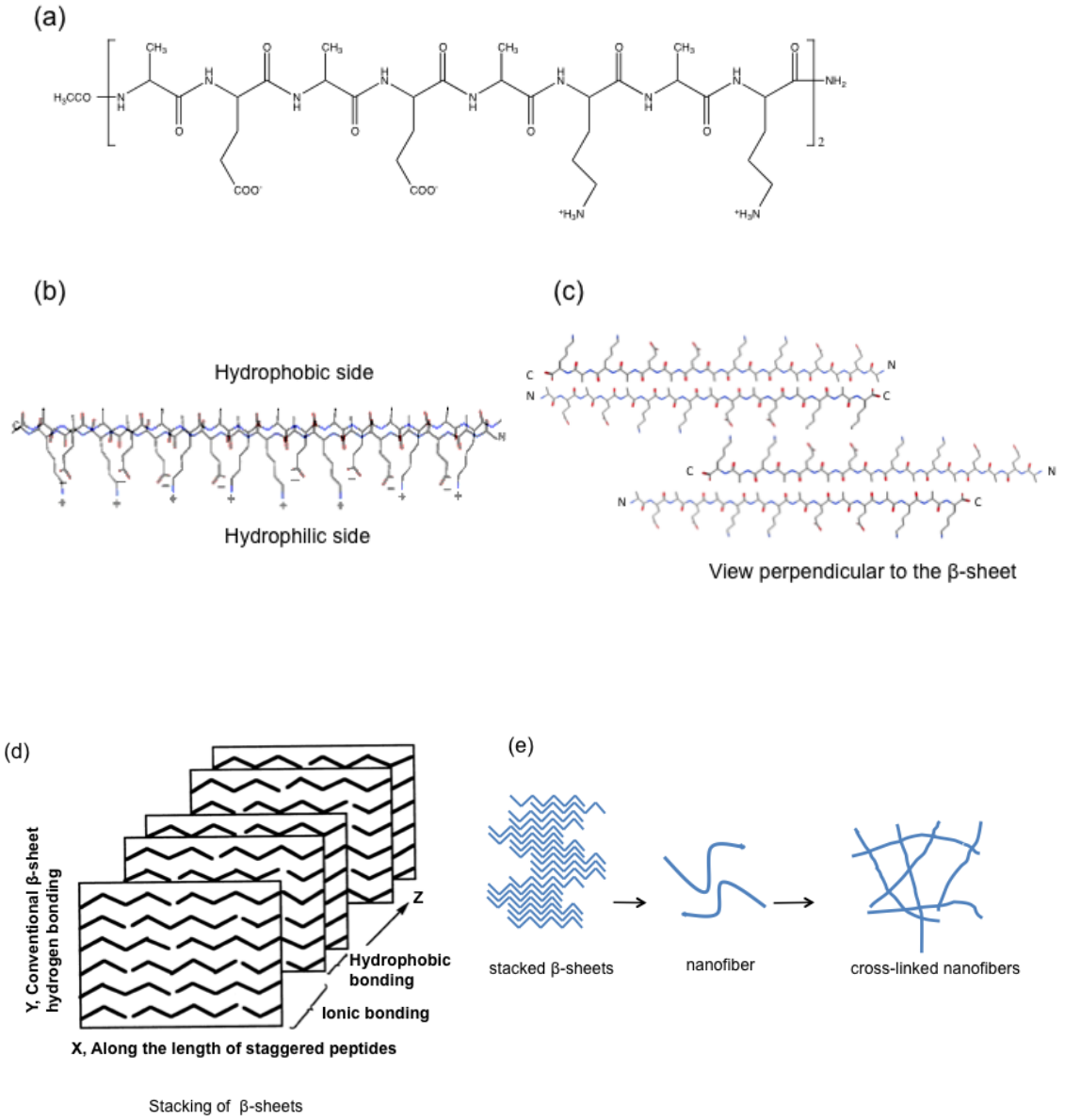

Figure 3-2: Schematic structures of EAK and EAK nano-structure. (a) chemical structure of EAK, (b) a single β-sheet formed from two molecules of EAK16, (c) a perpendicular staggered β-sheets, (d) stacking of β-sheets. The staggered peptides are oriented along the x axis. The z axis has the complementary ionic bonds between lysine and glutamic acid, as well as the hydrophobic bonds between alanines. The y axis contains the conventional β-sheet hydrogen bonds.[10] (e) nanofibers cross-linked to form the membrane.

Salt effect on the self-assembly

Zhang and coworkers further studied the effects of salts on the spontaneous-assembly process.[10, 56] It was observed that only monovalent cations are most effective in inducing assembly formation. The order of effectiveness has been determined as $Li^{+}>Na^{+}>K^{+}>Cs^{+}$, which is consistent with the hydrated radius of the ions: 3.4Å (Li^{2+}), 2.8Å (Na^{+}), 2.3Å (K^{+}) and 2.3Å (Cs^{+}). Divalent cations on the other hand induce disordered aggregation, rather than ordered periodic structures. $NH4^{+}$ and Tris•HCl are not able to induce EAK to form aggregates. It is an indication that the metal ions are more likely the components of the peptide structure, rather than as a catalyst only stabilizing the electronic charges. The salt-induced process is thought to be driven by charge screening by monovalent cations between the basic and acidic side chains on peptide molecules, resulting in decreased electrostatic repulsion. This however does not explain the differential effects of monovalent and divalent ions. A unifying perspective is that the spontaneous process is driven by free energy gained from entropic release of water molecules structured around the alanines into the bulk solution as two β-sheet stack upon one another at high concentrations.[60] When multiplied throughout many alanines in the system a significant amount of energy can be derived, making the process a spontaneous one. In this scenario the charged side chains reduce the entropic gain in free energy by decreasing the orderness of bound waters around alanines. The addition of monovalent and small ionic species dislodges the charged side chains from the alanine salvation spheres thereby allowing maximal orderness of water molecules surrounding the hydrophobic moieties.[61] The precise role of salts, however, remains under investigation.

Concentration effect on the self-assembly

Both Fung et al.[62] and Hong et al.[63] reported that there is a critical self-assembly concentration (CSAC), which is 0.1mg/ml (60μM) for EAK in pure water. Surface tension and self-assembled nanostructures formation were determined for a wide range of peptide concentrations using an axisymmetric drop shape analysis-profile (ADAS-P) and atomic force microscopy (AFM). The principle of the analysis was that changes in solution properties associated with molecular aggregation could be measured. A "break point", or minimum, is observable in the surface tension corresponding to the CSAC. AFM studies revealed that EAK formed fibrillar networks above the CSAC, while isolated filaments were observed at concentrations below the CSAC. The implication of these results is that mechanical properties of the assembly can be tuned by varying the concentration of the peptides in the system.

pH effect on the self-assembly

While interactions among the charged amino acids in EAK may not initiate stacking of β-sheets, they must contribute to the stability of the insoluble structures through electrostatic interactions. The ionization state of the four lysines and four glutamic acids in EAK can be tuned by pH in the environment, with all ionized at neutral pH. EAK contains four positively charged lysine and four negatively charged glutamic acid residues at neutral pH. In the aqueous environment, lysine has an estimated pKa of 10 and glutamic acid has an estimated pKa 4.4, with EAK having a calculated isoelectric point (pI) of 6.7. It was predicted that changes in pH would greatly affect the β-sheet structure of EAK. These effects have been studied systematically. Using circular

dichroism (CD), Zhang et al. reported a stable β-sheet structure for EAK from pH 1.5 to 11.[11] AFM images of EAK at various pH values indicated fibrillar nanostructures formed throughout the pH range from 4 to 11.[64] Given the purported configuration of the self-assembly, it is unexpected that no significant changes of EAK structures were registered. Such resistance to acidic and alkaline conditions is likely due to the complementary ionic bonds or hydrogen bonds between glutamic acid and lysine when EAK exists in the β-sheet form. Protonated and deprotonated carboxylic acids and amines may remain hydrogen bonded. Since the β-sheets are staggered and overlaid, the collective interaction energy should be much greater in for individual β-sheets. The additive interactions within the multilayer aggregate most likely cause the unusual stability.[56, 64]

Design rationale for self-assembling peptides

The sequence dependence of self-assembling peptides motivated the design of novel structures by changing the amino acid compositions. Assumed to be relatively low in immunogenicity and good biocompatibility, such sequences have been used mainly as scaffolds for tissue engineering in regenerative medicine and controlled drug release systems. Among these are peptides that are classified based on ionic complementary typed moduli (modulus I, modulus II, modulus III, modulus IV, etc., and mixtures thereof). This classification scheme is based on the pattern of alternating positively and negatively charged amino acids separated by one, two, three residues, and so on. For example, charge arrangements for modulus I, modulus II, modulus III, and modulus IV are − + − + − + − +, − − + + − − + +, − − − + + +, and − − − − + + + +, respectively.[57, 58]

Therefore, the first EAK peptide with the sequence Ac-$(AEAEAKAK)_2$-NH_2 is termed as EAK16-II.

Xiong et al. claimed that in self-assembling oligomeric peptides the polar/nonpolar periodicity could overwhelm the intrinsic propensities of amino acid residues, serving as the major determinant of peptide secondary structure.[65] Extending this notion, Zhang et al. hypothesized that if the charged residues in EAK are substituted with other amino acids with the same charge (i.e., Glu−>Asp or Lys−>Arg in the reversed EAK sequence) or hydrophobic residues with other hydrophobic amino acids (Ala−> Phe or Ala−> Leu), there would be essentially no drastic effects on the self-assembly process. [65, 66]

To test this hypothesis, another set of self-assembling peptides containing the RAD sequence, a similar motif found in EAK was characterized. These include RAD16-I, Ac-$(RADARADA)_2$-NH_2, and RAD16-II, Ac-$(RARADADA)_2$-NH_2. Indeed, RAD16-I has been comercially produced as PuraMatrix from BD Biosciences (MA, USA). [67]

Application of RAD16-I in controlled drug release

Because of the small diameter of peptide nanofibers (~10nm), nanofibers gels have a high surface:volume ratio compared to biopolymers with larger diameter fibers. This high surface ratio permits the adsorption of large quantities of drugs. [68]

Zhang et al. examined RAD16-I as matrices for controlled drug release. Microscopic images revealed that the peptide self-organizes into interwoven nanofibers with diameters of 10-20nm. These nanofibers further associate to form highly hydrated hydrogels (up to 99.5% w/v water), with pore size between 5 and 200 nm in diameter.[57, 69] The group reported that RAD16-I can be used to control the release of small molecules. Phenol red,

bromophenol blue, 8-hydroxypyrene-1,3,6-trisulfonic acid trisodium salt (pyranine, 3-PSA), 1,3,6,8-pyrenetetrasulfonic acid tetrasodium salt (4-PSA), and Coomassie Brilliant Blue G-250 (CBBG)) (figure 3-3) released through 5% w/v RAD16-I hydrogels were investigated. The mass-transfer kinetics for the release of the dyes were illustrated with mass released fraction (M_t/M_∞) monitored as a function of time (t). Phenol red, which is presumed to have no electrostatic interactions with the peptidic nanofibers, was released quickly; more than 50% of the loaded amount was released after 2 h and reached a plateau after 12 h. Although bromophenol blue has molecular structure similar to phenol red, it is not readily released from the matrices. Bromophenol blue has a lower pKa (4) than phenol red, which has a pKa of 7.9. Hence, the phenolic hydroxyl group of bromophenol blue tends to dissociate at neutral pH and thereby can interact strongly with the positively charged amines of the arginine residues in RAD16-I. Even after 7 days, bromophenol blue was essentially retained in the peptide scaffold. The mass fraction (M_t/M_∞) of release for 3-PSA and 4-PSA reached 26% and 9% after 7 days, respectively. Additionally, the diffusivity of 3-PSA was approximately seven times higher than that of 4-PSA. The difference in the release rate is most likely due to electrostatic interactions between the sulfonic acid groups and the positively charged amine groups of the peptide nanofibers. 4-PSA has 4 sulfonic side groups while 3-PSA only has 3. As CBBG binds strongly to proteins, it is concluded that this interaction impedes its release from the RAD16-I matrices. [69]

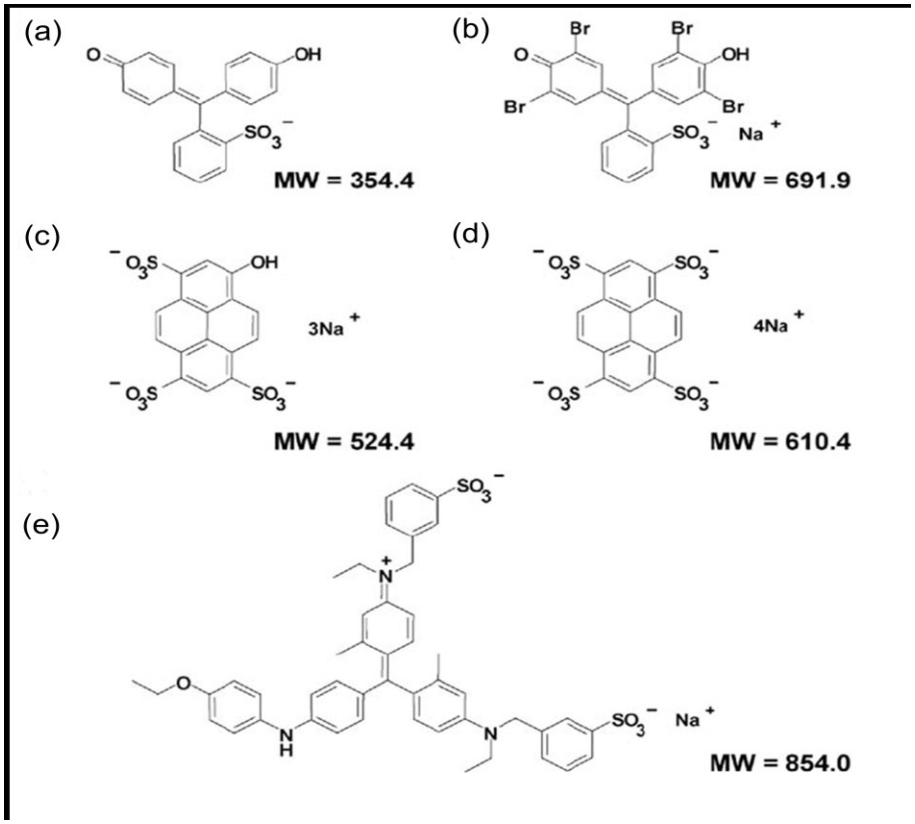

Figure 3-3: Molecular structure of the model drugs: (a) phenol red, (b) bromophenol blue, (c) 8-hydroxypyrene-1,3,6-trisulfonic acid trisodium salt (3-PSA), (d) 1,3,6,8-pyrenetetrasulfonic acid tetrasodium salt (4-PSA) and (e) Coomassie Brilliant Blue G-250 (CBBG).[69] Reprinted, with permission, from © 2006 Elsevier B. V.: [Journal of Controlled Release] (Vol.115 Page19, 2006).

Subsequently, the same group tested a series of proteins as model encapsulated drugs to study the kinetics of release from RAD16-I peptide hydrogel.[70] These include lysozyme, trypsin inhibitor, bovine serum albumin, and IgG, proteins with differing physicochemical properties (pI 4.6-11.4; molecular mass, 14.3-150kDa) and morphologies (listed in Table 3-1). The results showed that the peptidic matrix appeared to be a robust system for sustained release of proteins in aqueous environments. IgG has the slowest release among the proteins tested, with measurable concentration detectable only after 60 h. As expected, it was found that large proteins were retained inside the matrix for longer periods compared to smaller proteins, as in the case for most other fibrous matrices.[68] The implication being that the rate of release is more sensitive to physical size than charge. Lysozyme, the smallest (radius ~1.9nm) among the proteins studied, was released fastest. Trypsin inhibitor, which is slightly larger and oppositely charged compared to lysozyme, was released slower than lysozyme but faster than bovine serum albumin, a larger protein. Conversely, the release rates do not correlate with the isoelectric points of the proteins. The data also indicate that increasing the peptide concentration results in a higher density of nanofibers in the network, which could hinder the release of the proteins. Therefore, protein release through the RAD16-I can be controlled by varying the peptide concentration. In examining the functionality of the protein released, identical circular dichroism (CD) spectra and similar activity values were obtained for proteins recovered compared to the freshly prepared native proteins. Hence, it can be concluded that the encapsulation process and release mechanisms do not affect integrity of the proteins studied.

Protein	*Molecular mass (kDa)*	*Hydrodynamic radius (nm)*	*pI*
Lysozyme	14.3	1.9	11.4
Trypsin inhibitor	20.1	2.4	4.6
BSA	66.0	3.6	5.3
IgG	≈150.0	5.3	≈7.2

Table 3-1: Physicochemical properties and morphologies of the model proteins.[70]

Immunogenicity of RAD and EAK peptides

Zhang et al. attempted to produce antibodies using RAD16-II and EAK oligopeptides. However, when these peptides were either alone or conjugated with other proteins and injected into rabbits, they did not elicit a detectable immune response, and no significant titers of antibodies were obtained.[61] It was found that these peptides had a similar amino acid sequence as a segment in intermediate neural filament H, L and M proteins.[71] These sequence similarities may cause the lack of immunogenicity. Holmes et al. injected EAK and RAD (including RAD16-I and RAD16-II) peptides into the rats leg muscles to test for their induction of inflammation. The rats were killed 9 days or 5 weeks after the injections. The entire muscle was dissected and sectioned. The muscle sections were then stained with Nissl and thionin (specific for ribosomal RNA) and examined by using light microscopy for mononuclear cell infiltration and muscle fiber necrosis for signs of inflammation or necrosis. No apparent inflammation or any structural abnormalities were observed in the muscles that were injected with either saline or the peptides.[12] A collection of these results indicates that these self-assembling peptides are non-immunogenic, which is important so as to reduce immune rejection if these peptides are developed for tissue engineering or *in vivo* drug delivery.

In vivo application of RAD16-II in protein delivery

Lee et al. have investigated RAD16-II for myocardial protein delivery. [68, 72-74] In one application, platelet-derived growth factor (PDGF) was bound to RAD16-II non-covalently and resulted sustained delivery (~2 weeks) of the growth factor when the construct was injected into infarcted rat myocardium. After myocardial infarction, this

local protein therapy improved cardiac function, decreased cardiomyocyte apoptosis, and decreased infarct size.[72] This group also attached biotin to RAD16-II, and formed the biotinylated hydrogel by using 1:100 biotinylated peptides/nonbiotinylated peptides. Insulin-like growth factor 1(IGF-1) was then biotinylated as well and tethered to the peptide hydrogel with the aid of tetravalent strepavidin (figure 3-4). IGF-1 is a small protein that diffuses readily through tissues, a property that allows it to signal over great distances, but could restrict its retention within a tissue for prolonged periods. This biotin sandwich method is designed to deliver IGF-1 with biotinylated peptides to maximize the probability of peptide self-assembly and thus retention in the myocardium. After injection into rat myocardium, this "biotin sandwich" approach provided sustained IGF-1 delivery for 28 days, compared to 3 days for untethered IGF-1.[73] In order to incorporate protein stably into nanofibes, fusion protein was also made. For instance, this group constructed a fusion protein consisting of the stromal cell-derived factor-1 (SDF-1) sequence and the RAD16-II sequence, referred as SDF-1-RAD. SDF-1 is a potent chemoattractant for endothelial progenitor cells. Injected with a mixture of RAD16-II and SDF-1-RAD, the infarcted zone showed improved cardiac function and capillary density. [74]

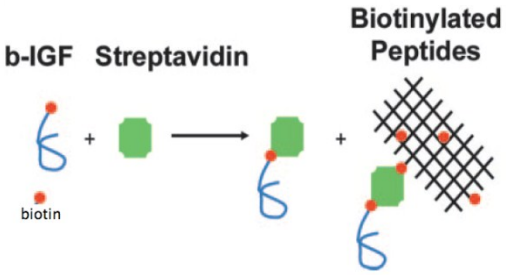

Figure 3-4: Schematic showing the biotin sandwich method: Tethering biotinylated IGF-1 (b-IGF) to biotinylated self-assembling peptides by using tetravalent strepavidin.[73] Reprinted with permission from ©2006 The National Academy of Science of the USA: [PNAS](Vol.103 Page 8156, 2006).

Design of KLD12 and its application in cell culture

In addition to the classical 16-mer peptides, smaller self-assembling sequences, including KLD12, Ac-$(KLDL)_3$-NH_2, have also been designed and tested.[75] Recall that the principal forces of the self-assembly are ionic complementary and hydrophobic interactions. It was subsequently determined that the proportion of hydrophobic residues in the sequence significantly influences the mechanical properties of the scaffolds and the speed of self-assembly[75]. The more hydrophobic the sequence, the shorter the length is required for aggregate formation with stronger mechanical properties. KLD12 was thus designed on the basis that leucine is more hydrophobic than alanine, and therefore more likely to pack tightly in the nanofibers in aqueous conditions, resulting in higher mechanical strengths.[75, 76] Grodzinsky et al. characterized KLD12 as a 3D scaffold for encapsulation of cells. Chondrocytes seeded within the KLD12-I matrix retained their morphology. The cell-peptide composite developed a cartilage-like extracellular matrix (ECM) rich in proteoglycans and type II collagen, indicative of a stable of chondrocyte phenotype. The results demonstrated the potential of KLD12-I as a scaffold for the synthesis and accumulation of a cartilage-like ECM within a three-dimensional call culture for cartilage tissue repair.[76] This peptide was also tested with bone marrow stromal cells (BMSCs). Only cells seeded with the peptide matrix but not agarose yielded high glycosaminoglcan content, spatially uniform proteglycan and collagen type II deposition (all indicating for cell proliferation).[77]

Design and application of β-hairpin peptides

Another configuration for assembly is a design through β-hairpin. In this conformation two adjacent strands in an oligopeptide oriented in an antiparallel arrangement are linked by a short loop of two or five amino acids, shaped as a hairpin. Schneider and Pochan have developed a set of β-hairpin peptides that self-assemble into rigid hydrogels.[78-84] These peptides contain a pair of turn inducing residues such as proline followed by glycine or threonin. The cyclic structure of proline causes a slight kink in the α-carbon backbone and in combination with the more comformationally flexible glycine or threonine residues that follow allows a complete reversal of the direction of the α-carbon backbone. The loop is cemented by the two residues before and after the turn-inducing pair and subsequent residues to hydrogen bond together, holding the peptide strand into a tight hairpin. Non-natural D form of proline is used in the turn sequence to permanently force a type II′ turn and prevents a cis-proly bond that could create heterogenicity in the unfolded population of peptides (figure 3-5 a).[79] A prototype of these is "MAX1" (figure 3-5),[80] which contains a total of 20 amino acids with alternating valine (V) and lysine (K) residues on two β-strands connected by a tetrapeptide (-V^{D}PPT-) sequence. These peptides are designed to remain freely soluble and unfolded due to electrostatic repulsions between the positively charged lysine side chains at neutral pH. When a physiologiacally relevant salt concentration is introduced, the electrostatic repulsions between the lysine side chains are screened and the peptide folds into a β-hairpin structure, stabilized by intramolecular hydrogen bonds. When folded, the hairpin exhibits facial amphiphilicity and the valine-rich face undergoes hydrophobic collapse, driving the self-assembly of the folded hairpins into fibrils. The β-hairpin peptidic gels are

cytocompatible with mammalian cells, including fibroblasts, mesenchymal stem cells, primary articular chondrocytes, and hepatocytes.[78, 81] Cells can be encapsulated during self-assembly, resulting in cells being homogeneously distributed throughout the fibrillar network. In addition, these peptide hydrogels possess the ability to shear thin and recover, allowing the gel-cell constructs to be delivered via syringe. [78, 82]

The Schneider series and other amphiphilic peptides demonstrate a key feature: it is possible to tailor matrices to specific biomedical applications through unique arrangements of secondary structures by careful selection of amino acids. This flexibility drives the imagination of designing capabilities for self-assembling structures. In addition to those already discussed, several other systems warrant mentioning. Peptide P_{11}-4 (Ac-QQRFEWEFEQQ-NH_2) was designed by Aggeli et al. to self-assemble to form β-sheets and nematic gels in the pH range 5-7 at concentrations ≥12.6 mM in water. This self-assembly is reversibly controlled by adjusting the pH of the solvent. A peptide P_{11}-3 (Ac-QQRFQWQFQQQ-NH^2) whose self-assembly behavior is independent of pH was first designed. pH control was then incorporated by appropriately positioning glutamate (E) side chains so that the peptide-peptide free energy of interaction in the tapelike substructure was strongly influenced by direct electrostatic forces between COO^- in glutamate.[85, 86] Collier and Messersmith described a similar peptide, Ac-QQKFQFQFEQQ-NH_2, which exists as β-sheets and self-assembled into fibrillar aggregates. The resultant structures contain several pendant glutamine residues that can be cross-linked with lysine containing peptides in the presence of transglutaminase and calcium ions.[87]

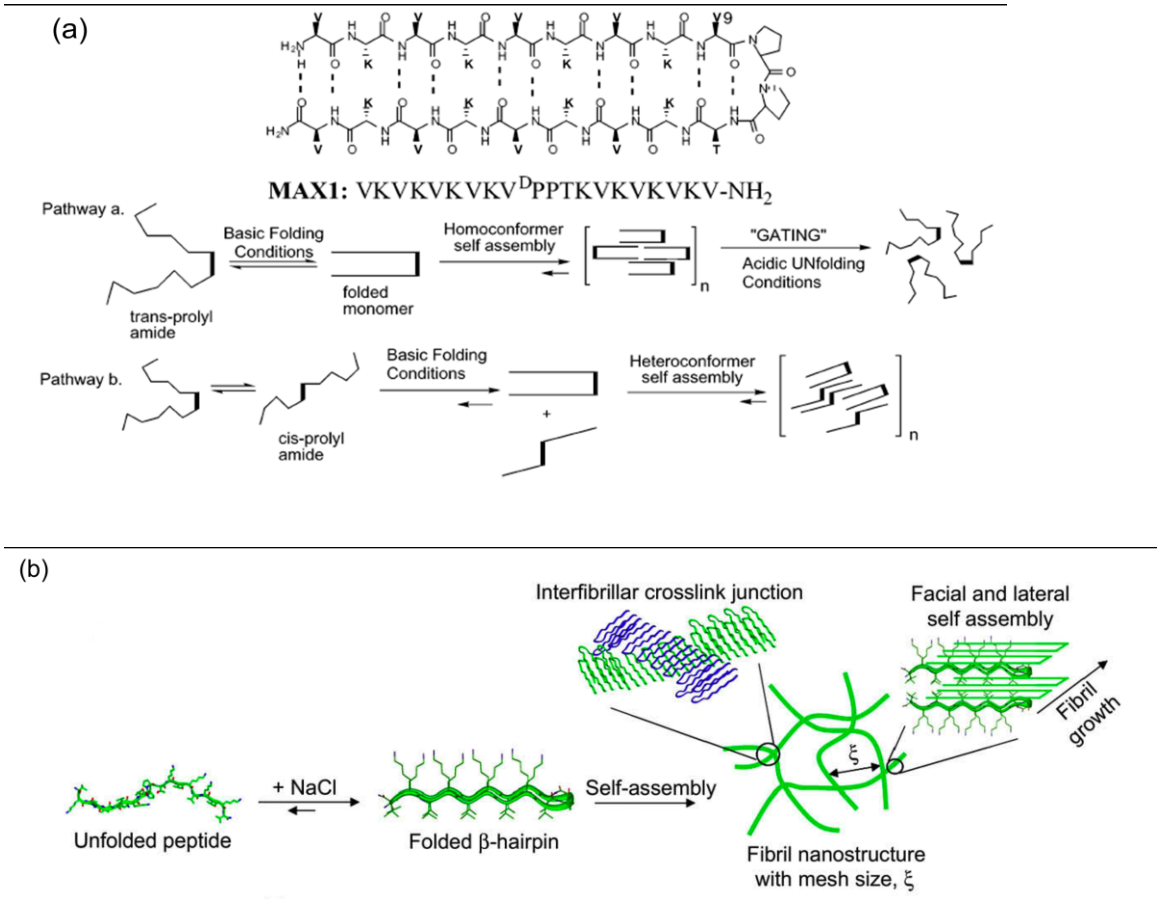

Figure 3-5: Schematic of β-hairpin peptide assembly. (a) Sequence and proposed β-hairpin structure of peptide MAX1. Alternate folding/self-assembly pathways dependent on turn structure contained within MAX1. Valine at position 9 strongly enforces a trans-prolyl amide bond geometry favoring hairpin formation prior to self-assembly (pathway a). A cisgeometry, which is designed against, may result in an extended conformation, which could undergo mixed self-assembly with correctly folded hairpins (pathway b). [79] Reprinted with the permission from © 2002 American Chemical Society: [Journal of the American Chemical Society] (Vol. 124, Page15031, 2002) (b) Proposed mechanism for the folding and self-assembly of β-hairpin hydrogels.[80] Reprinted with the permission from © 2008 Elsevier Ltd. [Biomaterials] (Vol. 30, Page 1340, 2009).

Taken together, synthetic self-assembling peptides have tremendous potential as biomaterials because they can be readily modified at the amino acid level. The responsive to stimuli, for example ionic strength and pH, is a major advantage in developing *in vivo* applications by designing around one or more physiological condition(s). The peptides appear to be non-immunogenic, and the matrices can be loaded with biologically active proteins for prolonged release.

CHAPTER 4

PHYSICAL CHARACTERIZATION OF EAK-EAKH6 COMPOSITE

INTRODUCTION

Both naturally occurring and synthetic materials have been used for protein delivery. Naturally occurring materials include collagen, gelatin, agarose, alginate, chitosan, etc. The advantage of naturally occurring materials is their known physiological activities, mechanical properties, and biodegradability. These materials may also be relatively inexpensive. However, potential transfer of infectious agents from animals, antigenicity and unstable material supply are potential disadvantages. Moreover, specific properties of naturally derived materials that are necessary for protein delivery are difficult to design. Synthetic polymers can be produced on a large scale, and their structural and mechanical properties can be more easily modified. Commonly used materials are polylactide (PLA), glycolide-lactide copolymer (PLGA), polyvinyl alcohol (PVA), and poly-ethylene glycol (PEG). Potential disadvantages of synthetic polymers are a decrease in local pH from acid breakdown products, bulk degradation, and inflammatory responses. [68]

In the past decades, self-assembling peptides have been developed for tissue engineering and protein delivery. These peptides recently attracted intense research interests because they are injectable, non-immunogenic, biocompatible, and flexible in design and modification.[56, 57, 88] The first member of this class of self-assembling peptides is EAK. Discovered in the sequence of the yeast Z-DNA binding protein zuotin, EAK (also referred to as “EAK16-II” in the literature) is prototypical of a class of self-assembling peptides characterized by periodic repeats of alternating polar and non-polar

amino acids. In water, EAK adopts a β-sheet conformation. In buffers containing monovalent metal ions (Na^+, K^+), the peptide assembles into an ordered stable quaternary β-sheet structure. This high molecular weight assembly is resistant to proteases, high temperature (up to 90°C) and acidic or alkaline conditions (pH 4-11). [9-11]

The EAK assembly has been used as a scaffold for promoting cell growth *in vivo*. Cells co-injected with the EAK peptide form cell-embedded matrices with biological functions. Such applications in tissue engineering represent a form of individualized medicine mostly practiced in academic settings. An "off-the-shelf" injectable capable of modulating host cells *in vivo* would have much wider applications. [58, 61]

The goal of this project is to develop a platform technology by introducing a His-tag onto the insoluble structure as "mounting sites". This was done by seeding into the assembly with EAKH6, which contains six histidines at the C terminus of the EAK sequence. It was hypothesized that the amphiphilic domain (AEAEAKAK)2 intercalates into the EAK β-sheets, with the C-terminal his-tag domain extruding out-accessible as binding sites. The assumption is that the histidine appendage does not interfere with the ability of the amphiphilic domain to engage the same in EAK oligomers in macroscopic insoluble structures.

This chapter describes preparation and characterization of assemblies made with EAK and EAKH6. The goal is to demonstrate the integration of EAKH6 into the EAK β-sheet network using analytical and biochemical means. It provides physical evidence on which subsequent functionalization is based. Four techniques were used to characterize the EAK-EAKH6 composite: UV-Vis, circular dichroism (CD), Fourier transformed infrared

spectroscopy (FTIR) and an enzymatic reaction using nickel-bound horseradish peroxide (HRP-Ni) as a probe of the H6 domain. Collectively, results from these analyses show evidence for EAKH6 integration into the EAK network.

MATERIALS AND METHODS:

Peptide assembly preparation

The peptides EAK and EAKH6 were custom synthesized by EZBiolab (Carmel, IN, USA) custom synthesis service. The purities of EAK and EAKH6 are 79.54% and 92.72% respectively. The peptides were acetylated at the N-termini and amidated at the C-termini to be chemically inert. Their identities were confirmed by mass spectroscopy. Upon arrival, the lyophilized peptides were reconstituted in sterile deionized water (18.2 MΩ at 25°C) at a concentration of 3.13mM (5mg/ml for EAK and 7.8mg/ml for EAKH6) and stored at -80°C until use. The peptide sequences are showed in figure 4-1.

To form the assembly, the peptides were thawed out. 10-20μl of the stock solution of EAK, or the mixture of EAK and EAKH6, was injected into 1.0 ml of phosphate buffered saline (PBS; 154 mM sodium chloride, 5.5 mM sodium phosphate dibasic, 1.2 mM potassium phosphate monobasic; pH 7.4; no calcium or magnesium). 2-4μl 0.1%(w/v) Congo red, which is the dye binding to β-sheet specifically, was added to visualize the structure.

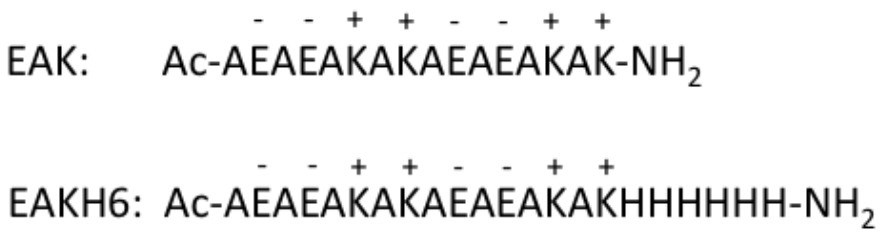

Figure 4-1: Amino acid sequence of EAK and EAKH6. Peptides are acetylated and amidated at the termini.

UV-Vis analysis

The UV absorbance of peptide bond has been determined to investigate how much percentage of EAKH6 can be incorporated into the EAK fibrillar structure. The samples were prepared as follows: 10µl of the stock solution of EAK peptide (5mg/ml) was mixed with 1µl of the stock solution of EAKH6 (7.8mg/ml) peptide. This mixture was added into 1ml PBS to initiate the structure formation. After that the sample was centrifuged at 16,000×g force for 20 min to spin the peptide assembly down. The supernatant was collected and absorbance at 205 nm was measured on a Lambda35 UV/Vis Spectrometer (PerkinElmer Instruments, Shelton, CT, USA). Meanwhile the groups of 50 µg of EAK and 7.8µg of EAKH6 by themselves were incorporated as well.

Fourier transform infrared spectroscopy spectroscopy

FTIR spectra were recorded on a Thermo Nexus 470 Infrared Spectrometer operated at a spectral resolution of 0.5 cm^{-1} over 1024 scans. Fibillar structures were formed in PBS (1ml) with 100µg EAK, or the same amount of EAK with 78µg EAKH6 for the composite. After centrifugation (16,000×g for 20min using an Eppendorf 5415R Centrifuge), the supernatant was removed and the structure was washed to remove unbound EAKH6. The fibrillar structure collected was then lyophilized by a Labconco Freeze Dry System/Freezone 4.5 prior to FTIR analysis under inert condition and scanned over 400-4000 cm^{-1}.

Circular Dichroism (CD) measurement

CD spectra were obtained on a Jasco J-810 spectropolarimeter (Jasco Analytical Instruments, Germany) with Jasco's Spectra Manager™ software for data processing.

Spectra were recorded from 190 to 250 nm at room temperature by accumulating 10 runs. After correction for solution blanks, absorbance values were converted to mean residue ellipticities according to the equation 4-1:

$$[\theta] = \frac{100 \cdot \theta_{obs}}{cnl} \qquad \text{Equation. 4-1}$$

Where θ_{obs} denotes the measured ellipticity, c the peptide concentration in mM, n the number of amino acid residues, l the path length of the quartz cuvette in cm. Finally the θ_{obs} was plotted against the wavelength using Excel 2007(Microsoft, USA). The secondary structure conversion of EAKH6 was evaluated by the comparing the CD spectra of EAKH6 by itself and the EAKH6 component in the mixture with EAK. Furthermore, the analysis of secondary structure composition has been performed using CD Pro software, which contains three popular methods (SELCON3, CONTINLL and CDSSTR) for CD analysis. The software is available at the website: http://lamar.colostate.edu/~sreeram/CDPro/main.html. A reference set containing 43 soluble proteins was chosen to execute the programs.

Nickel conjugated horseradish peroxidase (HRP-Ni) binding assay

HRP-Ni is a nickel (Ni^{2+}) activated derivative of horseradish peroxidase (HRP) used for direct detection of poly-histidine tagged proteins since nickel can form coordination interaction with histidine side chains. HRP-Ni was obtained from Pierce (IL, USA) as lyophilized powder. Upon arrival, the enzyme was reconstituted in sterile ddH_2O at a concentration of 4mg/ml, and stored at -80°C until use.

The peptide assembly was formed by injecting a mixture of 50μg EAK and 19.5μg EAKH6, mole ratio 1:4 (EAKH6: EAK), into 1ml PBS. The groups of individual 50μg

EAK and 19.5 μg EAKH6, and equal volume of PBS were included as well. 1μl of 0.1%(w/v) Congo red was also added to visualize the structure. After the membrane-like structure was formed, 1μl of 0.8μg/ml (1:5,000 dilution of the stock) HRP-Ni was added into each sample. The mixtures were incubated on ice for 1 hour. Then the samples were centrifuged at 16,000×g for 20 min to spin the assembly down. The supernatants were taken out and filtered through a 0.22μm filtered to remove any insoluble fragments. 100μl of the filtrate was mixed with 100μl of TMB substrate (BD Biosciences, CA, USA) in 96-well plate. Triplicates were done for each sample. The plate was incubated for 30 minutes at room temperature in the dark. Afterwards, 50μl stop solution (2N H_2SO_4) was added to each well, and the plate was read for absorbance at 450nm. The results were corrected by subtraction of the absorbance at 570nm. All the absorbance was determined using a PerkinElmer wallac 1420 multilabel counter (PerkinElmer Life and Analytical Sciences, Finland). A standard curve of HRP-Ni was also performed from serial dilution of 0.125ng/ml to 8ng/ml. The concentrations of unbound HRP-Ni in the supernatants were then calculated.

RESULTS AND DISCUSSION:

Peptide assembly

EAK assembly can be prepared and visualized by injecting 10µl of the stock peptide solution (5mg/ml) mixed with 2µl 0.1% (w/v) Congo red into 1ml PBS. The insoluble structure is red, due to the binding of Congo red purported to bind to hydrophobic grooves in fibrous β-sheet structures (figure 4-2 a).[10, 89] Figure 4-2c shows the self-supporting nature of the assembly prepared by mixing equal volume of EAK (5mg/ml) and PBS. This suggests that the peptide molecules assemble into a 3-dimensional structure.

EAK-EAKH6 assembly was prepared from injecting a mixture of 50µg EAK and 19.5µg EAKH6 into a volume (1ml) of PBS. The mixture produced an insoluble structure visually similar to EAK. On its own EAKH6 does not associate into aggregates as evidenced by the lack of Congo red binding (figure 4-2 b). Mixture of EAK and EAKH6 also form a 3-dimensional gel-like substance, as evidenced in figure 4-2 d.

This result indicates that the spontaneous assembly of EAK is not disrupted by the presence of EAKH6 at 4:1 (EAK: EAKH6) mole ratio. However, formation of insoluble structure does not prove the existence of EAK-EAKH6 composite. The presence of the Congo Red-stained structure could be caused by self-assembly of EAK with EAKH6 excluded and remained in the aqueous solution. Evidence will be presented in the following chapters to support the notion that EAKH6 is indeed integrated into the EAK network.

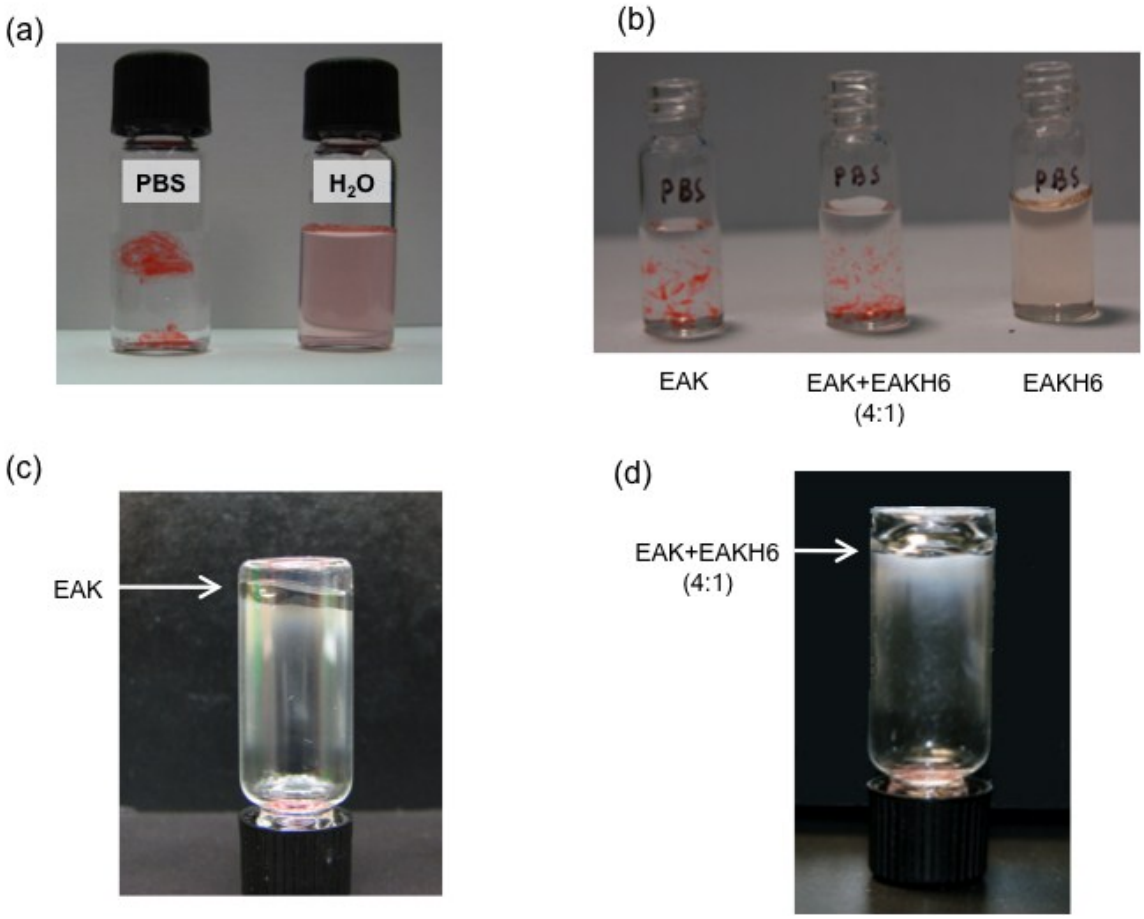

Figure 4-2: Formation of the peptide assembly. (a) Fibrillar structure formed from 50µg EAK was revealed by Congo red (1µg/ml) staining in 1ml PBS, but not in 1ml ddH_2O, (b) Congo red staining of β-sheet-rich structures in PBS containing EAK, EAK-EAKH6 and EAKH6 by itself, and self-supporting structure of (c) EAK, (d) EAK-EAKH6 gel-like structure in an inverted vial.

Characterization of the fibrillar structure composition

The fraction of EAKH6 associated with EAK was determined indirectly based on quantity of peptides remained in the aqueous phase after centrifugation. At 16,000×g EAKH6 associated with the EAK fibrillar structure can be removed from the aqueous phase. The concentration of EAKH6 remained in the aqueous phase was determined using UV-Vis (absorbance by peptide bond at 205 nm) based on Beer's law (figure 4-3 a). The results are summarized in figure 4-3 b. The difference between the mixture of two peptides and EAK alone is significantly lower than the equal amount of EAKH6 by itself. The percentage of EAKH6 incorporated into the fibrillar structure was calculated according to the equation 4-2.

$$\text{Percentage of EAKH6 in membrane} = \left(1 - \frac{A_{EAK+EAKH6} - A_{EAK}}{A_{EAKH6}}\right) \times 100\% \qquad \text{Equation 4-2}$$

Based on the results from three independent experiments, 54.9±5.6% of the EAKH6 was removed from the solution by centrifugation with the EAK assembly. The assumption here is that 100% EAKH6 on its own remain soluble and stay in the supernatant. These data indicate that more than half of the mixed EAKH6 can be incorporated into the network. This indirect measurement supports the fibrillar structure consists of both EAK and EAKH6.

UV-Vis absorbance assays are fast and convenient for determination of protein/peptide concentration, and do not consume the samples. Proteins in solution absorb ultraviolet

light with absorbance maxima at 280 and 190nm. Amino acids with aromatic rings, tyrosine and tryptophan, are the primary reason for the absorbance peak at 280 nm.[90] Since neither EAK nor EAKH6 contains these amino acid residues, the other strong absorbance by peptide bonds peaked at about 190 nm was used. Because of the difficulties caused by absorption by oxygen and the low output of conventional spectrophotometers at this wavelength, measurements are more conveniently made at 205 nm, at which the absorbance is approximately half that at 190 nm. The advantage of using peptide bond absorbance is that there is little variation in response between different proteins/peptides.[91]

Based on the outcome of UV-Vis analysis, a major part of EAKH6 was centrifuged away from the supernatant in the presence of EAK. Since EAKH6 is soluble by itself, it must associate with the EAK structure and get precipitated out.

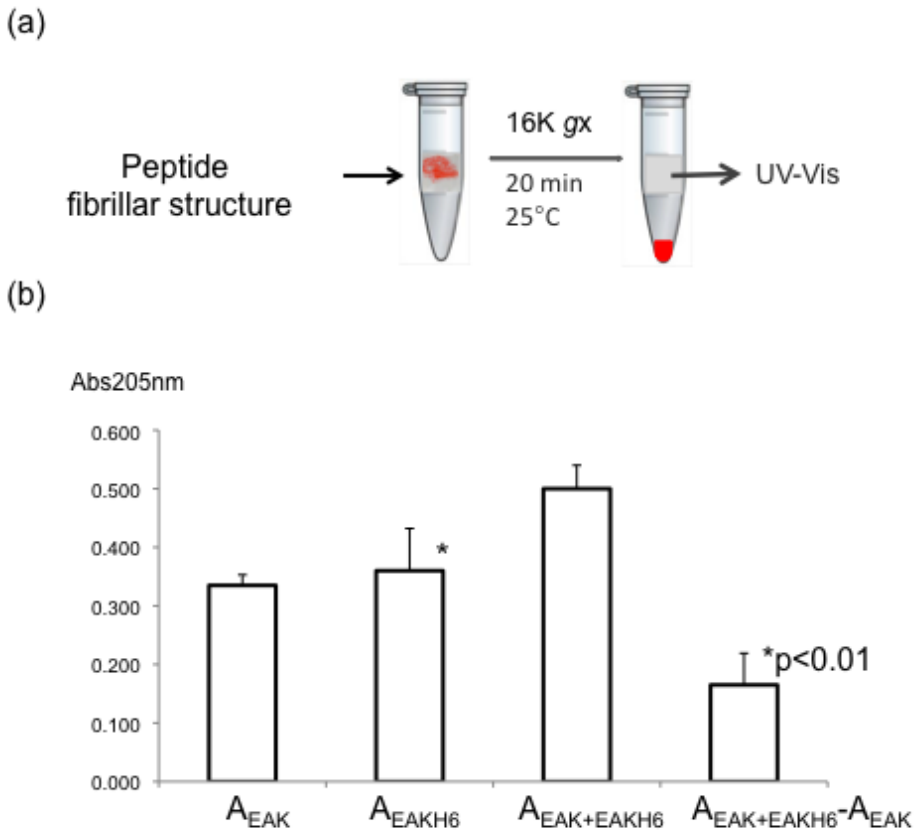

Figure 4-3: UV-Vis analysis of peptide aggregates. (a) Schematic of sample preparation, and (b) UV-Vis absorbance at 205 nm of the supernatants (n=3). The value of $A_{EAK+EAKH6}$-A_{EAK} is significantly lower than the value of A_{EAKH6} by one-tail t-test ($p<0.01$)

Chemical evidence of EAKH6 integration into EAK

The presence of the H6 domain in the EAK-EAKH6 composite was confirmed using FTIR spectroscopy (figure 4-4). The fibrillar structure was formed by injecting a mixture of EAK and EAKH6 (mole ratio 2:1, dissolved in water) into 1ml PBS, followed by centrifugation to remove unbound EAKH6. The aggregates collected were then lyophilized and subjected to FTIR scanning. The FTIR spectra of EAK-EAKH6 assembly and pure EAK were recorded and represented as percent transmittance as a function of wave-numbers (figure 4-4 a). Contribution of EAKH6 in the composite was obtained by subtracting the spectrum of EAK from that of EAK-EAKH6 (figure 4-4 c).

In figure 4-4 a, the spectrum of EAK-EAKH6 shows peaks in the 900-500 cm^{-1} region, while there is no such peaks in the spectrum of EAK. Aromatic and heteroaromatic compounds display strong out-of-plane C-H bending and ring bending absorption bands in this region.[92] The presence of EAKH6 in the EAK-EAKH6 assembly can be evidenced by these bands in the aromatic ring vibration region since EAKH6 contains imidazole rings in its histidine side chains (figure 4-6b).

Figure 4-6 c shows the net contribution of EAKH6 in the mixed peptide assemblies. The presence of histidine is evidenced by the characteristics bands consistent with the chemical features of the imidazole ring (figure 4-6 c).[92-94] Among these are peaks characteristics of stretching of the double bonds C4=C5 at 1529 cm^{-1}. The peak at 3274 cm^{-1} is assigned to the stretching vibration of C-H (C5-H and C2-H) in the imidazole ring.[94, 95] A broad band centered at 1134 cm^{-1} is typical of the tautomeric forms of imidazole in the stretching of C_2-N_3 and C_4-N_3. The peak at 1051cm^{-1} represents C-H

bending at C4 and C5 of the imidazole ring. The peaks at 541 and 721 cm^{-1} are consistent with deformation vibration of ring structures, again supporting the presence of imidazole. Since the EAK sequence contains no ring structures, the composite must contain the H6 domain. These spectroscopic results thus confirmed the presence of EAKH6 in the assemblies formed by a mixture of EAK and EAKH6.

(a)

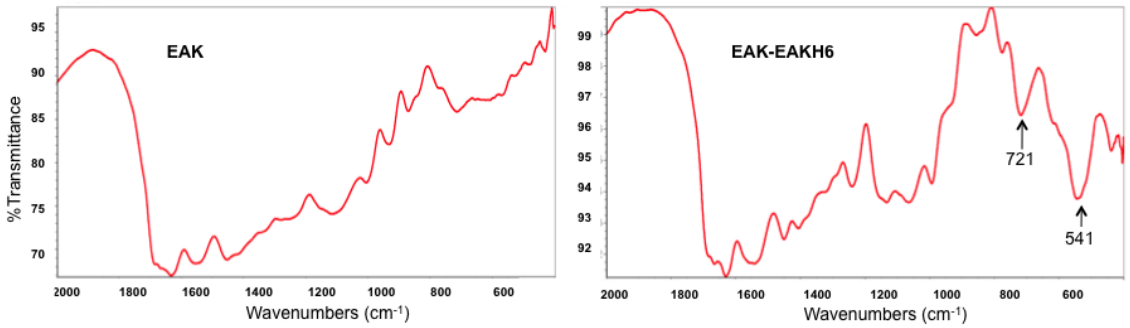

(b)

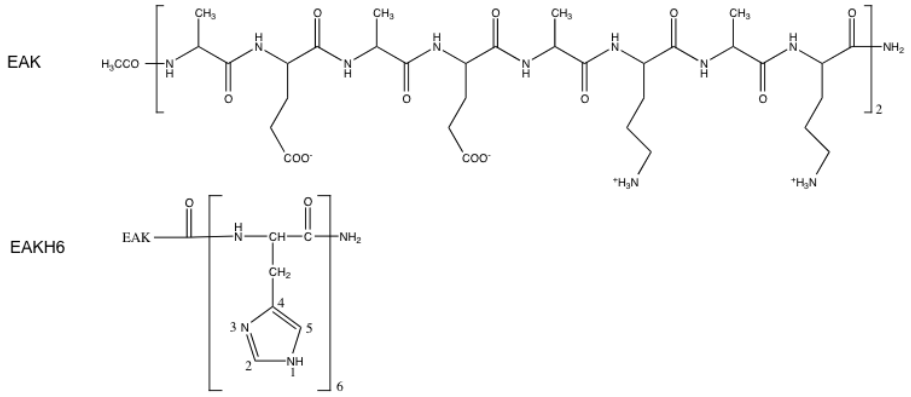

(c)

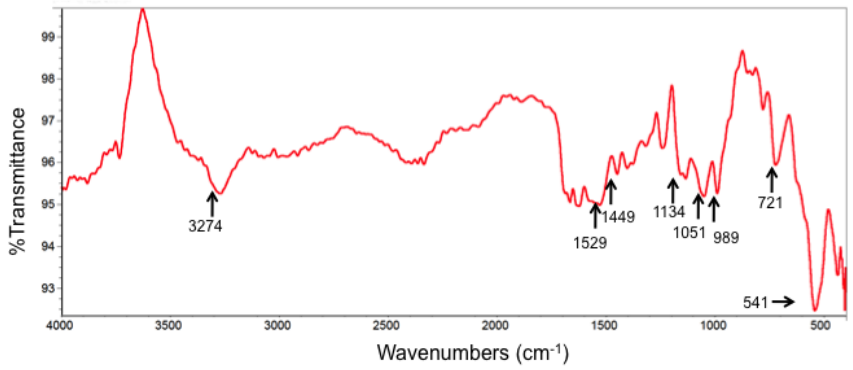

Figure 4-4: FTIR confirmation of EAKH6 in EAK-EAKH6 insoluble structure. (a) Fourier Transform Infrared (FTIR) spectra of lyophilized pure EAK and EAK-EAKH6 insoluble structure, (b) chemical structures of EAK and EAKH6, and (c) Imidazole-specific peaks were assigned to spectra of EAK-EAKH6 subtracted with EAK. Peptides (dissolved in deionized water) were pipetted into 1ml PBS and collected by centrifugation (16,000×g for 20 min at 25°C). Samples were washed with PBS to remove weakly bound peptides not integrated into the assembly and subsequently lyophilized before scanning over 400-4000cm^{-1}.

Infrared spectrum is obtained when radiation in the range of 4000-400 cm^{-1} is absorbed and converted by an organic molecule into energy of molecular vibration. There are two main types of molecular vibrations: stretching and bending. The stretching frequencies are usually higher than corresponding bending because it needs more energy to stretch a bond than bend it. The two important areas for a preliminary examination of a spectrum are the regions 4000-1300 and 900-500 cm^{-1}. The high-frequency portion of the spectrum is called the functional group region. This region tends to include motions, generally stretching vibrations, that are more localized and characteristic of the typical functional groups, e.g., O-H, C-H, N-H, found in organic molecules. Meanwhile the region of 900-500 cm^{-1} involves usually molecular bending motions, which are characteristic for an aromatic or heteroaromatic structure.[96] In the current system, the presence of imidazole ring in the EAK-EAKH6 composite can be confirmed by the peaks at 541,721 and 989 cm^{-1}.

The identification of a compound using IR spectroscopy relies heavily on the characteristic functional group frequencies. Certain groups of atoms give rise to bands at or near the same frequency regardless of the structure of the rest of the chemical environment. Based on this theory, the expectation is that the spectral contributions detected were only those of the poly-histidines by including the spectral signatures of the EAK as a background to be subtracted from the EAK-EAKH6 composite. In comparing to the spectrum of an authentic sample, most of the peaks in the subtraction spectrum match the characteristic peaks of histidine (i.e., C-H stretching at 3274 cm^{-1}, C=C stretching at 1529 cm^{-1}, C-N stretching at 1134 cm^{-1}). The analysis is completed over

1024 scans and results are presented as an average of all 1024 scans, which strengths the case for sufficient background subtraction, and supports the strength of this evidence for EAKH6 presence in the fibrillar structure.

The IR spectroscopic analysis of the assemblies (collected by centrifugation) indicates that at least some of the added EAKH6 associated with the EAK assembly. One possibility is that the EAKH6 intercalates into the β-sheet stacks of EAK, thus becoming an integral part of the fibrillar structure. The other possibility is that EAK form the structure by itself with EAKH6 adsorbed physically, perhaps on the surface of the assembly. Neither UV-Vis analysis nor IR spectroscopy could offer mechanism of EAKH6 association with EAK. Thus further investigations to reveal the conformational change of EAKH6 when associate with EAK are warranted.

EAK induces EAKH6 conformational change

For EAKH6 to integrate into the EAK β-sheets, the former must undergo a change in conformation. Circular dichroism (CD) was used to determine the dominant secondary structure of EAK, EAKH6 and EAKH6 in the presence of EAK (figure 4-5). The spectrum for EAK (figure 4-5 a) shows a broad negative maximum at ~216nm and a positive band near 200 nm, a profile consistent with a predominant β-sheet conformation. In contrast, the spectra of EAKH6 (figure 4-5 a) exhibits double minima at 206 and 222nm, which are characteristic of α-helix conformation.[97] These spectra of individual peptide formed the basis of analyzing EAKH6 in the presence of EAK.

Mixtures of EAKH6 and EAK at mole ratios of 1:2 and 1:4 were also analyzed. Spectroscopic contribution by EAKH6 was determined by subtracting the contribution of EAK based on the spectrum of the pure peptide. This analysis indicates that EAKH6 underwent conformational change from a predominant α-helix to contain β-strand conformation in the presence of EAK (figure 4-5 b).

The relative proportions of secondary structure compositions of the peptides were analyzed using the algorithms operated in the de-convolution program CD-Pro. The percentage of four secondary structure components, helix, strands, turn and random coil, were estimated by comparing with reference proteins from a database of 43 soluble proteins.[98, 99] Figure 4-5 c shows the results of the analysis. EAK, as expected, adopts a high percentage of β-strand conformation at 58%, with the rest in turn and random coil. By itself EAKH6 exhibits a mixed secondary structures, containing 14~17% of β-strand and 24~28% of helix conformation. In the presence of EAK, however, the β-strand

fraction of EAKH6 increased to 86% at the mole ratio 1:2 (EAKH6: EAK), and 92% at 1:4. Taken together, these data indicate that EAK induces EAKH6 undergo α→β conformational change at the microscopic level. It is consistent with the notion of integration of EAKH6 into EAK insoluble structure that consists of oligomerization of β-sheets.

The pathway of EAKH6 association with the EAK structure was explored based on secondary structure composition. CD measures the differential absorption of the left and right circularly polarized components of plane-polarized radiation. This effect will occur when a chromophore is chiral, or optically active.[97] All 20 natural amino acids, except glycine, possess a center of asymmetry at the α carbon atom. Hence different forms of regular secondary structure found in peptides and proteins exhibit distinct far-UV CD spectra at 180-250 nm, where the peptide bond is the chromophore. In solutions, EAK and EAKH6 adopted distinctly different conformations. The basic principle involved in the analysis of CD spectra, and used in the estimation of secondary structure factions, is that the CD spectrum (C_λ) can be expressed as a linear combination of CD spectra of individual secondary structure components (k), $B_{k\lambda}$.

$$C_\lambda = \sum f_k B_{k\lambda} \quad \text{Equation. 4-3}$$

Where f_k is the fraction of the secondary structure k. This equation has been validated by Sreerama et al., in 2000.[98] Spectra of model polypeptides or of a set of reference proteins with known structures are used to determine the component secondary structure spectra $B_{k\lambda}$. The secondary structure fractions for the reference proteins are determined from the corresponding crystal structure. The criteria to choose a reference set is based on

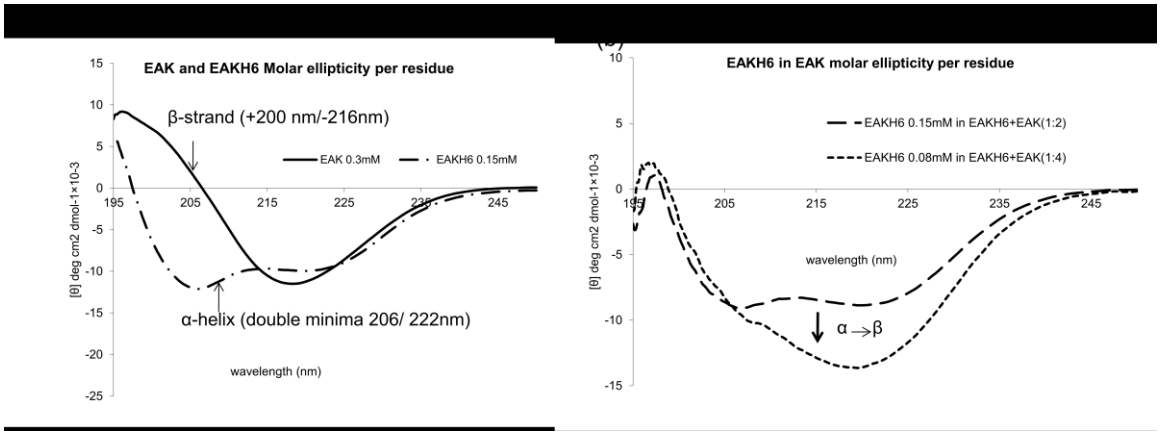

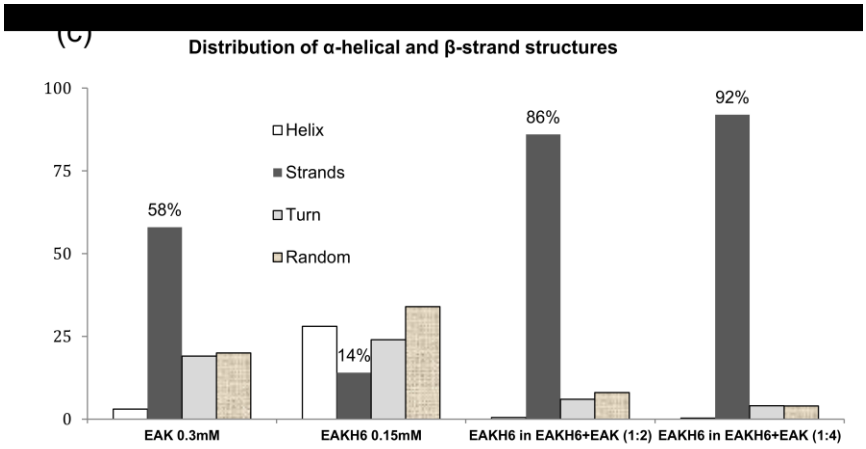

Figure 4-5: Conformational analysis of EAK and EAKH6. Spectra of EAK and EAKH6 in solution by itself (a) and net contribution of EAKH6 in the presence of EAK (b). Relative fractions of secondary structures in each were de-convoluted using CDPro (c). Data shown represents two independent experiments conducted.

the wavelength range and the nature of the sample peptides, native or denatured. Otherwise, a reference set with the largest number of proteins should normally be chosen.[98, 99] Therefore, the secondary structure fractions analysis used a 43 soluble protein set, in which the work of Johnson et al., Keiderling et al., Yang et al., and Sreerama et al., was combined. [100-103]

EAKH6 would most likely retain its helical conformation if it merely adsorbs onto the EAK structure. The CD analysis, however, reveals that EAKH6 undergoes α→β conformational change in the presence of EAK. The most likely cause for this change is that EAKH6 is integrated into the β-sheet stacks of EAK, forming complementary hydrophilic and hydrophobic interactions among glutamate/lysine and alanine, respectively.

The results further suggest that the higher the mole ratio of EAK to EAKH6, the more β-strand fraction in EAKH6. A possible explanation could be EAKH6 is much more dispersed in the matrix of EAK at higher mole ratio, and is forced to line up with the β-sheets by the surrounding EAK molecules. Based upon the β fraction of EAKH6 at various mixing ratio (figure 4-5b), a mole ratio of 1:4 (EAKH6 to EAK) is sufficient to obtain almost 100% of the added EAKH6 integrated into the β-sheets of EAK.

It is likely that only the amphiphilic domain $(AEAEAKAK)_2$ of EAKH6 intercalated into the β-sheets, with the non-complementary H6 domain extending from the EAK-EAKH6 assembly. To prove this, an evaluation of the accessibility of H6 domain in EAK-EAKH6 composite is required.

EAK-EAKH6 composite displays H6 domains

A biochemical assay based on the enzymatic reaction of nickel conjugated horseradish peroxidase (HRP-Ni) was performed to determine the accessibility of H6 domains in the EAK-EAKH6 composite. HRP is an efficient enzyme which converts the substrate 3,3',5,5' tetramethylbenzidine (TMB) into two-electron oxidation product, diimine, with the Km~3.6μM.[104] The reaction rate is coupled to colorimetric change.[104] Through nickel coordination HRP-Ni can bind to the histidines specifically.[105] The assay was performed by incubating HRP-Ni with the assemblies. EAKH6 integrated into the EAK assembly should display the non-complementary H6 domains for binding with HRP-Ni. Assembly associated HRP-Ni can be removed by centrifugation (16,000×g) and filtration (0.22μm) from solution in which unbound HRP-Ni would remain. The amount of unbound HRP-Ni remained in the solution was quantified by the catalysis of TMB manifested in chromogenic change measured (λ=450nm). The amounts of free HRP-Ni were then calculated according to a standard curve relating observed optical density to known concentrations of HRP-Ni. The results are summarized in figure 4-6. The concentration of HRP-Ni in EAK-EAKH6 group was found significantly lower than the other groups by ANOVA and Tukey's multiple comparison tests, which suggested most of the HRP-Ni bound to the composite.

Results are normalized to samples HRP-Ni processed without any peptides, which represent the maximal possible amount of the enzyme remained in solution. Only 7.8±4.5% of the added HRP-Ni remained in the supernatant of EAK-EAKH6 composite. 89.5±13.3% and 83.1±15.0% of HRP-Ni were found unbound in the supernatant of pure EAK and pure EAKH6, respectively. Therefore, it can be deduced that approximately at

least 90% of the HRP-Ni bound to H6 domains in the assembly and was removed from solution by centrifugation. Although EAK formed the assembly and was centrifuged and filtered removed, HRP-Ni remained in the filtrate because it does not bind to EAK. It is possible that HRP-Ni could bind to EAKH6, but these complexes are likely low molecular weight species and therefore passed through the filtration step. Hence, the disappearance of HRP-Ni from the supernatant of EAK-EAKH6 is caused neither by non-specific adsorption to the assembly, nor by complexation with free EAKH6. Taken together, these results add to the evidence of integration of EAKH6 into EAK and that the composite display solvent accessible H6 domain. These H6 domains extruding from the EAK-EAKH6 composite can be recognized by reactive agents, thus work as mounting sites to modify the peptide assembly.

Additionally, these results were repeated for samples taken from the supernatant with the EAK-EAKH6 formed and incubated at 37 °C, 5% CO_2 for days, figure 4-6 c. The H6 domain was thus demonstrated to be stable in EAK-EAKH6 structure over one week.

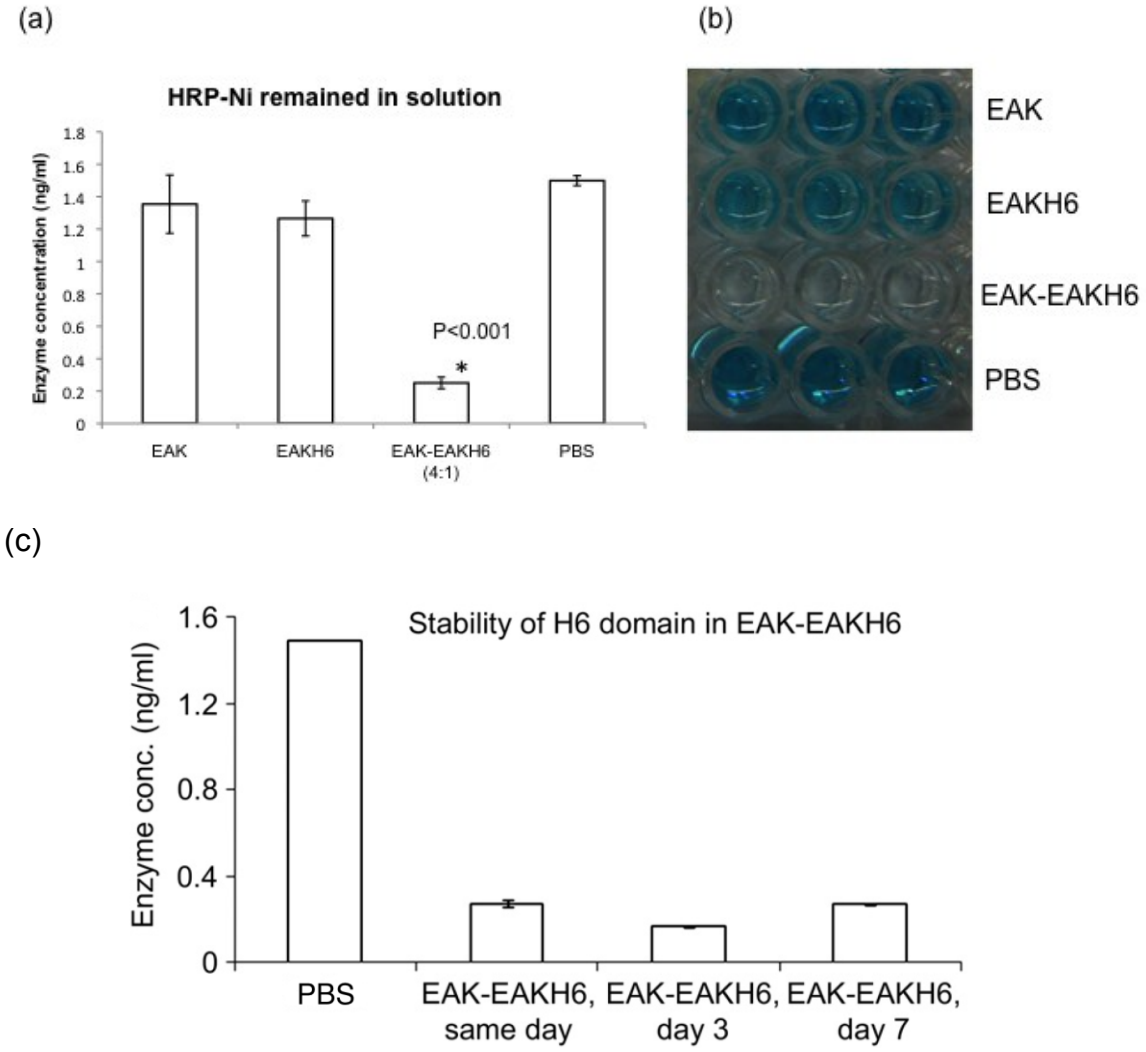

Figure 4-6: Probing H6 domains in EAK-EAKH6 composite. Peptide structures formed in PBS were incubated with HRP-Ni for 60 min at 4°C. Samples were then collected by centrifugation (16,000×g) and filtered (0.22μm) to remove residual aggregates. The amount of HRP-Ni remained in the filtrates (i.e. not bound to the structure) was quantified using a colorimetric method with TMB as the substrate (with reaction terminated with H_2SO_4, λ=450nm). (a) Concentrations of the enzyme were determined using a standard curve (range: 0.125 ng/ml to 8 ng/ml) reflecting a linear function: y=1.04x-0.15(r^2=0.98). Differences among EAK-EAKH6 and EAK, EAKH6 and PBS were statistically significant (*p<0.001, n=3) based on ANOVA and Tukey's Multiple Comparison Test (α=0.05). (b) Color contrasts among and absence of aggregates in the samples. Samples with HRP-Ni added to buffered saline without EAK or EAKH6 were included to reflect maximal enzyme recovery. (c) shows the stability of H6 function in the composite kept in PBS at 37°C and 5% CO_2 over seven days.

SUMMARY AND CONCLUSIONS

To transform the EAK β-sheet network into a structure for antibody immobilization a versatile mounting mechanism is needed. To this end, a modified EAK peptide with six histidines (H6) appended at the C-terminal was used to introduce mounting sites. H6 domains can be recognized by anti-poly-histidine (anti-H6) antibodies and interact with metals such as nickel and cobalt through coordination bonds. The modified peptide, referred hereafter as "EAKH6", was designed on the basis that the amphiphilic domain $[AEAEAKAK]_2$ intercalates into the crossed β-sheets of EAK to form a composite in which the H6 domains freely accessible. The assumption is that the histidine appendage does not interfere with the ability of the amphiphilic domain to engage the same in EAK oligomers. The integration of EAKH6 in the EAK structures was examined using UV-Vis FTIR, CD and a biochemical assay (HRP-Ni). FTIR spectra clearly show the presence of imidazole ring in the EAK-EAKH6 composite. In the presence of EAK, EAKH6 undergoes a distinct conformational change, from α-helix to β-strand. A biochemical assay based on the enzymatic reaction of HRP-Ni was performed to determine the accessibility of H6 domains in the EAK-EAKH6 composite. Results from this study show that the EAK-EAKH6 composite can capture up to 90% of the metal-enzyme conjugate, thus proving the functional property of H6 domains. Collective interpretation of the results in the aforementioned studies confirms the integration of EAKH6 into EAK assembly and that the associated H6 domains are accessible.

CHAPTER 5

FUNCTIONALIZATION OF EAK-EAKH6 COMPOSITE WITH PROTEIN A/G AS THE ADAPTOR

INTRODUCTION

Results described in the previous chapter demonstrate that H6 domain can be introduced into the peptide assembly by the integration of EAKH6. H6 associated with the assembly can be recognized by anti-H6 antibodies and interact with the divalent metal nickel. In the current chapter, results will be shown to demonstrate the functionalization of the EAK-EAKH6 assembly via the H6 domain. Specifically, IgG molecules will be mounted onto the insoluble structure such that the (capture) antibodies are displayed and clustered. To this end, a linker is needed to connect the capture antibody and H6 domains of the assembly. Protein A/G, which contains six Fc-binding sites for immunoglobulins, will be used to form the construct on which IgG molecules can be concentrated for the purpose of binding cells or soluble molecules.

Protein A/G is a recombinant fusion protein with six Fc-binding domains combined: four from protein A and two from protein G.[106] Protein A is a cell wall component produced by several strains of *Staphylococcus aureus*. It consists of a single polypeptide chain with M.W 42,000Da with four high-affinity ($K_a=10^8$/mole) binding sites capable of interacting with the Fc region of IgG structures. Maximal interaction occurs at pH8.2, although good binding takes place at neutral or physiological conditions (pH 7.0-7.6) (figure 5-1 a).[107, 108] Protein G is also a bacterial cell wall protein isolated from group G Streptococci. Native protein G contains two Fc-binding sites, as well as albumin and cell

surface interacting domains. In the recombinant form, the albumin and cell surface binding domains are eliminated to reduce nonspecific interactions. It has been reported that most mammalian immunoglobulins bind with greater affinity to protein G than protein A. Maximal binding occurs at pH 5, although good interaction is observed at pH 7.0-7.2.[109-111] Recombinant DNA of Fc-binding domains of protein A and protein G results in a chimeric protein with broader binding activity than either protein A or protein G alone. Recombinant protein A/G (hereafter referred to as rpAG) thus binds to all human and mouse IgG subclasses. Binding of rpAG is also less pH-dependent, with good interaction in the pH range between 5 and 8 (figure 5-1 a). [106]

By taking advantage of the Fc-binding capability of rpAG, a bi-functional complex was designed by coating rpAG with both the capture antibody and an anti-H6 antibody. The EAK-EAKH6 assembly is thus functionalized via its H6 domains through anti-H6 antibodies (figure 5-1 c). IgG is a "Y"-shaped macromolecule, with typical molecular weight greater than 150KDa. The structure consists of three distinct domains. Limited digestion with the protease papain cleaves antibody molecules into three fragments, yielding two identical fragments termed the Fab (i.e. fragment antigen binding) and the Fc fragment. The Fc domain plays an important role in the functions of antibodies by activating the complement pathway, or recruit cytolytic effects of phagocytes and natural killer cells via Fc receptors.[4, 112] Such structural configuration and functional segregation allows one to use Fc as an anchoring site to display Fab for binding antigens, as demonstrated in the studies to be described in the following chapter.

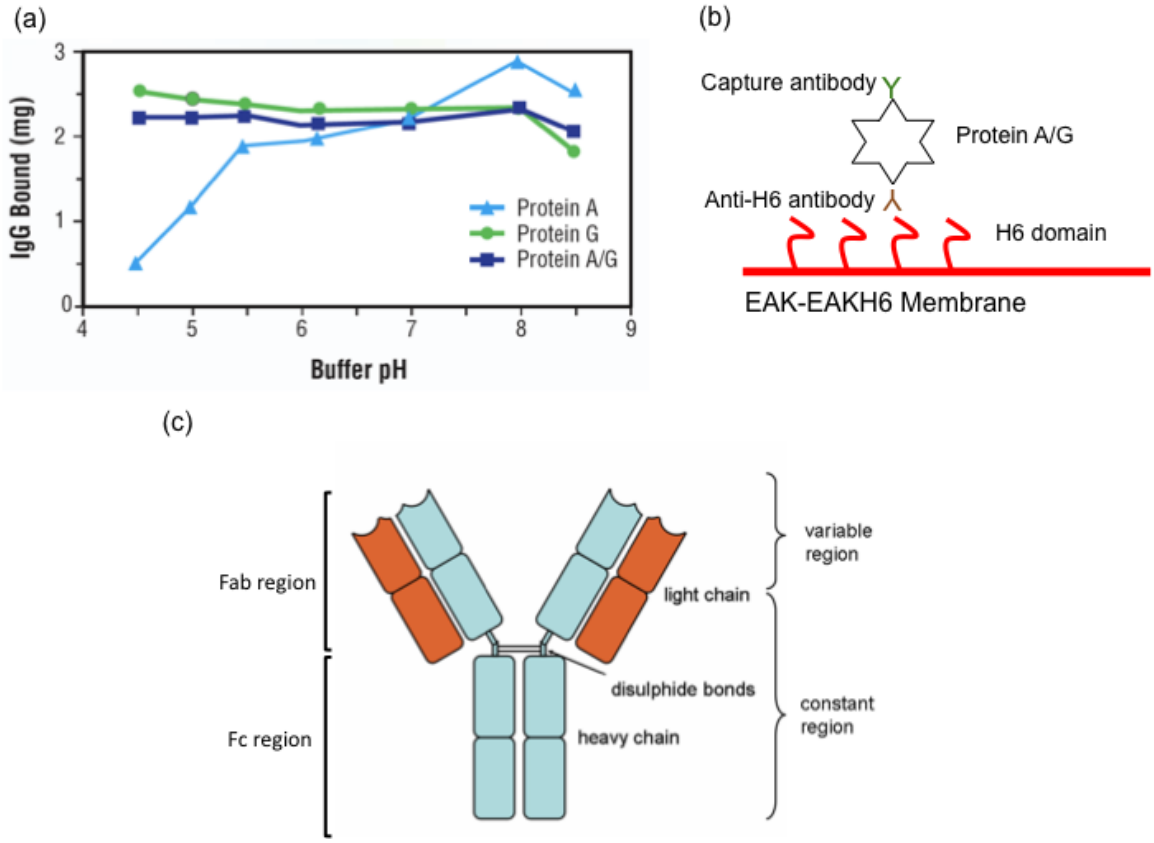

Figure 5-1: Protein A/G and antibody. (a) Comparison of the binding characteristics of mouse IgG at various buffer pH levels. Reprinted by permission from International Scientific Communications (ISC): [American Biotechnology Laboratory] (Vol.7 Page 42), 1989. (b) Schematic of using protein A/G as the adaptor to mount the capture antibody to EAK-EAKH6. (c) Structure of an IgG and its fragments. Reprinted with permission from © 2005 Grand Sciences Publishing: [Immunobiology] (6th edition, Page17).

MATERIALS AND METHODS

Protein A/G and antibodies

rpAG was obtained from Pierce (Rockford, IL, USA). This protein was expressed in Bacillus and secreted into the surrounding medium during fermentation. It was supplied as salt-free lyophilized powder. Upon receiving, it was reconstituted into a stock concentration of 2.5mg/ml in sterile deionized water, and stored as aliquots of 50µl in the freezer (-80°C) until use. The strong binding affinity of rpAG to mouse and rabbit IgG subclasses has been proved. Rabbit anti-H6 polyclonal antibody was obtained from AnaSpec, Inc (San Jose, CA, USA). This antibody was affinity purified and supplied as 0.2mg/ml solution in PBS (pH 7.4) with 0.2% bovine serum albumin (BSA) and 0.05% sodium azide. It was stored in the refrigerator (4 °C) until use. Fluorescein isothiocyanate (FITC) conjugated anti-mouse CD8a antibody was obtained from BD Biosciences (San Jose, CA, USA). This fluorescent antibody was provided as 0.5mg/ml in aqueous buffered solution containing ≤0.09% sodium azide. Up on arrival it was stored in the refrigerator (4 °C) and protected from exposure to light。

Loading antibodies onto EAK-EAKH6 assembly

The complexes of rpAG and antibodies were prepared by incubating the antibodies with rpAG. 0.1µg rpAG was coated with 1µg anti-H6 antibody first (molar ratio 1:3). The capture antibody, anti-CD8a antibody, 1µg (mole ratio of rpAG to anti-CD8a 1:3) was then added to make the complexes. Thus the six Fc binding sites of a rpAG were saturated, and each molecule of rpAG carried both anti-His6 and anti-CD8a antibodies. A FITC conjugated anti-CD8a antibody was used for the purpose of confocal analysis. The

complexes were then mixed with peptides solution, and the mixture solution was injected into 1ml PBS containing 10% fetal bovine serum (FBS) to initiate the insoluble structure forming. FBS was added here to minimize the nonspecific binding. Aggregates were mounted onto slides for confocal analysis.

Preparation of primary murine splenocytes suspension

Six to eight weeks old female (certified virus free) C57BL/6 mice were purchased from Charles River Laboratories International Inc. (Wilmington, MA, USA) and housed in the Duquesne University Animal Care Facility. All experimentation was handled in accordance with institutional animal care policy. To obtain primary murine splenocytes, the spleen was removed from the mouse, and grinded in 5 ml Rosewell Park Memorial Institute (RPMI) medium (HyClone Laboratories, Inc. Logan, UT, USA) containing 10% heat-inactivated fetal bovine serum (FBS) (HyClone), 50 μM 2-mercaptoethanol (Acros Organics, Geel, Belgium), 1% antibiotics (penicillin/streptomycin) (Lonza Walkersville, Inc. Walkersville, MD, USA). The cells were then spun down and resuspended in ACK lysis buffer followed by incubation in ice for 5 min to remove red blood cells. After that, the splenocytes were purified by passing through a nylon mesh (70 micron pore size), washed and suspended in PBS containing 10% FBS to the final concentration of 1×10^6 cells /ml.

Apply splenocytes to antibody mounted EAK-EAKH6 assembly

The anti-CD4 antibody mounted EAK-EAKH6 assemblies were formed as described above in 6-well plate containing 2 ml complete RPMI (10% FBS and 1% antibiotics included) in each well. Assembly formed with EAK alone with everything else was

included as a control. 2ml murine splenocytes suspension (1×10^6 cells/ml) in complete RPMI medium was applied to each well to achieve a final concentration of 0.5×10^6 cells/ml. The plate was then incubated at 37°C for 24 hours. The peptide assemblies were then imaged for investigation of their integrity.

Microscopic imaging

Peptide assemblies with cell captured were mounted onto microscope slides with ProLong Gold antifade reagent (Invitrogen, OR, USA). A Zeiss AxioObserver Z1 inverted microscope (Carl Zeiss MicroImaging GmbH, Germany) was used to collect imaging data. The microscope is equipped with digital image correlation (DIC) capability illuminated by 100w bright-field and 300w liquid light-guide channeled Xenon light sources for white light and fluorescence wide-field observation. The bright-field images and fluorescent images are captured by QImaging MicroPublisher 22159 digital CCD color microscope camera and high-sensitivity Hamamatsu C9100-02 electron multiplier CCD camera, respectively. The images were analyzed using a SimplePCI imaging software program (Hamamatsu Corporation, Sewickley, PA, USA).

RESULTS AND DISCUSSION

The objective of this study was to determine the ability of EAK-EAKH6 assembly to display a specific antibody via rpAG as the adapter, building upon the work described in chapter 4, which shows the presence and accessibility of H6 domains in the EAK-EAKH6 assembly. In this study, a fluorescent conjugated antibody was used for detecting its association with the peptide assembly.

Immobilization of FITC conjugated antibodies on EAK-EAKH6 assembly

Capture antibodies were immobilized on EAK-EAKH6 assembly by using rpAG as the adapter. rpAG (22 pmol) was coated with anti-H6 (67 pmol) and the capture antibody (67 pmol), resulting in mole ratio of 1:3:3 (rpAG to antibodies) (table 5-1). Thus, all six Fc binding sites on rpAG should be saturated. The now bi-specific rpAG was then mixed with EAK and EAKH6 (dissolved in water), and injected into a volume of PBS containing 10% serum. The ability of the adaptor to concentrate antibodies on EAK-EAKH6 was first tested using rpAG equilibrated with an anti-H6 antibody and a fluorescent (FITC)-conjugated anti-CD8a IgG.

rpAG complexed with the antibodies mixed with EAK-EAKH6 showed concentrated fluorescence (figure 5-2), while only a low level of fluorescence was observed when the antibody was complexed with the EAK assembly. These results indicate for the immobilization of the anti-CD8a antibody on the EAK-EAKH6 assembly. The assembly prepared with EAK only did not concentrate the antibody, suggesting a lack of interaction between the rpAG complex with the structure. When kept in serum containing PBS at

4°C for one week, the EAK-EAKH6/antibody construct remained intact, as evidenced by the fluorescence observed on day 7 of incubation (figure 5-2).

These data are consistent with the interpretation of the analytical results described in Chapter 4. In particular, the presence of functional H6 domains in the EAK-EAKH6 assembly is reinforced. In addition, the current data confirm the feasibility of the design of using anti-H6 antibody coated rpAG to mount capture antibodies onto the assembly. Furthermore, in the presence of serum proteins, which saturated the non-specific binding sites, the complex did not bind to EAK assembly. One can therefore assume that the H6 domains are indispensable for loading the FITC-conjugated antibodies.

	M.W	*Stock Conc.*	*Total mass used for the construct*	*Moles used for the construct*	*Mole Ratio*
rpAG	50kDa	0.25μg/μl	1.1μg	2.2×10^{-11}	1
Anti-H6 antibody	150kDa	0.2 μg/μl	10μg	6.7×10^{-11}	3
FITC-anti-CD8a antibody	150kDa	0.5 μg/μl	10μg	6.7×10^{-11}	3
EAKH6	2479.7	7.8 μg/μl	78μg	3145.5×10^{-11}	1430
EAK	1656.2	5μg/μl	200μg	12075.8×10^{-11}	5489

Table 5-1: Stoichiometry of rpAG, antibodies and peptides. Peptides assembly was formed by EAK and EAKH6 at mole ratio of (4:1). The six Fc binding sites of rpAG were saturated by anti-H6 and anti-CD8a antibodies, both at the mole ratio of 1:3 (rpAG to antibody). The mole ratio of EAKH6 to anti-His6 antibody is about 500:1 to ensure there are plenty of H6 domains to bind with.

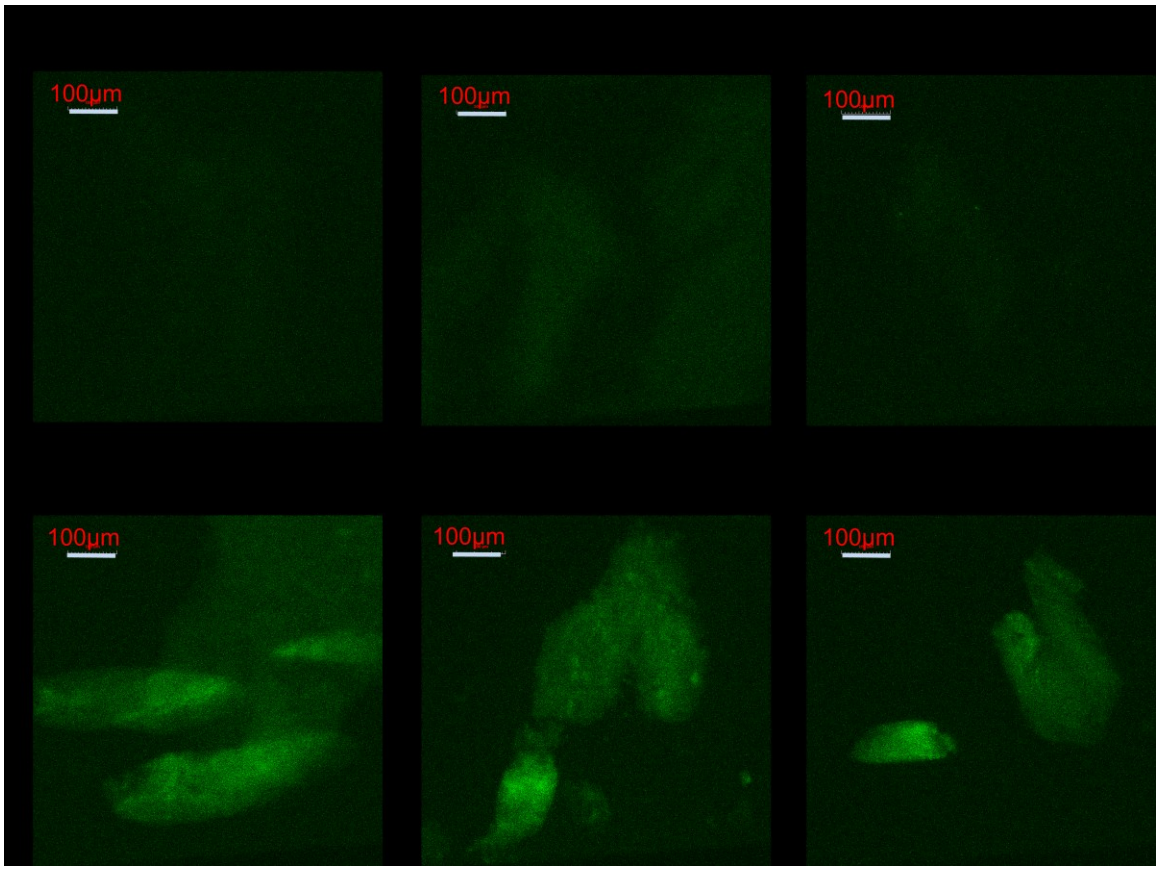

Figure 5-2: Displaying IgG molecules on (a) EAK and (b) EAK-EAKH6. (a1), (b1) incubated in serum containing PBS for 24 hours; (a2), (b2) incubated for 5days; (a3), (b3) incubated for 7days. Peptide structures were mounted with rpAG equilibrated with rabbit anti-H6 Ab and a fluorescein-conjugated IgG with a molar ratio of 1:3:3 such that all six Fc binding sites on protein A/G are occupied by either antibody. Bovine sera (10% v/v) were included to minimize non-specific binding. The peptide structures were transferred to glass slides and analyzed using a Zeiss AxioObserver microscope (operating the SimplePCI imaging software). Images shown are representative of two independent experiments conducted.

As stated above, each rpAG molecule has six Fc-binding sites for antibody. In order to use rpAG as the adaptor to bridge the capture antibody to the EAK-EAKH6 assembly, every rpAG molecule carrying the capture antibody must have at least one anti-H6 antibody attached as well. To achieve this goal, rpAG was coated with anti-H6 antibodies at the mole ratio of 1:3 as the first step in the process of making the constructs. By this way, half of the antibody-binding sites in rpAG molecules were occupied and the other half remained available for the capture antibody. The assumption is that anti-H6 antibody molecules added are evenly equilibrated with rpAG. This strategy was validated by the results showed in figure 5-2.

The results in figure 5-2 support the use of rpAG-antibody complex to mount capture antibody onto EAK-EAKH6 assembly. However, it is possible that the capture antibodies lose their biological activities during the process. They could form aggregates, be denatured, or the antigen-binding sites be covered by other components of the assembly. Thus it is important to test the bio-function of the antibodies after they are mounted onto EAK-EAKH6 assembly. Further studies will be conducted to test the ability of peptide-antibody construct to capture cells.

Cellular compatibility of EAK-EAKH6 assembly

Materials developed as injectables or implants must be compatible with cells. As a preliminary study, the integrity of the EAK-EAKH6 structure was examined when co-cultured with leukocytes. Primary murine splenocytes suspended in complete RPMI medium were applied to mouse IgG mounted EAK-EAKH6 assembly. The samples were incubated at 37°C for 24 hours.

The peptide assemblies were examined before and after incubated with cells, as shown in figure 5-3. A group of peptide-IgG constructs formed in medium without any cells was included as a control. As the images showed, overall integrity of the peptide assembly remained largely the same after 24 hours culture with mouse spleen cells. The accumulation of cells metabolites did not impact the β-sheet structures. No apparent effects were seen from accumulation of carbonic and lactic acids released from metabolic active cells. Components in animal (bovine) serum, including peptidases and proteases appeared inert against the structure. Thus the results suggest that EAK-EAKH6 composite can reasonably sustain typical environment of living systems. It should be noted that the issue of biological compatibility require long-term in vivo studies beyond the scope of this work.

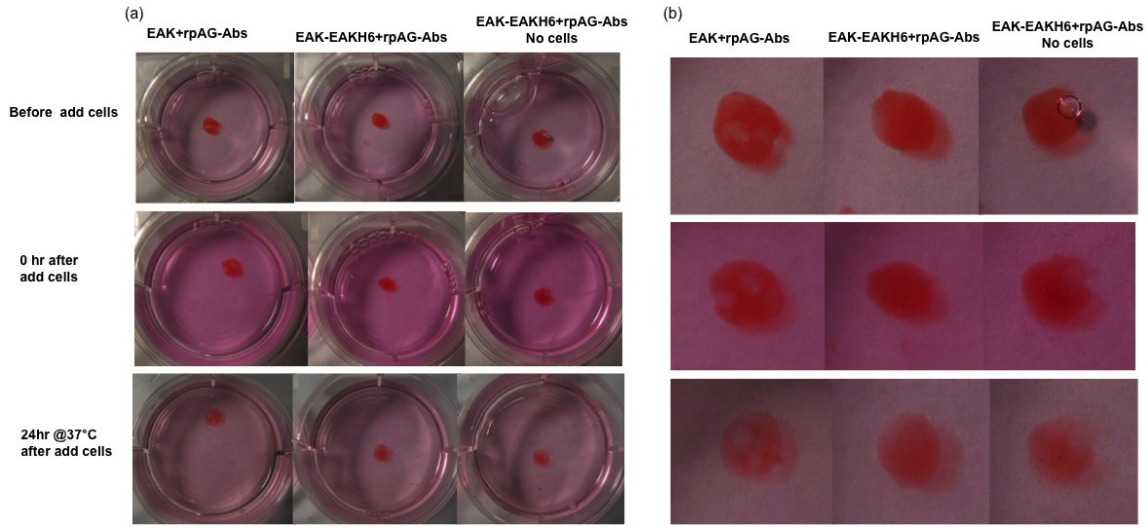

Figure 5-3: Cell compatibility of EAK-EAKH6 IgG construct. (a) Images of peptide assemblies in the cell culture wells. Primary mouse splenocytes were applied with complete RPMI medium containing 10% FBS and 1% antibiotics. (b) Zoomed in (digitally magnified) images.

Concentration of IgG in vivo via EAK-EAKH6

The ability of the construct to assemble *in vivo* was examined in a preliminary study. A solution of EAK and EAKH6 dissolved in deionized water mixed with rpAG equilibrated with an anti-H6 antibody and IgG (conjugated with the PE dye) was injected subcutaneously next to B16 tumors established in living animals (figure 5-4 a). Mice received the injection were allowed to move freely in their cage and euthanized on the next day, with the tumors and the adjacent tissues excised for analysis. The subcutaneous small tumor was used as a reference point for *ex vivo* identification of the injection site.

All mice injected with the complex were found to behave normally, with no unusual eating, drinking or grooming activities observed. Care was taken to preserve the tissue integrity when tumors were excised. The insoluble EAK-EAKH6 structure could be observed with Congo red staining (figure 5-4 b). Figure 5-4 c and d represent bright-field image and xenon wide-field image of a same region of the recovered peptide assembly, respectively. Observed was an area with significant red fluorescence, which could only come from the PE-conjugated IgG molecules, injected with the EAK-EAKH6 assembly. The locale of the fluorescence is in the same vicinity of the injection site. In contrast, when IgG-PE was injected without the peptide assembly at a tumor established on the opposite flank in the same mouse, no fluorescence could be detected (Figure 5-5). These results indicate that free IgG administered in vivo failed to remain at the site of injection but congregated when injected with EAK-EAKH6 and rpAG (anti-H6). Based on these data, it can be concluded that EAK-EAKH6 serves to form His-tag displaying assemblies *in vivo*. Concentration of antibody sustains for at least 24 h *in vivo* in the subcutaneous space.

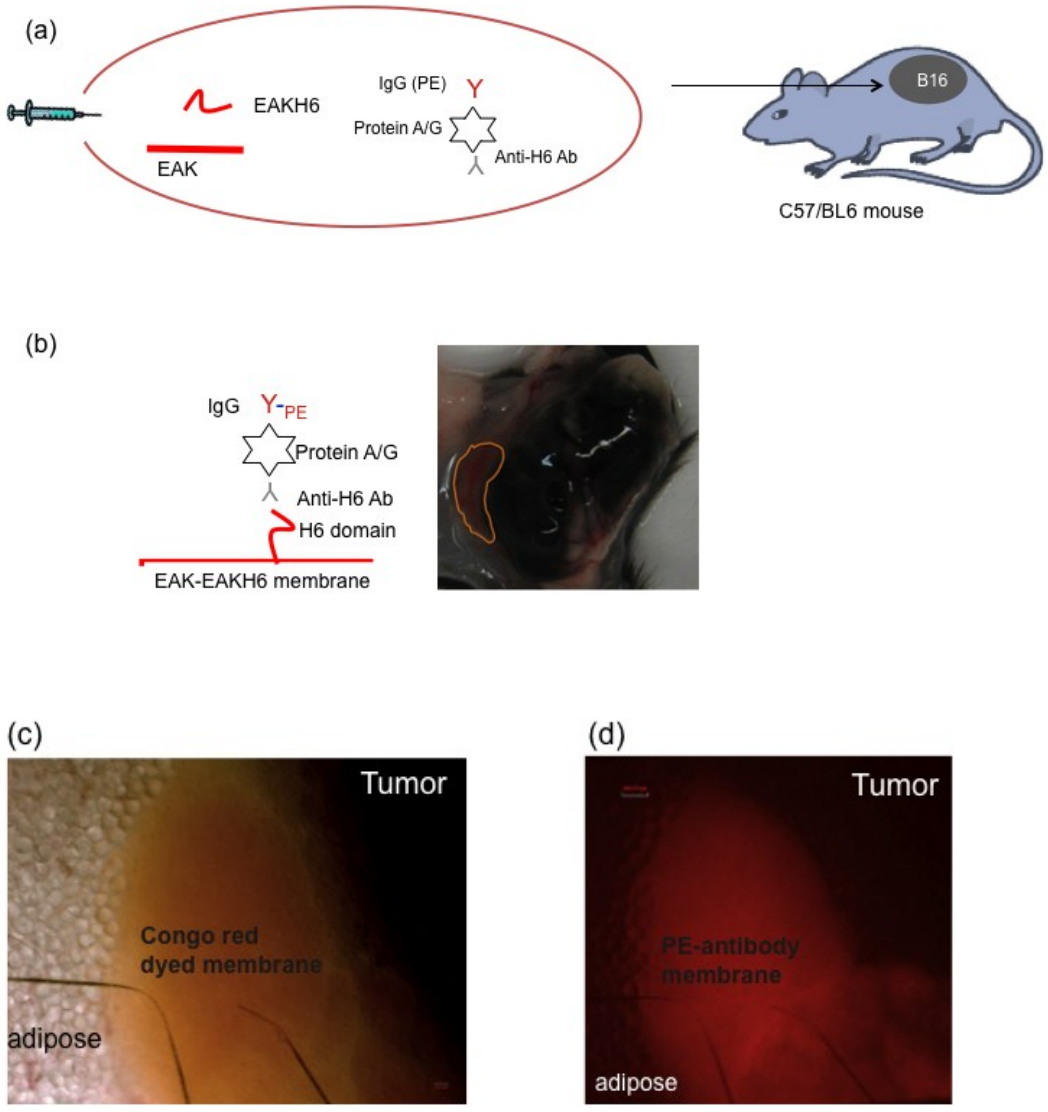

Figure 5-4: Self-assembly of EAK-EAKH6 in vivo. (a) A solution containing EAK, EAKH6, rpAG equilibrated with anti-H6 antibody and a IgG conjugated with the red fluorescent dye (PE) was injected subcutaneously adjacent to a B16 tumor (~3 mm in diameter) established in a C57BL6 mouse. (b) After 24 h, the area (the tumor and surrounding tissues) was excised and imaged. (c) Bright-field image showing the outline of the membrane; (d) Xenon wide-field image showing the red fluorescence concentration in the membrane.

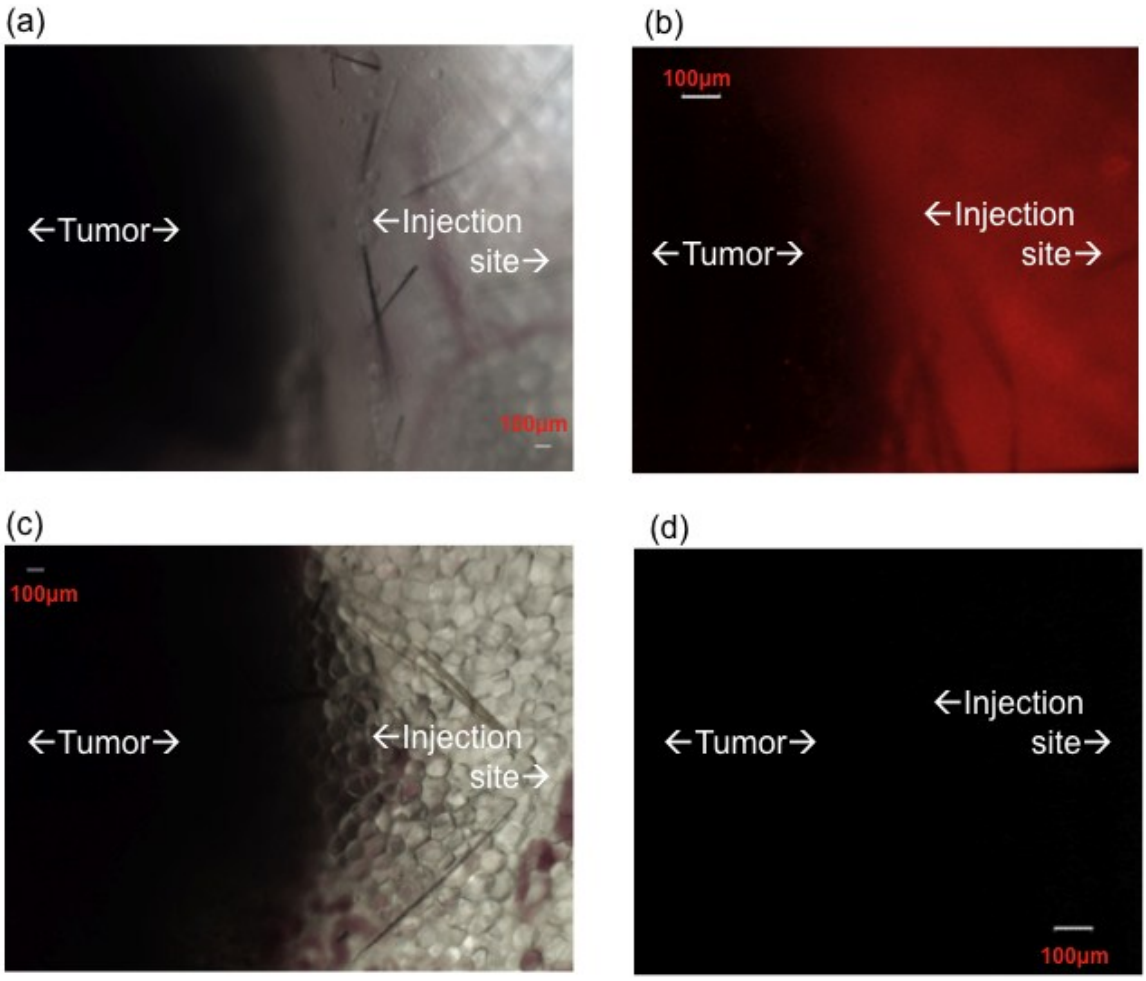

Figure 5-5: Fluorescence conjugated anti-mouse IgG concentrated with peptide assembly in vivo. (a), (b) PE-IgG complexed with rpAG and anti-H6 was injected with EAK-EAKH6 composite. (c), (d) same amount of PE-IgG was injected by itself. (a) and (c) are bright-field images of the injection sites next to the tumors. (b) and (d) are xenon sourced wide-field images of the fluoresce. . No fluorescence was detectable when IgG-PE was injected by itself at a tumor established on the opposite flank in the same mouse.

Immunohistochemical analysis of self-assembling peptides injected *in vivo* did not show overt inflammation.[68] Although these results suggest that self-assembling peptides are non-immunogenic, studies testing long-term immunogenicity *in vivo* have still to be performed. rpAG and the antibodies could dissociate and phagocytosed by APCs, but the high-affinity interactions render this unlikely. The generation of neutralizing antibodies against rpAG and/or the antibodies could occur in 10-14 days after digestion by APCs, but in the absence of adjuvant, these entities should elicit only weak and short-lived IgG or IgM responses. The use of humanized antibodies should reduce the overall immunogenicity of the constructs. Protein A has also been used in immunoadsorption treatments (apheresis) for rheumatoid arthritis and dilated cardiomyopathy (ClinicalTrials.gov Identifier NCT00558584). The incidence of adverse events, mainly vasculitis, is low. [113] A Phase I clinical study of administering staphylococcal protein A (PRTX-100) directly into healthy volunteers has been completed (ClinicalTrials.gov Identifier NCT00517855). The lack of safety concerns drove the initiation of an ongoing trial studying the effects of multiple doses of staphylococcal protein A in adult patients with idiopathic thrombocytopenia purpura (ITP) in Australia (ClinicalTrials.gov Identifier NCT00571467). These examples of clinical usage suggest an acceptable level of biocompatibility of rpAG.

SUMMARY AND CONCLUSIONS

The studies described in this chapter have implications for the applicability of the system. The data show that IgG molecules can be concentrated via rpAG-antibody complex directed toward H6 domains. This observation opens the possibility of a system that can interact with cells and soluble molecules in a specific manner. Building upon the data showing spontaneous integration and assembly of EAKH6 into EAK, the *in vivo* experiments demonstrates a similar process can take place in the subcutaneous space. The system proves to be amenable as an injectable material. A solution of EAK, EAKH6, rpAG, anti-H6 antibody and IgG-PE injected subcutaneously assembled to concentrate the fluorescent antibody at the injection site for at least 24 h. Presumably, the triggering stimulus is the salt in the physiological environment. This stimuli-responsive nature of EAK-EAKH6 is particularly useful. Because the crossed β-sheets insoluble structure forms only in the presence of metal ions, the components of the construct can be kept as a soluble system, allowing injecting through regular syringes, without the need for surgical placement often required in the use of implanted drug delivery devices. Importantly, complexation of rpAG with the antibodies remained intact during the injection, sustaining the shear stress applied through the needle ($25^{5/8}$G). Taken together, the data support the notion that EAK-EAKH6 can be used as a platform for displaying antibodies *in vivo*. Ultimately, I envision the design may change how therapeutic antibodies are used and delivered in man.

CHAPTER 6

CAPTURE OF LEUKOCYTE SUBSETS IN FUNCTIONALIZED EAK-EAKH6 COMPOSITE

INTRODUCTION

Recent evidence has demonstrated that Treg cell-mediated immunosuppression is one of the crucial mechanisms of unsuccessful tumor immunotherapy. Approaches to physically deplete or functionally inactivate Treg cells have been developed to reverse the tumor induced Treg cell expansion.[40, 42] Anti-Treg mAb can be used to deplete the cells through antibody-dependent cellular cytotoxicity (ADCC) or block signaling through surface receptors. The depleting anti-CD4 and CD25 have been tested in mice with some success, and the signal modulators anti-CTLA4[7] and anti-GITR[54] have shown promise. Several of these, including daclizumab (anti-CD25), and ipilimumab (anti-CTLA4) are being tested in humans. A common feature from the results of the clinical trials is autoimmune syndrome such as thyroditis (daclizumab) and colitis (CTLA-4).[40, 42] Thus a more specific therapeutic strategy is required to prevent high-dose and sustained therapy in refractory diseases. Another possible reason for the poor clinical efficacy is that although the level of Treg cells is increased in tumor microenviornment, the number of lymphocytes is still not comparable to tumor cells. The tumor infiltrated lymphocytes were found to be <0.5% of the entire tumor cellularity.[41] Given these, it is envisioned that a localized delivery system that enhance the functions of the aforementioned anti-Treg antibodies could be decisive as adjuvant in tumor immunotherapy. The EAK-EAKH6 structure characterized could be a potential carrier of the antibodies. The objective of the research in this chapter was to determine the ability

of EAK-EAKH6 assembly to trap T cells specifically *in vitro* via mounted surface molecule specific antibodies. Achieving this milestone will provide an initial assessment of EAK-EAKH6-antibody construct as a viable platform for engaging specific subset of T cells *in vivo*. The rationale is that the selective and multiple binding between the surface molecules and the antibodies displayed by EAK-EAKH6 should render a particular type of T cells immobilized onto the peptide assembly. Anti-CD4 antibody was used in the experiments to trap Treg cells. The level of Foxp3 expression was monitored in the lymphocyte population since Foxp3 is the most distinctive marker for the regulatory lineage.[114]

MATERIALS AND METHODS

Apply murine splenocytes to constructed anti-CD4 antibody mounted EAK-EAKH6 composite

The purified unlabeled rat anti-mouse CD4 antibody, 0.5mg in 1.0ml of 100mM borate buffered saline (pH 8.2), was purchased from SouthernBiotech (AL, USA). rpAG was complexed with rabbit anti-H6 antibody and rat anti-mouse CD4 antibody at the mole ratio 1:3:3 as described in chapter 5. The rpAG-antibody complexes and EAK, EKAH6 in water were then injected into 600µl serum containing PBS holded in BD Falcon^{TM} cell culture inserts (BD Biosciences, NJ, USA) with polyethylene terepthlate (PET) membrane (8.0 µm pore size) accompanied by BD Falcon^{TM} cell culture insert companion 24 well plate. The membrane insert made possible removal of residual peptides and antibodies through repeated washing steps. Murine lymphocytes were obtained from the spleen of a female C57BL/6 with late stage of melanoma, and made into lymphocytes suspension, as described in chapter5, in PBS containing 10% FBS to a concentration of 2×10^6 cells per ml. 2×10^6 cells were then applied to each well, and gently shake for 1 hour at 4°C. The unbound cells were rinsed away by serum containing PBS. This process was repeated for 4 times. The peptide assemblies with cell captured were stained with FITC conjugated rat anti-mouse CD25 antibody (SouthernBiotech, AL, USA), 2µg antibody per well, and mounted onto microscope slides for microscopy analysis. Unbound cells were collected for semi-quantitative reverse transcription polymerase chain reaction (RT-PCR). The procedure is illustrated in figure 6-1.

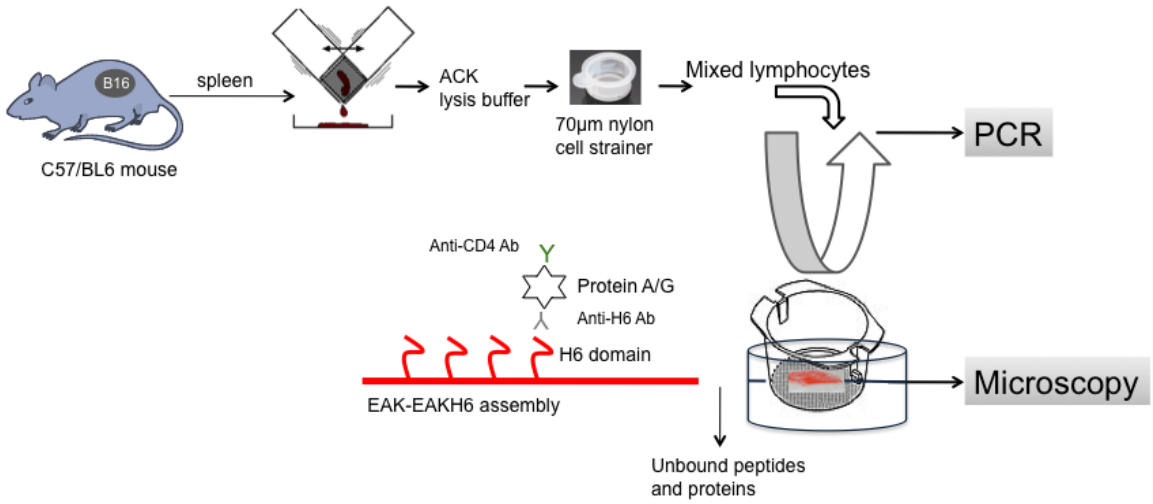

Figure 6-1: Schematic of applying murine splenocytes to anti-CD4 antibody mounted EAK-EAKH6 membrane. Lymphocytes were harvested from the spleen of mice carrying B16 tumors. Single cell suspensions ($2x10^6$ cells/ml), depleted of erythrocytes and monocytes, were placed onto aggregates of EAK and EAK-EAKH6 established on mesh filters (pore size: 8 μm) for 4 h at 4°C. This process was repeated four times. Samples on filters were transferred to glass slides and analyzed under microscope. Unbound cells were collected for PCR analysis.

Microscopic imaging analysis

Peptide assemblies with cell captured were mounted onto microscope slides with ProLong Gold antifade reagent (Invitrogen, OR, USA). A Zeiss AxioObserver Z1 inverted microscope (Carl Zeiss MicroImaging GmbH, Germany) was used to collect imaging data. The microscope is equipped with digital image correlation (DIC) capability illuminated by 100w bright-field and 300w liquid light-guide channeled Xenon light sources for white light and fluorescence wide-field observation. The confocal capability is provided by three acousto-optic tunable filter (AOTF) software-selectable (488/568/647nm) Melles Griot Kr/Ar laser lines fed into a Yokagawa QLC 100 spinning disc confocal head that is capable of analyzing 360 frames/sec. The bright-field images and fluorescent images are captured by QImaging MicroPublisher 22159 digital CCD color microscope camera and high-sensitivity Hamamatsu C9100-02 electron multiplier CCD camera, respectively. The images were analyzed using a SimplePCI imaging software program (Hamamatsu Corporation, Sewickley, PA, USA). The cells were counted by the program of NIH ImageJ.

Semi-quantitative reverse transcription polymerase chain reaction (RT-PCR)

Total RNA of collected unbound cells was isolated using a SV total RNA isolation kit (Promega, WI, USA). The qualities and concentrations of template RNA were investigated by absorbance at 260nm and 280nm using a Beckman DU530 Life Science UV/Vis Spectrometer (Beckman Coulter, Inc., CA, USA). Coupled RT-PCR was performed using Masterscript Kit & Masterscript RT-PCR System (5 PRIME GmbH, Hambrug, Germany) in an Eppendorf MasterCycler (Eppendorf, Hamburg, Germany). 2 μl of primer pairs (one reverse and one forward, 10μM each) specific for Foxp3 and β-

actin (R&D Systems, Minneapolis, MN) were added to 0.1-0.5 μg of RNA sample in a reverse transcription (50 °C for 50 min) step, followed by denaturation (94 °C for 4 min). The amplification steps consisted of 35 cycles of template denaturation (94 °C for 45 s), primer annealing (55 °C for 45 s) and primer elongation (68 °C for 45 s). PCR products were separated in 2% agarose gel, visualized by of ethidium bromide staining, and analyzed using NIH ImageJ.

RESULTS AND DISCUSSION

Evidence of CD25 positive T cells captured by anti-CD4 antibody mounted EAK-EAKH6 composite

The EAK-EAKH6 structure was loaded with an anti-CD4 antibody to test the capacity of the design to capture CD4+ T cells. The construct was exposed to a mixed population of mouse lymphocytes (including CD4, CD8 T cells, B cells and NK cells). These cells were harvested from mice carrying B16 tumors, which have spleen populated with Treg cells. Cell suspensions were applied onto the EAK-EAKH6 anti-CD4 construct formed on polycarbonate mesh filters. Cells bound to the construct were stained with FITC conjugated rat anti-mouse CD25 antibody and examined under microscope.

Bright-field images were captured on the same region at different magnifications. As presented in figure 6-2, a greater extent of cell capture is evident in anti-CD4 antibody mounted EAK-EAKH6 assembly (a1 through a4) compared to that in the EAK aggregate (b1 through b4). Using ImageJ the cell density was estimated to be 200-1000 cells/mm^2 in the EAK-EAKH6 construct, whereas only 10-40 cells/mm^2 were captured by the EAK structure. The micrographs show that cells are not adsorbed randomly at the surface, but are ordered in heterogeneous clusters.

The captured cells in the EAK-EAKH6 structure were examined for their identities. Figure 6-5 shows a representative for two independent experiments indicating that the cells captured in the EAK-EAKH6 construct express CD25. Most likely, the cells are Tregs. This result compliments the findings in the bright-field images to suggest that cells were captured specifically through the antibodies displayed with minimal non-specific cell adsorption to the EAK aggregate.

Taken together, the data show that the design of EAK-EAKH6 and rpAG/anti-H6 can be used to display mAb for purpose of capturing specific cell populations. The structure formed by self-assembling structure with pores of about 5–200 nm have an extremely high water content, >99.9–99.5% or 1–5 mg/ml (w/v).[57] These structures closely mimic the porosity and structure of extra-cellular matrices, which allow tissue cells to reside and migrate in a 3D environment. Hence these peptide scaffolds have been used for 3D cell culture, controlled cell differentiation, tissue engineering, and regenerative medicine applications. However, the non-specific adsorption of cells to the peptide assembly was suggested not to be stress resistible. As figure 6-2 a1-a4 showed, most of the EAK assembly adsorbed cells were washed away. In the meantime, the cells immobilized with anti-CD4 antibodies stayed within the EAK-EAKH6 assembly after washing steps, indicating a stable interaction with the peptide structure. This property is important for *in vivo* application, especially in the tumor microenviorment that has higher perfusion rate and interstitial pressure than normal tissues.

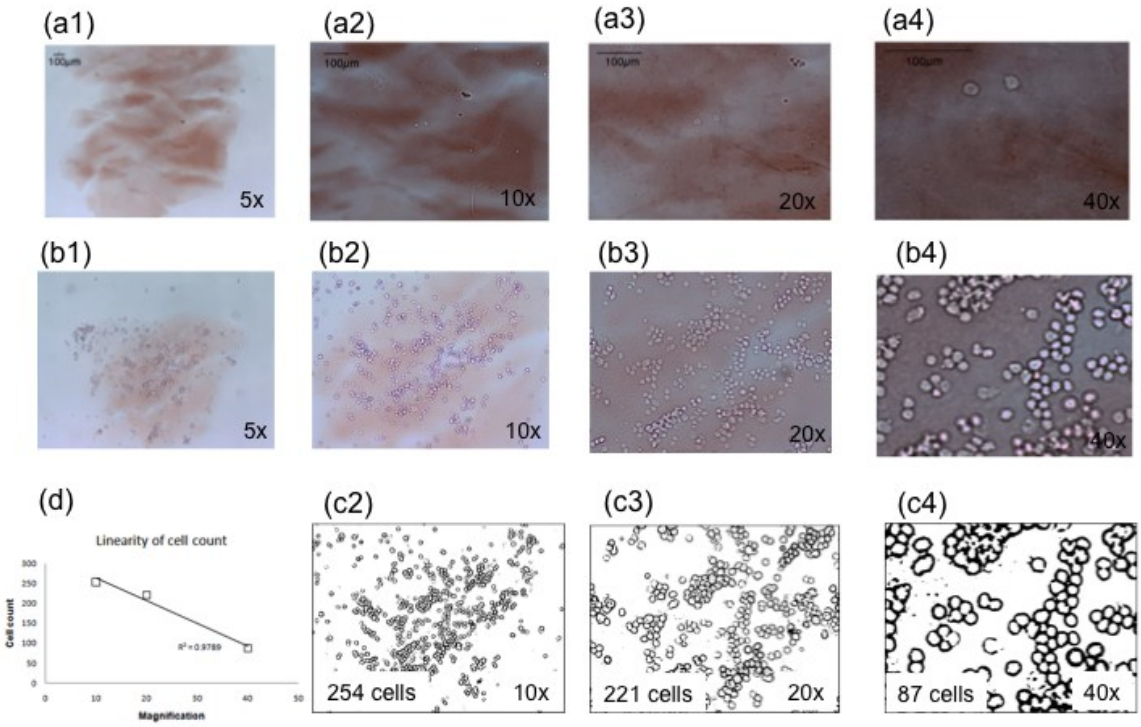

Figure 6-2: Capability of the anti-CD4 antibody mounted EAK-EAKH6 assembly to capture cells. Lymphocytes were harvested from the spleen of mice carrying B16 tumors. Single cell suspensions (2×10^6 cells/ml), depleted of erythrocytes and monocytes, were placed onto aggregates of (a) EAK, (b) EAK-EAKH6 established on mesh filters for 4 h at 4 °C. This process was repeated four times. Samples on filters were transferred to glass slides and analyzed at 5x (a1), (b1); 10x (a2), (b2); 20x (a3), (b3); 40x magnification (a4), (b4). (c2), (c3), (c4) cells associated with EAK-EAKH6 were enumerated using ImageJ. (d) Cell count per area (mm^2) at different magnifications was found related linearly ($y=-5.7x+321$, $R^2=0.9789$).

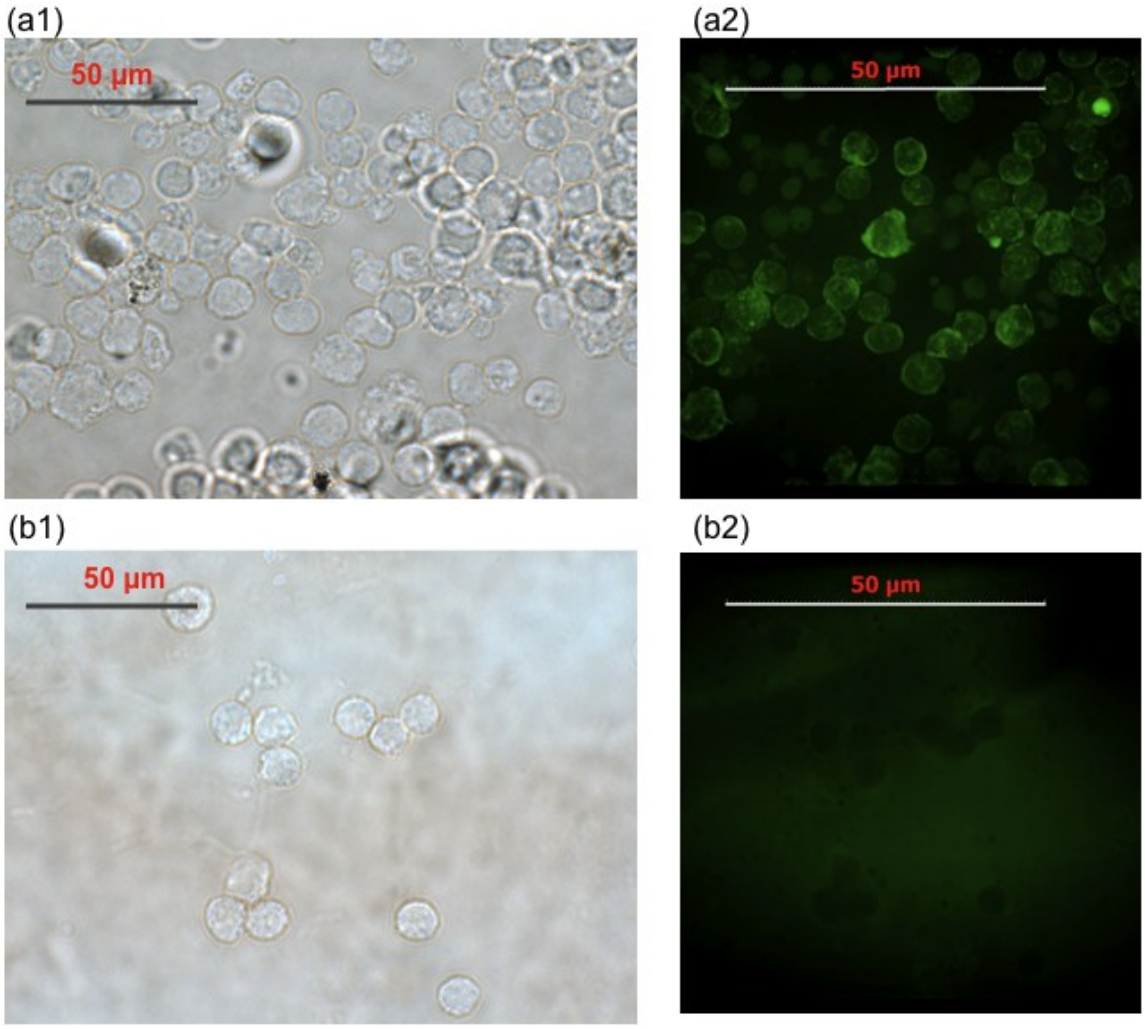

Figure 6-3: Laser confocal images of CD25 staining. Cells bound to EAK-EAKH6 (a) were stained with a fluorescein-conjugated Ab against CD25, a surface molecule expressed by regulatory T cells. The same experiment was performed with EAK aggregate (b) for comparison. (a1), (b1) bright-field images; (a2), (b2) Kr/Ar laser sourced confocal images.

Depletion of *Foxp3 in unbound fraction*

Unbound cells from figure 6-1 were collected and analyzed for Foxp3 expression level by semi-quantitative PCR with specific primers. Foxp3 is a distinct intracellular marker for Tregs.[115] Cells without passing through the anti-CD4 construct were used as the control.

Figure 6-4 shows the Foxp3 expression in the respective cell fraction in agarose electrophoretic migration. As expected, only products of Foxp3 (177 bp) and β-actin (154 bp) were detected. Band intensity was quantified to determine the relative amount of transcripts in the cells. Unbound cells collected from the EAK assembly showed a high level of Foxp3 expression, at approximately the same level with that of cells without passing through any peptide construct. In contrast, Foxp3 expression was found decreased by 90% in cells recovered from the EAK-EAKH6 construct. It can thus be concluded that regulatory T cells can be depleted from the heterogeneous lymphocyte suspension. These data are consistent with the microscopic images indicating that specific cell subsets are captured onto the anti-CD4 EAK-EAKH6 construct. The ability of the functionalized EAK-EAKH6 assembly to specifically capture cells via mounted mAb was thereby confirmed *in vitro*.

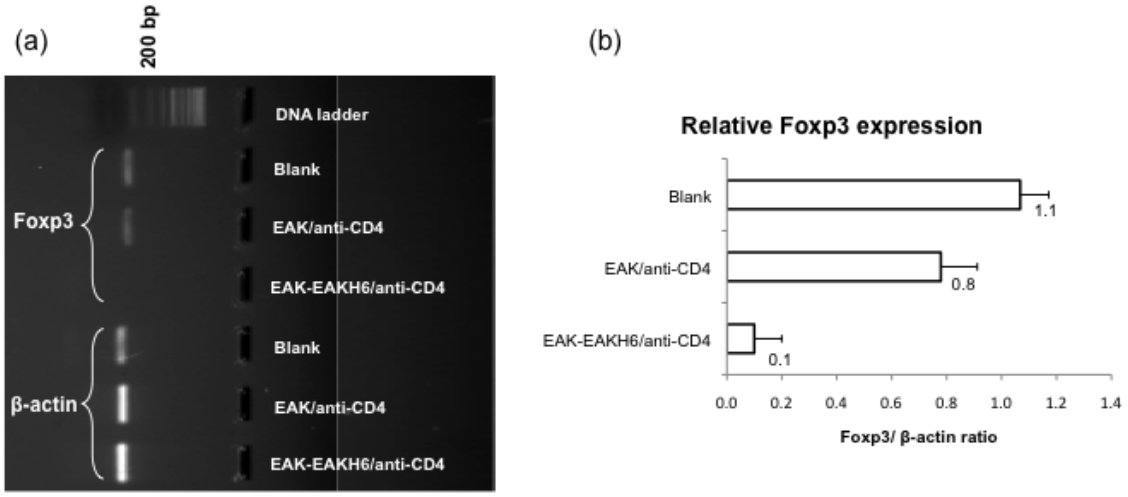

Figure 6-4: Evidence of EAK-EAKH6 used to deplete a specific T cell population. The relative fractions of regulatory T cells remaining apart from EAK-EAKH6 were quantified using semi-quantitative PCR based on expression of Foxp3, a transcription factor that largely defines regulatory T cells. The cells with no peptide-antibody construct incubation (referred to as blank) were used as a control here to evaluate the effect of culture condition on the Foxp3 expression. The band sizes were consistent with predicted PCR products of Foxp3 (177 bp) and β-actin (154 bp). Data represent two independent experiments conducted.

It has been established that Foxp3 is a crucial factor for the functional development of CD4+CD25+ regulatory T cells.[114] Initial support for the role of Foxp3 came from the observation that high Foxp3 expression in peripheral and thymic CD25+ Treg cells in mice. Conversely, Foxp3 could not be detected in CD25+ conventional activated T cells.[114] The expression of Foxp3 in CD4+CD25+ thymocytes in wild-type mice and the diminished numbers of CD4+CD25+ T cells in scurfy and Foxp3-knockout (Foxp3−) mice implied a role for Foxp3 in Treg cell development. Ectopic expression of Foxp3 in mouse CD4+CD25−Foxp3− T cells results in acquisition of suppressor properties. Foxp3 appears to exert parallel functions in mouse and humans. In humans, Foxp3 is also highly expressed in CD4+CD25+ T cells with suppressor function and that Foxp3 gene transfer confers suppressor functions to naive human CD4+ T cells.[33, 39, 114, 116] In light of these, the evidence presented above suggests the construct has the potential to regulate the abundance or accumulation of Treg cells in a defined microenvironment.

SUMMARY AND CONCLUSIONS

In the previous chapter (5), evidence was presented to demonstrate that rpAG, anti-H6, and EAK-EAKH6 could be combined to display mAb. The studies described in this chapter serve to extend the feasibility of the construct by mixing with mouse lymphocytes in vitro. The EAK-EAKH6 construct captured significant number of cells (figure 6-2), and the lack of cells bound to the EAK construct suggest specific interaction in the former. Two lines of evidence support specificity. Cells bound to the EAK-EAKH6 construct express CD25 (figure 6-3), and that unbound cells recovered had lower (90% decreased) level of Foxp3 transcript than that of the same from the EAK assembly (figure 6-4). It can thus be concluded that the EAK structure first reported almost two decades ago could be transformed from a non-specific matrix to a cell-selective structure in the EAK-EAKH6 construct.

The EAK-EAKH6 composite coated with mAb can be loaded with bioactive molecules, such as siRNA. Unlike the traditional concept of targeted drug delivery, in which the therapeutic agent is required to travel through the systemic fluid to arrive at the target cells, the current concept relies on co-localization of target cells with the therapeutics. Characterization of this injectable system described herein is a step towards applying the concept "reversed drug targeting" by which target cells are brought to a reservoir of drug molecules. I have begun to explore this in two formats. First, the membrane could be loaded with nucleic acids (used as a model drug) in the membrane. Preliminary data (not shown) indicate a 90% loading efficiency of oligonucleotides in the EAK-EAKH6 membrane, but only approximately 30% of that loaded was released after seven days at 37˚C. A second option is to mount polymeric particles loaded with nucleic

acids in or on the membrane. In this case the nucleic acids are released as a function of particle degradation. Both scenarios are aimed to exploit the close proximity of target cells and bioactive nucleic acids co-localized on a defined structure.

CHAPTER 7

CHARACTERIZATION OF POL-(D, L-LACTIC-CO-GLYCOLIC ACID) PARTICLES AS CARRIERS OF NUCLEIC ACIDS INTO PRIMARY DENDRITIC CELLS AND T CELLS

INTRODUCTION

Dendritic cells (DCs) are pivotal in the regulation of immune responses.[117] Modulation of DCs phenotypes with oligodeoxynucleotide (ODN) as decoys or anti-sense molecules can affect T-cell functions and immunity.[118, 119] Direct administration of ODN in intact animals, however, results in unpredictable and often suboptimal effects.[120] This can be attributed to inefficient accumulation of the ODN inside DCs due to extracellular physicochemical (e.g., anionic charges of DNA) and enzymatic (e.g., nucleases) barriers.

Nanoparticles have been used as carriers of ODN to overcome these barriers.[121, 122] The biodegradable co-polymer poly(D,L-lactide-co-glycolide) (PLGA) is a suitable building block for forming nucleic acids carriers.[123, 124] PLGA particulates are stable *in vivo*[125] and can be effectively engulfed into APCs by endocytosis.[126, 127] Theoretically, a large number of DNA molecules can be internalized with each particle entry. A key remaining barrier, however, is that internalized DNA molecules are channeled to lysosomes and degraded. *In vitro*, this may be overcome by delivering a large amount of the DNA and hope that some would escape. This is an inefficient process and high local DNA concentration may not be possible to attain *in vivo*.

Another challenge is the poor efficiency of loading macromolecules in PLGA particles because the DNA is often damaged during the encapsulation process. Several groups have addressed this by incorporating cationic species into PLGA to increase entrapment of the DNA. Capan et al. have detailed the physical characteristics of microparticles of plasmid DNA formulated with PLGA and poly-L-lysine (PLL).[128, 129] Ravi et al. described the preparation and characteristics of cationic PLGA nanospheres with PVA−chitosan to adsorb DNA intended for gene delivery applications.[130] Li et al. have used calcium-phosphate to precipitate plasmid DNA to form PLGA microparticles.[131] Stearylamine[132] and polyethylenimine (PEI)[133] have also been used to encapsulate plasmid DNA into PLGA microparticles. Kasturi et al. have shown that plasmid DNA adsorbed on PEI-surface conjugated PLGA microparticles leads to enhanced gene delivery in macrophages.[134]

In the work presented in this chapter, O10H6, an ornithine–histidine cationic peptide, was employed to fulfill the dual functions of improving loading and enhancing the escape of DNA from lysosomes. It has been shown previously that O10H6 forms stable condensates with nucleic acids on the surface of carboxylate polystyrene microspheres and this self-assembled system can facilitate DNA uptake in DCs.[135, 136] The imidazole in histidine facilitates endosomal escape by disrupting the osmotic balance of the vesicles.[137, 138] Herein the physical characteristics and cellular uptake of PLGA nanoparticles loaded with ODN pre-condensed with O10H6 were examined. The results show that $PLGA_{O10H6}$ is an effectual nucleic acids carrier capable of delivering ODN into primary DCs. Evidence is shown for the cellular internalization and escape of the ODN

from the lysosomal pathway in DCs. These results raise the prospect of applying DNA-loaded $PLGA_{O10H6}$ in DC modulation.

MATERIALS AND METHODS

Peptide and oligodeoxynucleotide

The peptide O10H6 (figure 7-1 a; 1982 Da) was custom synthesized by Sigma-Genosys (Houston, TX, USA) custom synthesis service. Crude peptides were purified by HPLC (>90%) and their identities were confirmed by liquid chromatography-mass spectrometry. Upon arrival, the lyophilized peptides were reconstituted in sterile ddH2O at a concentration of 200 μg/μl (100 mM) and stored in 50-μl aliquots at −80 °C until use. ODN with a phosphorothioate-modified backbone containing the NF-κB binding sites (sense strand: 5′-AGGGACTTTCCGCTGGGGACTTTCC-3′) were custom synthesized by Alpha DNA (Montreal, Quebec, Canada). The DNA was labeled with fluorescein isocyanate (FITC) at the 5′ end. PLGA (50:50; 16.5–22 kDa; I.V.= 0.66–0.80) was obtained from Polysciences (Warrington, PA, USA). Polyvinyl alcohol (PVA) (Fig3.1 a) with a molecular mass of 22 kDa and 88% hydrolyzed was purchased from Sigma-Aldrich (St. Louis, MO, USA).

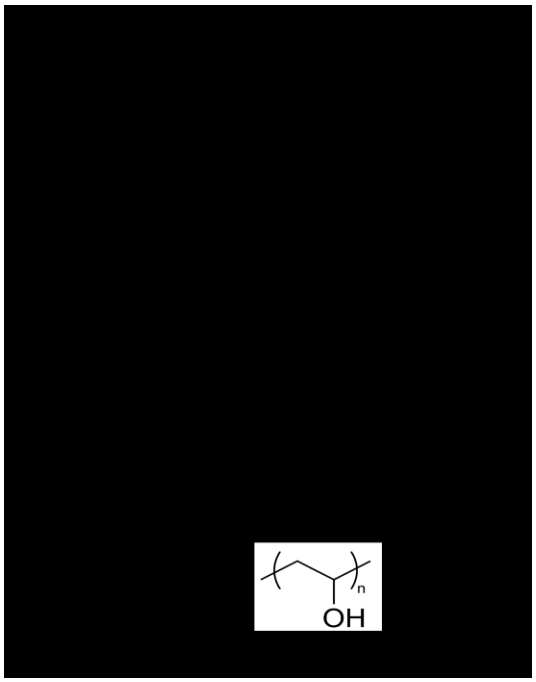

(b)

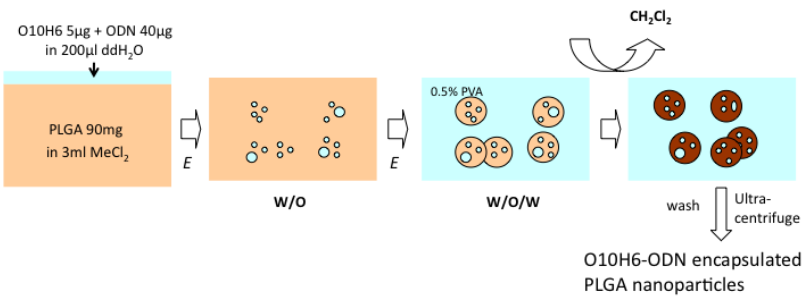

Figure 7-1: Materials and methods of particles preparation. (a) Chemical structures of PLGA, O10H6 and PVA used in making the particles. (b) A schematic diagram of the particle fabrication process. A double-emulsion solvent evaporation method was used.

Preparation of $PLGA_{O10H6}$-ODN nanoparticles

$PLGA_{O10H6}$-ODN particles were prepared using a double-emulsion (w/o/w) solvent evaporation technique (figure 7-1 b).[139] 5µg O10H6 was added to 200 µl of an aqueous solution containing 40 µg of the ODN and gently shaken for 0.5 h at room temperature. This aqueous solution was incorporated into a methylene chloride ($MeCl_2$) solution of PLGA (3%, w/v) by sonication. A Fisher model 100 sonic microprobe was used to introduce 24 W of energy (over 2 min) to form this water-in-oil emulsion. This primary emulsion was added drop wise with energy input (24W, 4 min) into 20 ml of aqueous solution of PVA (0.5%, w/v) to form a water-in-oil-in-water emulsion. The resulting double emulsion was stirred for 4 h in chemical fume hood to allow the $MeCl_2$ to evaporate. Particles were recovered by ultracentrifugation and washed twice with ddH_2O to remove excess PVA and un-trapped DNA. The particles used in the experiments described were freshly prepared prior to each analysis. We have, however, determined that the particles can be freeze-dried, stored, and be reconstituted in distilled water. Freeze-dried $PLGA_{O10H6}$-ODN retains 90% of their physical characteristics (particle size and zeta potential) upon reconstitution. Addition of sucrose (2%, w/v) improves the recovery to close to 100%. Loading efficiency was determined by dissolving the particles in chloroform (2 h constant shaking) followed by extraction with Tris-EDTA buffers. The aqueous phase was analyzed for DNA content with OligoGreen (Invitrogen/Molecular Probes, Eugene, OR, USA; detection limit 100 pg/ml) to determine the amount entrapped in the particles.[140] Loading efficiency was calculated based on the amount of ODN determined divided by the amount of ODN initially added in the primary emulsion.

Particle size and zeta potential analysis

The Nicomp 380 ZLS analyzer (Particle Sizing Systems, Santa Barbara, CA, USA) was used to determine particle size distribution and zeta potential. Mean hydrodynamic diameter was measured with particles suspended in ddH_2O. The radius was calculated using the Stokes–Einstein equation based on diffusion coefficient of the particles in the medium. Data were integrated over 10 min in duplicate experiments and were test fit for Gaussian and non-Gaussian functions. The instrument operates based on the dynamic light scattering principle, capable of detecting particle size ranging from 5 nm to 5 μm. Zeta potential measurement was performed with the samples diluted with ddH_2O (pH approximately 7.2) The measurement is based on electrophoretic mobility of the sample particles when subjected to an electric field.

Transmission electron microscopy and infrared measurement

Transmission electron micrographs were obtained using a JEM-100 CXII electron microscope (Jeol, Tokyo, Japan). A cool beam electron gun (60 kV) was used to illuminate the samples. A $PLGA_{O10H6}$-ODN suspension was dried on a copper grid support (G200-CU; Electron Microscopy Sciences, Hartfield, PA, USA) and stained with 1% uranyl acetate for image capture. Images were captured from films developed using high contrast D-19 developer (Kodak, Rochester, NY, USA). Reflectance FTIR spectra were recorded on a Thermo Nexus 470 Infrared Spectrometer operated at a spectral resolution of 0.5 cm^{-1} with 1024 scans. Particles were dried overnight in desiccators. Samples were analyzed under inert conditions are scanned over the range of 400–4000

cm^{-1}. Independent measurements of PLGA, O10H6 and plastic support were obtained for subtraction.

Mice and generation of primary DCs

Female certified virus free BALB/c ($H\text{-}2^d$) mice (6–8 weeks old) were purchased from Hilltop Lab Animals (Scottsdale, PA, USA) and housed in the Duquesne University Animal Care Facility. All experimentations were handled in accordance with institutional animal care policy. Primary DCs were generated from mice using the Inaba protocol[141] with minor modifications.[142, 143] Total bone marrow cells were harvested from femurs and cultured overnight in serum-free RPMI medium (Life Technologies, Gaithersburg, MD, USA). Non-adherent cells were then re-plated at 10^6 cells/ml in 24-well tissue-culture plates (Costar, Cambridge, MA, USA) in RPMI containing 10% heat-inactivated FBS, 50 μM 2-mercaptoethanol, antibiotics (penicillin/streptomycin/fungizone) (all from Life Technologies) and cytokines (5 ng/ml of murine GM-CSF and 5 ng/ml of murine interleukin-4; R and D Systems, Minneapolis, MN, USA) and maintained at 37°C in 5% CO_2. On day 4, non-adherent cells were removed by aspirating 80–90% of the media and adherent cells were re-fed with culture medium (1 ml/10^6 cells) containing GM-CSF and IL-4.

For flow cytometric analysis, cultured DCs on day 6 of differentiation were exposed to FITC-labeled free ODN (0.5 μM) or ODN encapsulated in PLGA or $PLGA_{O10H6}$ (estimated ODN concentration = 100 nM) in 2 ml of Opti-MEM media for 2 h at 37°C and 5% CO_2. Particle density in the experiment was estimated to be 2.2×10^7 particles/ml, based on the number of particles per unit area enumerated in TEM micrographs. After

incubation, cells were then washed with PBS and analyzed using a Beckman Coulter EPICS XL bench-top flow cytometer. At least 10^4 events were sampled for each group.

Confocal imaging

Cultured DCs were adhered to coverglasses, washed with PBS and incubated with $PLGA_{O10H6}$-ODN for 2 h at 37°C. Dendritic cells have an intrinsic propensity to adhere to glass or plastic surface. A Fisher brand coverglass (22 × 22 mm) was placed in each well in the bone marrow cultures. On day 6, the coverglass was recovered and adhered cells were washed with PBS and fixed in 4% paraformaldehyde for 15 min at 4°C before mounting on slides with an anti-fade medium (MOWIOL 4-88, CalBiochem, Darmstadt, Germany). Images were collected using a Leica TCS SP-2 spectral microscope (Leica Microsystems, Wetzlar, Germany) with an argon/helium laser and FITC filter. Internalized DNA was visualized by fluorescence detection based on FITC-labeled ODN. Lysosomes were illuminated by staining the cells with LysoTracker Red DND-99 (Invitrogen/Molecular Probes), a red-fluorescent dye that illuminates acidic compartments in live cells.

Foxp3 specific siRNA and preparation of siRNA adsorbed PLGA naoparticles

Double-stranded murine Foxp3-targeted siRNA (21bp) was designed and synthesized by Ambion (Austin, TX, USA) (Figure 7-2). Upon arrival, the lyophilized siRNA were reconstituted in sterile ddH_2O at a concentration of 0.5μg/μl (100 mM) and stored in 50-μl aliquots at −80 °C until use. In the uptake study, the siRNA was labeled with carboxyfluorescein (FAM) at one of the 5′-ends.

Figure 7-2: Sequence of Foxp3-targeted siRNA.

Plain PLGA particles were prepared in our lab using a double emulsion (w/o/w) solvent evaporation technique described above. Particles were recovered by ultracentrifugation and washed twice with ddH_2O before lyophilization to remove excess PVA and PLGA fragments. 60 mg of lyophilized PLGA was first coated with 200 mg of O10H6 in 300 μL of ddH_2O. To assure sufficient binding of O10H6 to the particles, the components were equilibrated in a 1.5 mL Eppendorf tube with gentle shaking for 2 hours at room temperature on a mini shaker at a setting that is equivalent to the second lowest speed. The resulting positively charged particles (denoted as $PLGA_{O10H6}$) were then equilibrated with the siRNA for an additional 30 min with gentle shaking at room temperature. The N: P ratio for O10H6 to siRNA was estimated to be 10:1. The final particle had siRNA condensed by O10H6 associated with the PLGA particle surface and was referred to as $PLGA_{O10H6}$-siRNA.

Physiochemical characterization of $PLGA_{O10H6}$-siRNA

A Nicomp 380 ZLS analyzer (Particle Sizing Systems, Santa Barbara) was used to determine the size and zeta potential of plain PLGA particles and $PLGA_{O10H6}$-siRNA particles.

In order to confirm the binding of siRNA onto the surface of $PLGA_{O10H6}$, the electrophoretic mobility of naked siRNA or the respective siRNA complexes ($PLGA_{O10H6}$-siRNA) was evaluated by agarose gel electrophoresis. Samples were analyzed in 1% agarose gel (MP Biomedicals, Solon, Ohio) with or without the addition of low molecular weight heparin sodium (Eikins-Sinn, Inc., Cherry Hill, NJ) (50 U/mL) that can release charge-bound nucleic acids. To test the protection effects of the particles,

free siRNA and $PLGA_{O10H6}$-siRNA were incubated with 10% FBS at 37°C for overnight prior to loading in sample reservoir.

Mice and cell line

Six to eight weeks old female certified virus free C57BL/6 mice were purchased from Charles River Laboratories International Inc. (Wilmingto, MA, USA) and housed in the Duquesne University Animal Care Facility. B16 (B6-derived melanoma)-F10 cell line was obtained from American Type Culture Collection (ATCC) (Manassas, VA, USA) and cultured in ATCC-formulated Dulbecco's Modified Eagle's Medium (DMEM) supplemented with 10% (v/v) FBS and 1% (v/v) antibiotics.

Flow cytometric analysis of RNA uptake

Fresh splenic T cells from C57BL/6 were exposed to FAM-labeled free siRNA (3 μg) or $PLGA_{O10H6}$-siRNA in 2 ml of Opti-MEM media for 4 h at 37ºC, 5% CO_2. After incubation, cells were then washed with PBS and analyzed using a Beckman Coulter EPICS XL bench-top flow cytometer. At least 10,000 events were sampled for each group.

In vivo effect of Foxp3 specific siRNA carried by $PLGA_{O10H6}$ particles

B16-F10 cells (passage number 5-10) were seeded subcutaneously into six to eight weeks old female C57BL/6 mice. After 7 days, $PLGA_{O10H6}$-siRNA particles were injected intra-tumorally. 48 hours later, mice were euthanized and the spleens were pulverized to make single cell suspension. For flow cytometric analysis, the splenic cells were stained for CD4, CD25 and Foxp3 with fluorescent-conjugated antibodies. For RT-PCR analysis, these splenic cells were selected for CD4 positive population. Total RNA was extracted and one-step RT-PCR analysis was performed in an Eppendorf

MasterCycler (Eppendorf, Hamburg, Germany). Murine Foxp3 primer pairs (SuperArray Bioscience, Frederick, MD, USA) were used to generate cDNA from total RNA and amplify the product, and mice β-actin primer pairs were used for semi quantification purpose. The DNA products were analyzed by electrophoreses on 2% agarose gel and visualized by ethidium bromide staining.

Tumor assay

Mice were inoculated with 0.5×10^6 B16-F10 cells (passage number 5-10) in 0.2 ml PBS subcutaneously. The diameter of the tumors was measured with calipers twice at right angles to calculate the tumor volume. Each experiment group consisted of five mice.

RESULTS AND DISCUSSION

$PLGA_{O10H6}$-ODN particles were fabricated from PLGA polymer with the ODN pre-condensed with O10H6 using a double-emulsion/solvent-evaporation method (figure 7-1b).[139] In contrast to a similar lysine-based peptide, O10H6 is nontoxic to DCs.[144] Ornithine is a non-natural amino acid that contains a side chain (−CH2−CH2−CH2−NH2) that is fully protonated at physiological pH. The histidine imidazole (pKa~6.7) is partially ionized (<5%) at pH 7.4, but is progressively protonated as pH decreases. Once inside endosomes (pH 5–6), the histidines in O10H6 may act as a buffer and induce the vesicles to burst by promoting influx of protons and water[137, 138] and release their content into the cytosol.

Physicochemical characteristics of $PLGA_{O10H6}$-ODN particles

The $PLGA_{O10H6}$-ODN particles have an average diameter of 373.5±29nm (n=3) based on dynamic light scattering analysis (figure 7-3 a). Additions of ODN and/or O10H6 do not affect the particle size since blank PLGA and PLGA-ODN (referred to as no O10H6) have similar diameters, 379±34nm (n=3) and 391±43nm (n=3), respectively. Blank PLGA particles have an average surface charge of −14.4 ± 3.2mV (n=3), most likely due to the PVA (surfactant) adsorbed on the surface.[145-147] As expected, addition of anionic ODN to PLGA (PLGA-ODN) results in a more negative potential (−17.3±1.8mV, n=3) compared to blank PLGA. Incorporation of the cationic O10H6 (in $PLGA_{O10H6}$-ODN) leads an average potential of −16.9±5.2mV (n=3 figure 7-2 b). The changes in the zeta potentials are consistent with the respective compositions of the particles.

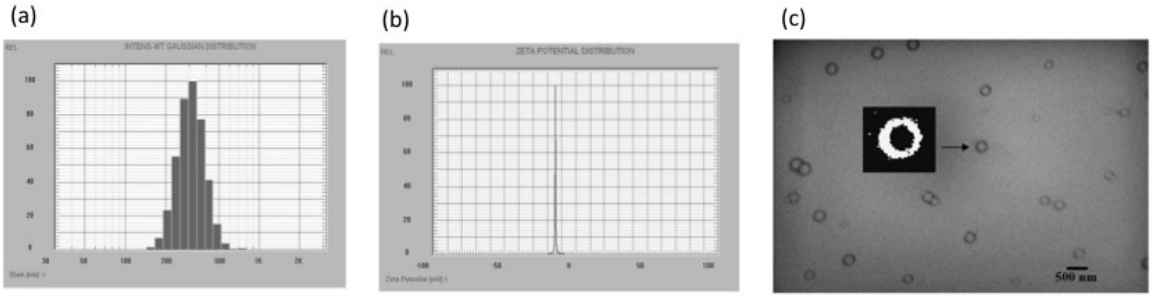

Figure 7-3: Physical characteristics of $PLGA_{O10H6}$-ODN particles. (a) Particle size determined by dynamic light scattering. (b) Zetapotential: determined with samples suspended in ddH_2O. (c) Transmission electron microscopy micrograph of $PLGA_{O10H6}$-ODN (diluted 10 times) at 10^4 × magnification. Inset: An inverted image of a selected particle was analyzed for circularity using the NIH ImageJ software. Circularity was determined to be 0.7 based on the function $4\pi \times area/perimeter^2$ (a perfect circle would have a value of 1.0). All data are representative of at least three independent experiments.

Transmission electron microscopy confirmed the spherical morphology (calculated circularity=0.7; 1.0 indicates a perfect circle) of the particles (figure 7-3 c). Loading efficiency of $PLGA_{O10H6}$-ODN was determined to be 42.3%, which is in the same order of magnitude in microparticles formed with PLGA and poly-L-lysine reported by Capan et al.[124] DNA loading in PLGA-ODN was poor, at only 1.3%.

A subtractive FTIR method[148, 149] was used to confirm the presence of ODN in the particles (figure 7-4). The spectra of $PLGA_{O10H6}$ and $PLGA_{O10H6}$-ODN were collected with PLGA as the subtracted background. The addition of ODN clearly changes the spectral profiles. The alkyl groups of the ODN can be clearly identified by the peaks at 2922 cm^{-1} and 2852 cm^{-1} assigned to C-H asymmetrical and symmetrical stretches (figure 7-4 a). In $PLGA_{O10H6}$ (without ODN), the broader bands at 3051 cm^{-1} and 2944 cm^{-1} can be attributed to the gauche conformation of the alkyl chains in peptides (figure 7-4 b). DNA structure leads to all-trans conformation of alkyl bands and a more consistent structure across the sample compared to peptides. The sharpening of the peaks, taken together with the changes in zeta potentials, confirms the presence of the ODN in $PLGA_{O10H6}$-ODN particles.

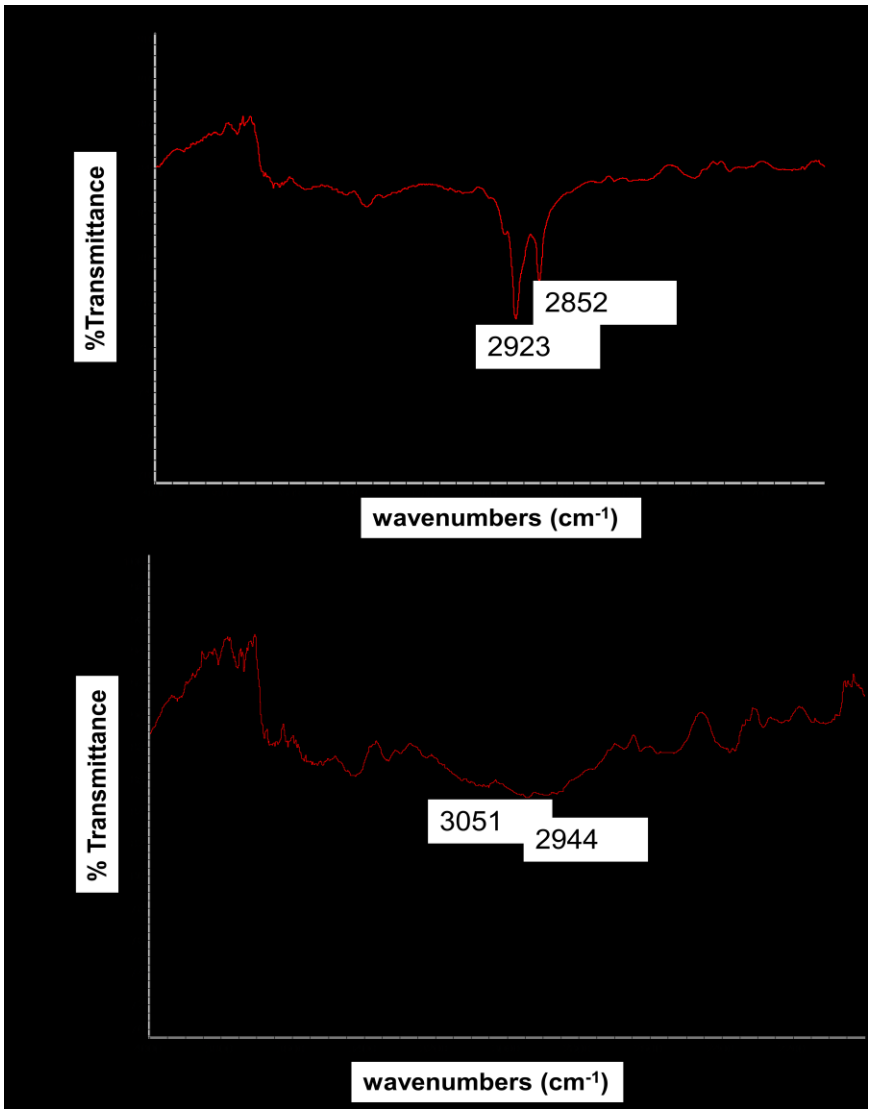

Figure 7-4: Transmittance infrared spectra of $PLGA_{O10H6}$-ODN. (a) $PLGA_{O10H6}$-ODN and (b) $PLGA_{O10H6}$, both with PLGA as subtracted background. x-axis, wavenumbers (cm^{-1}); y-axis, % transmittance. Data are representative of three independent experiments conducted.

Flow cytometric analysis of ODN uptake in primary DCs

Bone marrow-derived murine DCs were used as the target to determine the capacity of $PLGA_{O10H6}$-ODN to deliver ODN into cells. We used flow cytometry to determine the frequency of cells that had taken up the ODN based on FITC fluorescence. Each analysis was conducted based on at least 10^4 cells. Background fluorescence was determined in control cells that had not exposed to DNA or particles. Treatment with PLGA-ODN (broken line) results in lower uptake compared to $PLGA_{O10H6}$-ODN (dark line) (figure 7-5 a). Cells exposed to $PLGA_{O10H6}$-ODN have a higher level of ODN than those treated with equivalent concentration of 'naked' ODN (thin line). Collective analysis of three independent experiments confirmed that treatment with $PLGA_{O10H6}$-ODN consistently resulted in superior uptake compared to PLGA-ODN or 'naked' ODN (figure 7-5 b). We determined that 25–30% of the dendritic cells had taken up the ODN (labeled with FITC). With PLGA-ODN particles, the same analysis yielded uptake of less than 5%. This was expected because of the poor DNA loading in PLGA-ODN. Incorporating O10H6 into PLGA particles clearly contributes to the delivery.

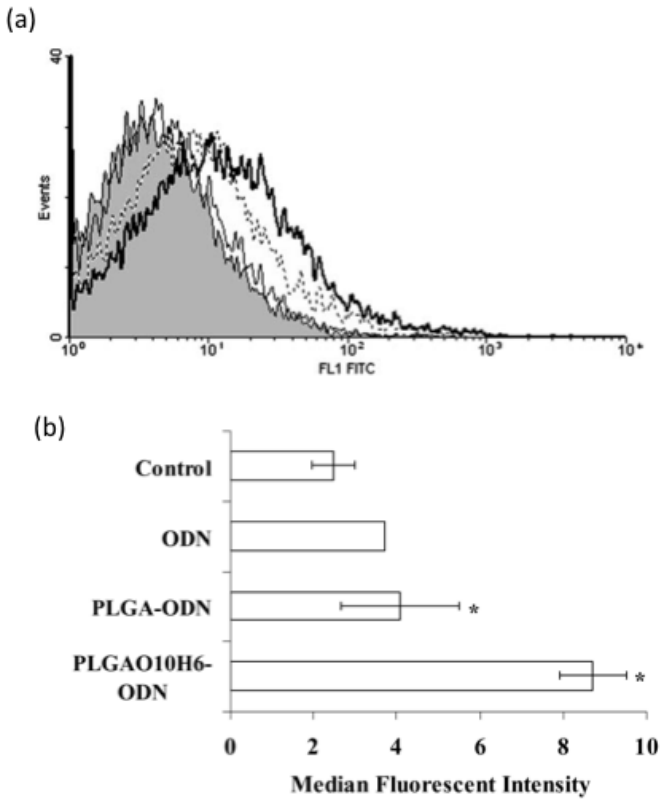

Figure 7-5: Uptake efficiency of FITC-labeled ODN by various carriers was determined in murine bone marrow-derived DCs. (a) Histograms from a representative experiment of control DCs (shaded solid), ODN (thin line), PLGA-ODN (broken line) and $PLGA_{O10H6}$-ODN (thick line). (b) Composite analysis of data from three independent experiments showing percentage of cells taken up the ODN. Error bars represent standard error of mean. Control DCs were cultured under the same conditions with treatment ($^{*}p < 0.05$).

Evidence of internalization and endosomal escape

Internalization of ODN into DCs was confirmed using laser confocal microscopy (figure 7-6). In concordance with the flow cytometric results, we observed consistent superior ODN accumulation in cells exposed to $PLGA_{O10H6}$-ODN compared to PLGA-ODN (figure 7-6). Again, this was expected because of the poor loading of DNA in PLGA-ODN. Diffused fluorescence can be seen in a cell exposed to $PLGA_{O10H6}$-ODN (figure 7-6 b, see arrow), indicating non-sequestrated ODN in the cytoplasm.

To confirm the fate of the ODN in DCs delivered by $PLGA_{O10H6}$-ODN, cells were stained with a LysoTracker (red) dye to illuminate acidic compartments. Based on the differential localization of green and red clusters, we concluded that DNA could escape from the lysosomes (figure 7-7). Delineation of FITC and red fluorescence in selected clusters confirmed that ODN (FITC) could be found outside of acidic compartments (figure 7-7 b, cluster 1). An example of internalized ODN sequestrated in an acidic compartment is also shown (figure 7-7 b, cluster 2). Cluster 3 represents an empty lysosome (figure 7-7 b). Inclusion of O10H6 in the current system is intended to facilitate loading and lysosomal escape of the DNA. Although it has been reported that PLGA itself can also facilitate endo-lysosomal escape by charge reversal in acidic compartments,[150] the buffering capacity of the histidines in O10H6 may neutralize lactic and glycolic acids generated in the particle interior as the polymer chains are hydrolyzed.[151-153] Thus, O10H6 may also serve to protect the DNA from degradation inside hydrated particles. It should be noted that Babensee and colleagues have reported that the effect of PLGA on dendritic cell maturation is dependent upon the density (or

surface area) of the particles.[154, 155] In our experience, this can be controlled by using particles with high payloads (amount of DNA/density of particles), thereby minimizing the surface area of PLGA particles the dendritic cells encountered.

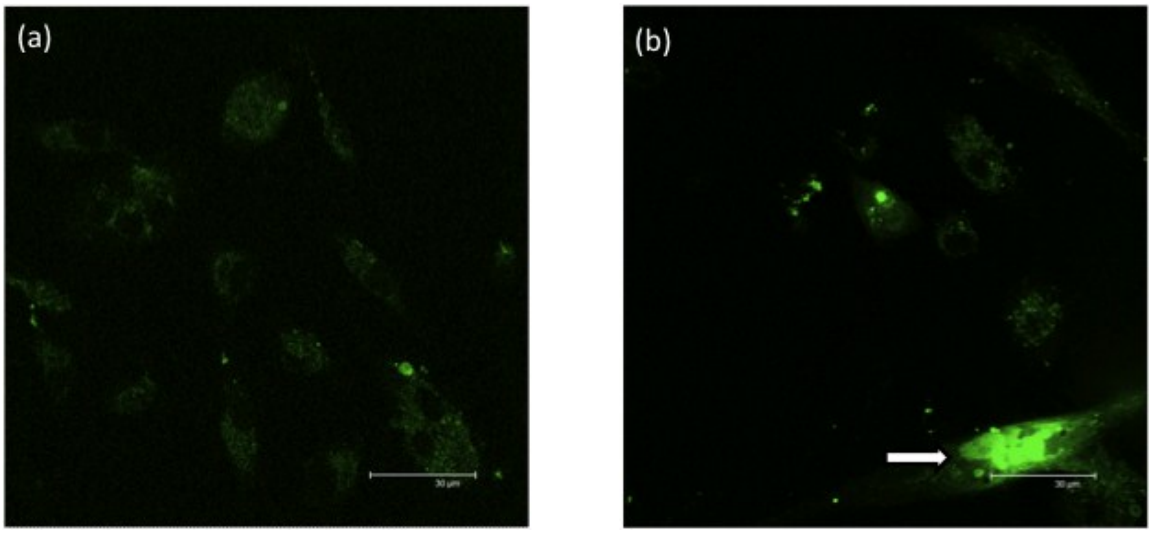

Figure 7-6: Confocal image analyses of DCs incubated with (a) PLGA-ODN or (b) $PLGA_{O10H6}$-ODN for 2 h at 37°C. The arrow indicates a region of diffused fluorescence. Mounted slides were imaged at 100× magnification on a Leica TCS SP-2 spectral microscope. Data are representative of three independent experiments conducted.

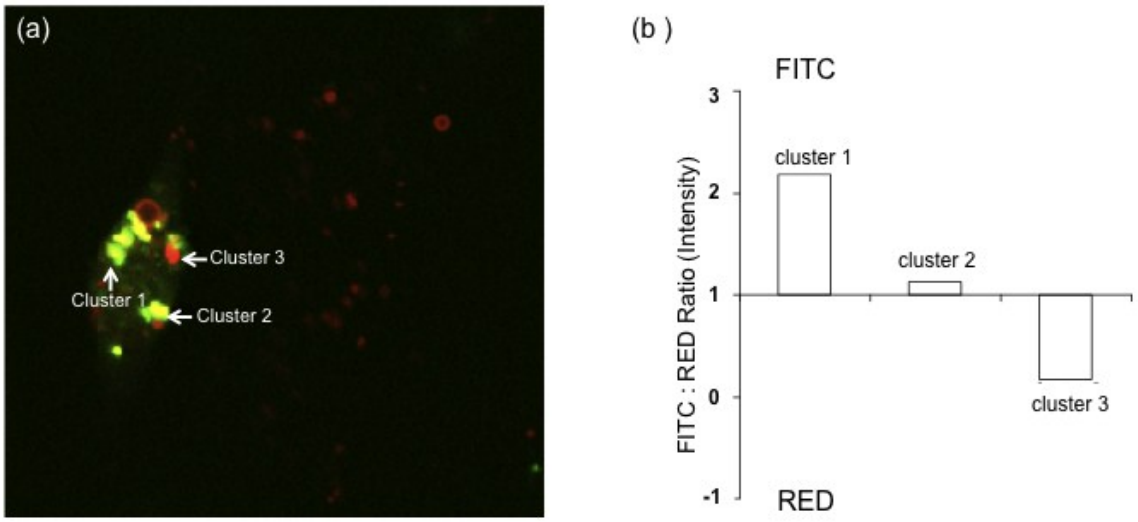

Figure 7-7: Intracellular fate of internalized ODN. (a) Image overlay of DCs stained with LysoTracker red and incubated with $PLGA_{O10H6}$-ODN. (b) Delineation of the location of acidic compartments and ODN in the image based on the ratio of red and FITC intensity. Data are representative of two independent experiments conducted.

Delivery of anti-Foxp3 siRNA

Another application of the carrier system is to deliver RNA molecules aimed to downregulate specific functions in T cells. In many forms of cancer, Treg cells that express the protein Foxp3 are associated with cancer progression.[40] These cells can be indentified by CD4 and CD25, molecules expressed on the cell surface. Foxp3 regulated in a dose-dependent manner the development and functions of Treg cells. Suppressive functions of peripheral Treg cells require a continuous expression of Foxp3.[156, 157] Studies have shown that downregulation of Foxp3 can increase the ability of other immune cells to destroy tumors, e.g. cytotoxic T cells (CTL) revert back to anti-tumor phenotypes.[45] RNA interference (RNAi) is a mechanism in which RNA molecules bind to and degrade specific messenger RNA (mRNA) in a sequence-dependent manner such that expression of the encoded protein is terminated.[158] Inhibition of Foxp3 expression can be accomplished by introducing double-stranded small-interfering RNA (siRNA) with sequence complementary to the Foxp3 mRNA. *In vitro*, the activity of siRNA is long lasting, with 50% knockdown observed up to 10 days, and is mainly limited by dilution of the siRNA through cell division. The activity of siRNA *in vivo*, however, is hindered by rapid degradation in biological fluids prior to reaching target molecules. Efficient application of RNAi requires a carrier system to facilitate the uptake of siRNA by cells.[159]

In this chapter, nanosized PLGA particles coated with the polycation O10H6 (with the resultant particles designated as $PLGA_{O10H6}$) was used to adsorb siRNA that bind to the mRNA encoding Foxp3. The surface molecules CD4 and CD25 were used in quantifying Tregs in flow cytometric analysis. The level of Foxp3 expression was estimated using

semi-quantitative PCR. The performance of the siRNA-loaded particles was determined in mice carrying B16 tumors in which Treg cells have been found to congregate.

Physiochemical characterization of $PLGA_{O10H6}$-siRNA Particles

Zeta potential measurement showed that plain PLGA particles have an average surface charge of -16.92±1.1mv. The surface adsorption of O10H6 and siRNA (figure 7-8 a) caused this negative charge neutralized, resulted in an average potential of -0.30±1.0mv. The size of the RNA-loaded particles remained below 300 nm in hydrodynamic diameter, figure 7-8.

Heparin is a highly sulfated glycosaminoglycan, which has a high negative charge density. In the electrophoresis, heparin was added to liberate RNA bound via ionic interaction. In figure 7-9 a, upper panel showed that RNA were retained in loading wells when complexed with $PLGA_{O10H6.}$ When heparin was added, comparable level of RNA was released from $PLGA_{O10H6}$-siRNA particles (figure 7-9 a middle panel). Serum was used to test the ability of $PLGA_{O10H6}$ to protect the RNA from enzymatic digestion and protein destabilization. Compared to free siRNA, which were mostly degraded, RNA complexed with $PLGA_{O10H6}$ ($PLGA_{O10H6}$-siRNA) remained largely intact after incubated with 10% FBS at 37°C for overnight, figure 7-9 a lower panel. The band intensity was quantitatively analyzed and summarized in figure 7-9 b. It shows that compared to free siRNA, which is totally degraded in serum digestion, approximately 60% of the siRNA were protected by $PLGA_{O10H6}$ particulates and remained intact through serum incubation.

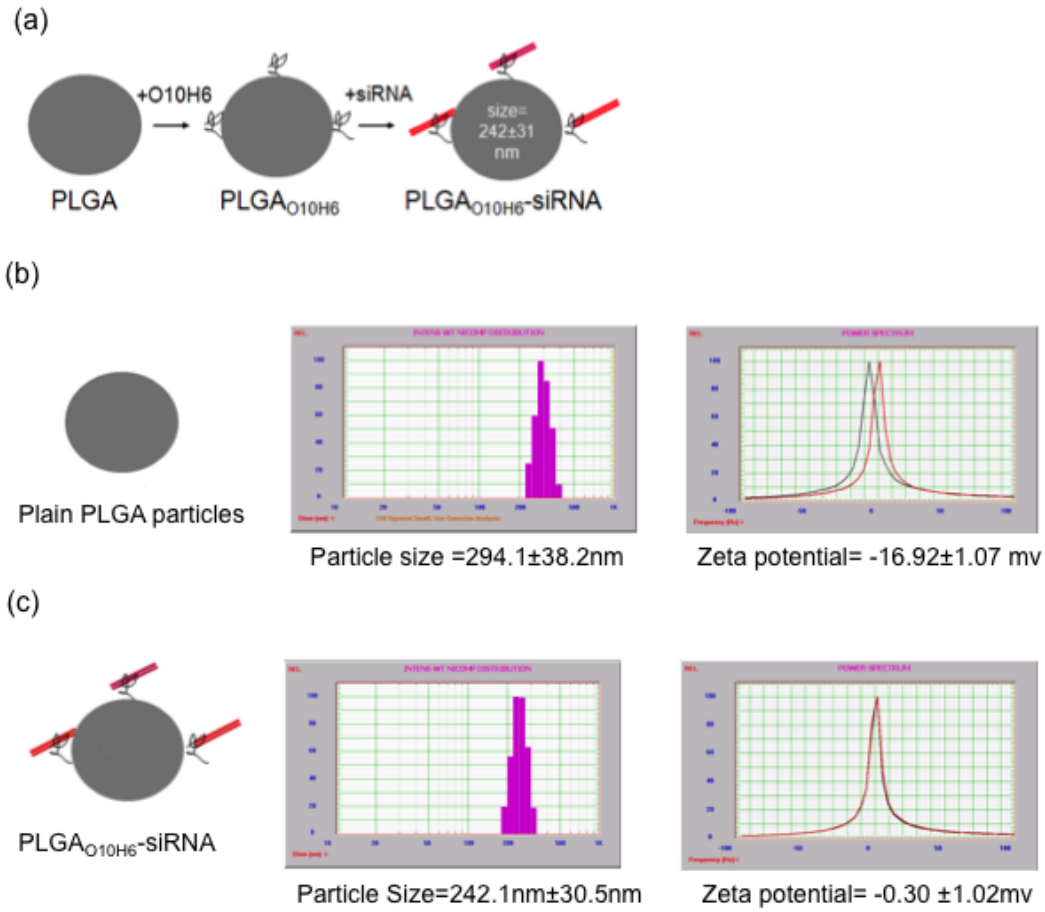

Figure 7-8: Physical properties of plain PLGA and PLGA$_{O10H6}$-siRNA particles. (a) Mode of RNA loading and physical properties. Particle size and zeta potential of (b) plain PLGA particles and (c) PLGA$_{O10H6}$-siRNA particles. The adsorption of O10H6 and siRNA did not change the size range of PLGA particles, but neutralize the negative surface charge.

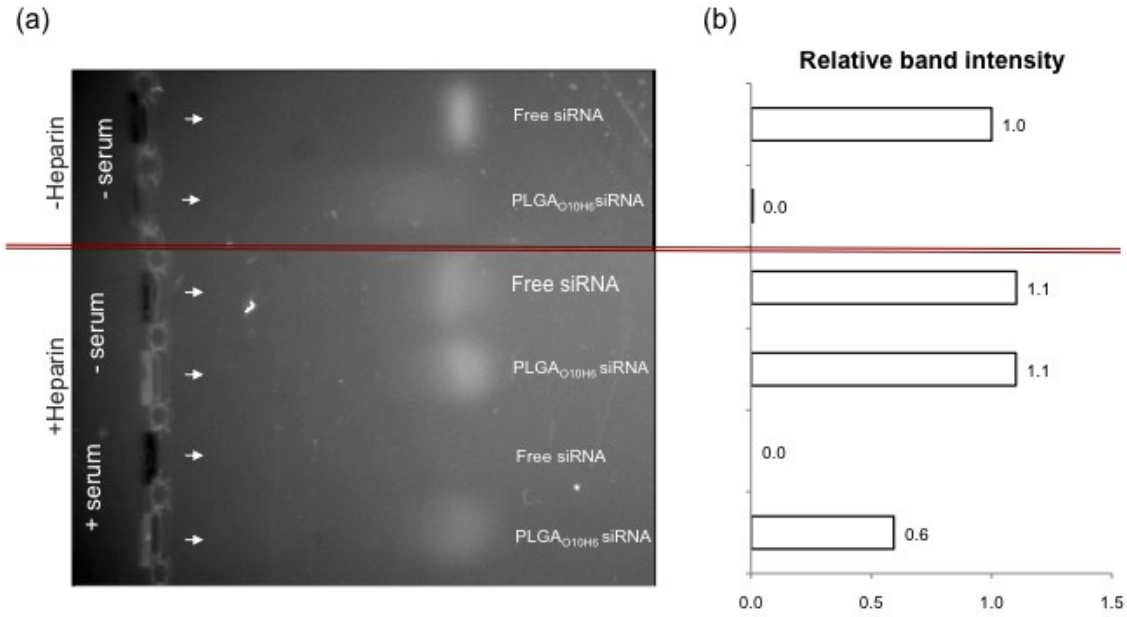

Figure 7-9: Gel electrophoresis of RNA complexes. (a) Agarose (1%) gel image. Heparin sulfate was added to liberate charge-bound RNA from the surface of particles. In the "+serum" groups, naked siRNA or the respective RNA complexes were incubated with 10% FBS at 37°C for overnight to test the protection effects of $PLGA_{O10H6}$ particles. (b) Relative fractions of RNA were quantified with the free siRNA as the control.

Uptake of RNA into primary mouse T cells

Confocal and flow cytometric analyses have been performed to test if the particles could assist uptake of RNA into primary mouse T cells. The uptake efficiency of FAM-labeled siRNA in mouse spleen T cells was improved from 3.2±0.2% for free siRNA to 20.1±3.9% when carried by $PLGA_{O10H6}$ particles. Furthermore, in CD4+ T cells, this level was increased from 2.7±0.2% to 27.1±1.3% when $PLGA_{O10H6}$ was employed. These differences were statistically significant in three experiments conducted ($p < 0.01$), figure 7-10 a and b. Approximately, one in four CD4+ T cells isolated from a mouse spleen took up FAM-labeled siRNA when loaded on $PLGA_{O10H6}$, compared to one in 24 when free siRNA were applied. Confocal imaging revealed that the RNA was internalized into the T cells (figure 7-10 c).

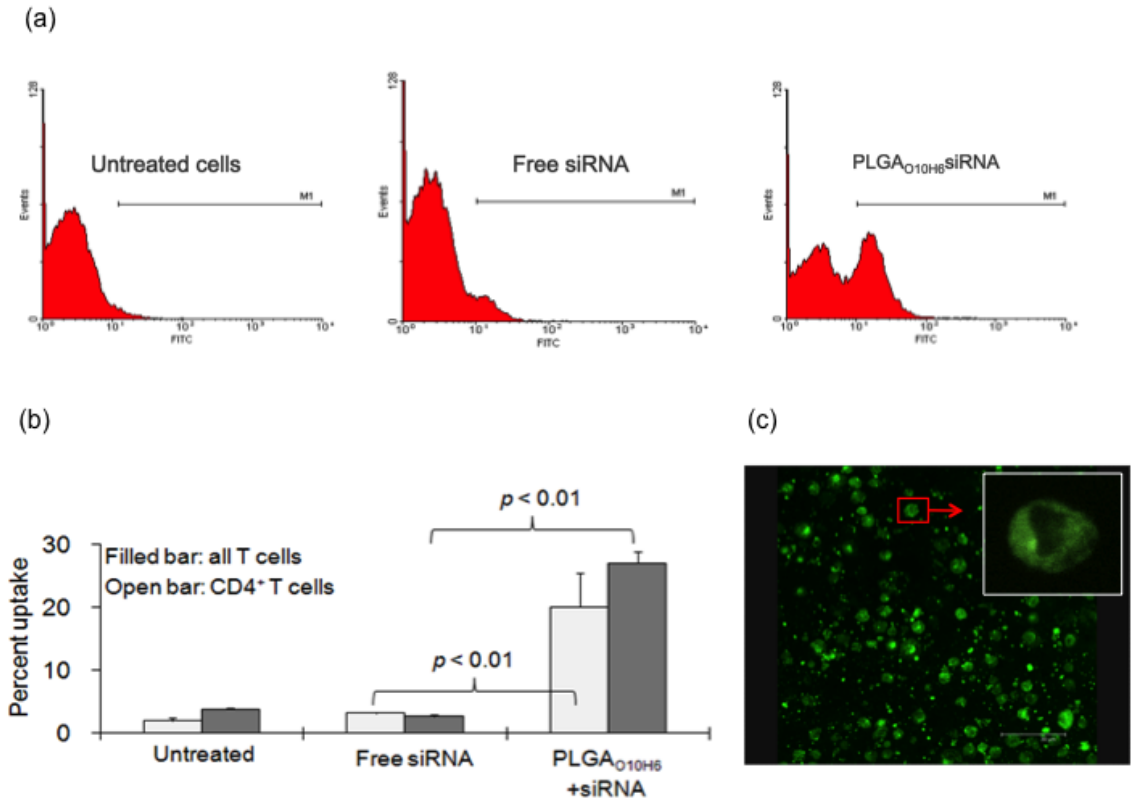

Figure 7-10: Evidence of siRNA (fluorescein labeled) in mouse T cells. (a) Histograms from a representative experiment of flow cytometric analyses. (b) Statistical analysis of data from three independent experiments. Error bars represent standard error of mean. (c) Confocal images of mouse splenic T cells exposed to PLGA$_{O10H6}$-siRNA. Primary mouse spleen T cells were incubated with PLGA$_{O10H6}$-siRNA particles for 4 hours at 37°C. Images were captured by a Leica confocal microscope at 63× magnification.

In vivo function of $PLGA_{O10H6}$-Foxp3siRNA particles in mouse B16 melanoma tumor model

B16 tumor-bearing C57BL/6 mice were treated with $PLGA_{O10H6}$-Foxp3siRNA particles. Spleen T cells were taken from these mice and fluorescently stained for CD4, CD25 and Foxp3. Flow cytometric analysis showed that Treg cells, measured based on cells expressing a high level of CD25, decreased from 24% to 14% in splenic CD4+ T cells. While measured based on intracellular expression of Foxp3, Treg cells decreased from 14% to 11% in CD4+CD25+ cells, figure 7-11 c. RT-PCR analysis (figure 7-11 d) showed that Foxp3 transcripts were downregulated about 50% in CD4+ spleen T cells isolated from these mice. Negative RNA that does not target any endogenous transcript was used as a control for nonspecific effects on gene expression caused by introducing any siRNA.

In figure 7-12, retarded tumor growth was observed in mice subjected to $PLGA_{O10H6}$ complexed with Foxp3 siRNA. Although the tumor would grow out eventually, the growth was delayed at the primary phase. Particles were injected when lesions were visible (5-7 days after B16 inoculation). It is envisioned that the regimen would be effective as an adjuvant when combined with cancer vaccines or chemotherapy. Mice administered with the particles or particles complexed with the siRNA showed no overt signs of acute toxicities.

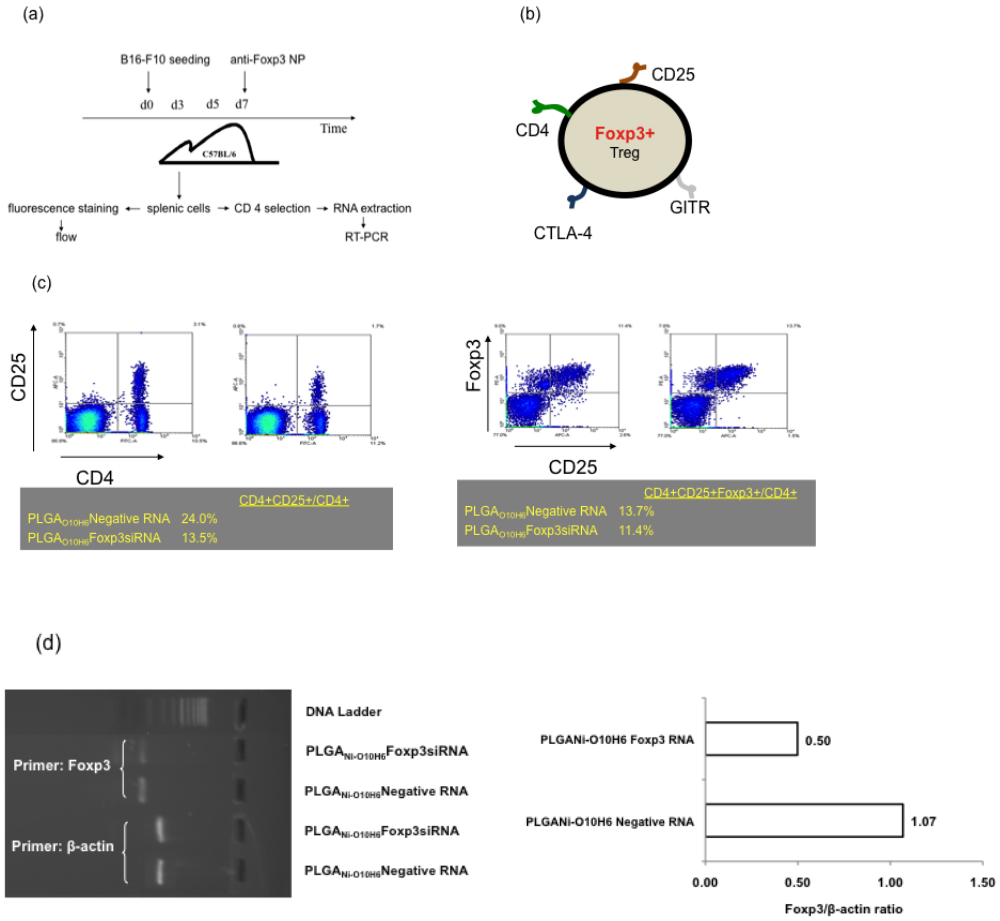

Figure 7-11: In vivo effects of PLGA$_{O10H6}$-Foxp3 siRNA particles. (a) Schematic of in vivo function study. (b) Surface and intracellular molecules expressed by Treg cells. (c) Flow cytometric analysis showed that CD4+CD25^{high} T cells and CD4+ CD25+Foxp3+ T cells were down regulated in vivo. (d) Foxp3 mRNA expression in spleen CD4+ T cells taken from PLGA$_{O10H6}$- siRNA treated mice. Bands identified were consistent with predicted PCR products of Foxp3 and β-actin at 221 and 302 bp, respectively. Negative RNA, that does not target any endogenous transcript, was used as a control for nonspecific effects on gene expression caused by introducing any siRNA.

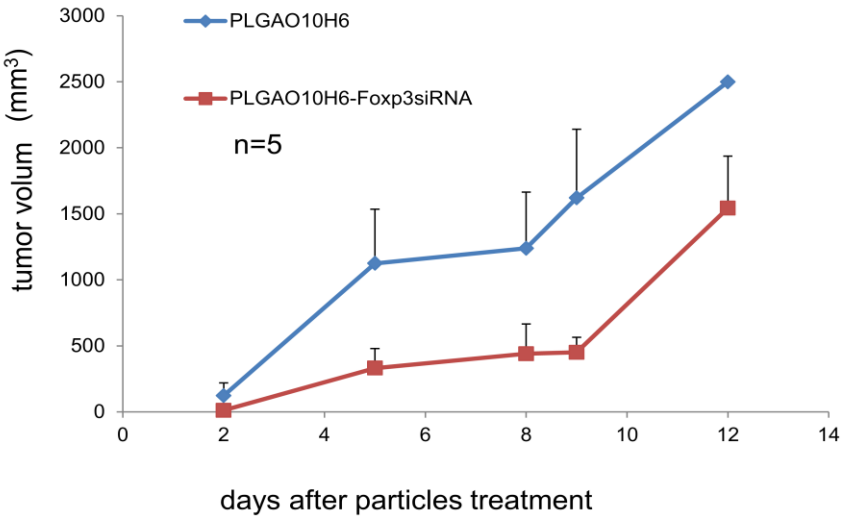

Figure 7-12: B16 melanoma tumor growth in mice treated with Foxp3siRNA-loaded or empty particles. Each experimental group consisted of five mice. Error bars represent standard error of mean. The difference between the two groups is not statistically significant (p=0.137). In the group treated with $PLGA_{O10H6}$-Foxp3siRNA, 5µg siRNA were used for each mouse.

SUMARRY AND CONCLUSIONS

The present study shows that efficient delivery of ODN into primary DCs can be achieved with $PLGA_{O10H6}$-ODN. The change in the zeta potentials and the infrared reflectance analysis indicate the presence of both O10H6 and ODN in the particles (figure 7-3 and 7-4). The colloidal nature of the particles suggests the system is a stable formulation. The combination of PLGA and O10H6 in particle formation is superior to PLGA or with O10H6 alone in the delivery of ODN (figure 7-5 and 7-6). Importantly, internalized ODN can escape from lysosomal degradation, suggesting that effective concentration can be attained in the cytosol (figure 7-7). In conclusion, the physical characteristics and cellular uptake of DNA loaded particulates fabricated with PLGA and O10H6 were reported. This unique combination should be further investigated for developing carriers of DC modulators.

In the delivery of Foxp3 specific siRNA, the change in surface zeta potential and electrophoretic pattern of the complexes indicated adsorption of the RNA onto the $PLGA_{O10H6}$ particles (figure 7-8). The size of the RNA-loaded particles remained below 300 nm in hydrodynamic diameter. Additionally, $PLGA_{O10H6}$ particles protected siRNA from serum digestion (figure 7-9). Confocal and flow cytometric analyses showed the particles assisted uptake of RNA into primary mouse T cells (figure 7-10). Mice administered with Foxp3-siRNA complexed with the particles had lower frequency of Treg cells (figure 7-11 c) and decreased expression of Foxp3 transcripts (figure 7-11 d). Early results revealed that intra-tumoral injection of the Foxp3-siRNA particles caused a delay in B16 tumor growth in mice (figure 7-12). In conclusion, the polymeric particle $PLGA_{O10H6}$ facilitated the delivery of siRNA in primary mouse T cells. When complexed

with $PLGA_{O10H6}$, Foxp3 specific siRNA is effective in down-regulation the level of Foxp3 *in vivo*.

CHAPTER 8

SUMMARY, CONCLUSIONS AND FUTURE DIRECTIONS FOR: A PEPTIDE-BASED PLATFORM FOR DISPLAYING ANTIBODIES TO ENGAGE T CELLS

In this work, I investigated the EAK-EAKH6 composite as a mAb-displaying platform and a potential nucleic acids delivery system. In this concluding narrative, I summarize the main findings from the aforementioned studies and share some of my thoughts in the next step in advancing the concept towards application.

A series of experimental studies were performed to test the concept that assembly of amphiphilic peptides could be exploited biomedically through functionalization. Chapter 4 contains data showing integration of EAKH6 into the EAK structures. When the mixture of EAK and EAKH6 was exposed to physiological concentration of salts solution, e.g. PBS, an insoluble, gel-like structure formed. Whereas EAKH6 itself remained in solution, about 50% of the EAKH6 was removed from the solution when mixed with EAK. The composite was found to be stable at 37°C for at least 7 days. Upon establishing the EAK-EAKH6 composite with H6 domains for binding, Chapter 5 sets out to determine whether this design can be used to load mAb to the peptide assembly. rpAG proved to be a reliable adapter to link anti-H6 antibody and capture mAb. The data show unequivocally immobilization of mAb onto the EAK-EAKH6. Importantly, the construct could be formed *in vivo*; aggregates displaying a fluorescent-labeled mAb could be observed when a mixture of EAK, EAKH6, rpAG, anti-H6 and IgG (PE) dissolved in water was injected subcutaneously next to a tumor in a mouse. The anti-CD4 construct was shown to capture CD4 positive cells in a mixture of mouse

lymphocytes. Collectively, the results indicate that the insoluble peptide structure can cluster mAb in which the antigen-binding function remains intact. This work thus raises the prospect of using EAK-EAKH6 as an antibody delivery platform to modulate immune cells inside or near pathogenic locales. The "reversed drug targeting" concept, to be elaborated below, requires a mechanism to build a reservoir of drug molecules for co-localization with captured cells. To this end, polymeric particles were explored as drug loading mechanisms (Chapter 7).

Monoclonal antibodies have emerged over the past decade into a mainstay of therapeutic options for a wide range of diseases, including autoimmunity, inflammation, cancer and organ transplantation. However, the clinical efficacy of therapeutic antibodies is limited. It is caused by short serum half-life, systemic side effects, or lack of effector functions which are Fc-mediated antibody properties that involved in target cell destruction: antibody-dependent cell-mediated cytotoxicity (ADCC), antibody-dependent cellular phagocytosis (ADCP) and complement-dependent cytotoxicity (CDC). As an alternative, additional functions can be endowed on antibodies by conjugation to other drugs. In cancer therapy, antibodies or the antigen binding fragments (Fab) can be conjugated with radioactive isotopes, chemotherapeutics, toxins or the surface of drug-loaded particles/liposomes to create highly targeted agents.[2] In diagnostic techniques, antibodies are conjugated to light-active molecules, e.g. quantum dots[160], for live imaging. Additionally, drugs conjugated to insulin receptor antibodies can achieve significant brain delivery through receptor-mediated transport.[161] However, using immobilized mAb to capture cells has not been examined extensively. This strategy could potentially provide a novel application of mAb, by which the limitations of rapid

degradation and poor tissue penetration can be avoided. Although this approach is restricted to cell surface molecule specific antibodies; and the target cells have to be leukocytes that are capable of migrating via diffusion, it suggests a new idea to design and use mAb.

Self-assembling peptides have been explored extensively for drug delivery, including small molecules and proteins. Most of them are loaded by physically mixing with the peptides; therefore the release kinetics are significantly varied due to various interactions (could be electrostatic interaction or hydrophobic interaction) between the drugs and the peptides. To achieve controlled delivery, self-assembling peptides can be biotinylated, which allows binding with high affinity to any molecule (such as a protein) that can be biotinylated using strepavidin.[73] However, typical conjugation methods require the use of organic solvents, resulting in at least partial denaturation detrimental effects on the biological activity of themacromolecules. Self-assembling peptides can also deliver signals by fusion proteins designed with incorporating proteins at the N- or C-terminus of the sequence of self-assembling peptides by a linker sequence.[74] This method is limited due to lack of versatility, since each peptide-drug conjugate would have to be custom synthesized. Our work demonstrated that H6 domain could be introduced into the EAK assembly as a way to introduce binding sites. Thus the points of functionalization are an integral part of the structure. This strategy confers a degree of flexibility, for the specificity of the construct can be readily changed by simply using a different mAb. The most promising aspects are the injectability of all components as a solution and the reconstitution of the structure in vivo.

Abnormally skewed lymphocytes populations have been reported in cancer patients. Although the primary solid tumor can be removed by surgery or killed by chemotherapy, the tumor-favored trend still exists in the patient's immune system, which allows the reoccurrence of the tumor, or even worse, metastasis. This work suggested an immune-focused strategy as a potential post-surgery treatment to reduce the incidence of reoccurrence, rather than directly target the tumor cells.

The demonstrated ability to capture cells is an important validation. Conventionally "targeted drug delivery" refers to chemical (e.g. ligand) or physical (e.g. magnetic)-guided localization of agents to diseased tissues (e.g. tumor). However, T cells are usually widely distributed in the pathogenic sites and difficult to be targeted. It has been reported that less than 5% of the entire tumor cellularity are infiltrated lymphocytes.[41] Therefore, the traditional drug delivery may not work efficiently. Taking the advantage that a specific subset T cells could be congregated in the peptide structure, we herein suggest a new concept of reversed drug targeting. In this reversed approach, the drugs are immobilized while the target cells are brought to the drugs. Even the antibody is not potent enough to cause the target cells destructed; other therapeutics can be pre-loaded to the peptide assembly. In the work of Chapter 7, we employed PLGA particles as delivery vectors for nucleic acids to DCs and T cells. These PLGA particles could be decorated with nickel by incorporating Ni-NTA-DOGS in the primary polymer solution. These $PLGA_{Ni}$ particles have been tested in a study described in chapter 9. It would be of great interest to load $PLGA_{Ni}$ particles as drug carriers onto the EAK-EAKH6 composite through coordination with the H6 domain. With each component characterized, it is thus

possible to develop a system to test the concept of reversed drug targeting by bringing specific cells (via mAb) to a reservoir of drug molecules (particles).

CHAPTER 9

The experiments described below were part of a separate project concerning genetic modification of allogeneic transplant tissues. The study lies outside the scope of the main thesis described in the chapters above but nevertheless represents an element in of my graduate work.

MODULATION OF ALLOGRAFT IMMUNOGENICITY WITH IL-10 GENE PARTICLES

INTRODUCTION

More than 20,000 patients undergo solid organ transplantation every year in the U.S (source: Organ Procurement and Transplantation Network: http://optn.transplant.hrsa.gov/). Organ transplantation improves the quality of life for patients suffering from otherwise incurable diseases, including those of cardiovascular nature and malignancies. Inhibitors of T cell receptor signaling (e.g. tacrolimus) represent the mainstay in managing transplant rejection.[162-164] These agents exert their therapeutic effects by dampening the cytolytic actions of all T cells. Patients exposed to these drugs chronically have increased risks of developing opportunistic infections and malignancies.[164] Consequently, transplant recipients rarely live to normal life expectancy. In most cases, the initial encounter between the allograft and recipient's immune system dictates the outcome. Attenuating acute rejection improves the long-term viability and function of the transplant. The time between organ harvest and implantation provides an opportunity to modulate the immunogenicity of the allograft, prior to encountering recipient's T cells *in vivo*. We envision that during the transit period (up to 24 hours), between organ harvest

and implantation, gene treatment can be applied as an *ex vivo* intervention to generate selective immunosuppression. The health impact of the proposed research lies in developing new strategies enabling tapered use of non-specific immunosuppressive drugs in transplant recipients by reducing the incidence and severity of acute rejection.

Interleukin-10 (IL-10) is an anti-inflammatory cytokine that has been used to induce allograft tolerance in animal models. IL-10 regulates the functions of neutraphils, mast cells, T cells, macrophages, and other tissues,[165] but the protective effect of the cytokine on allografts is mediated primarily through DCs.[166-168] DCs cultured with IL-10 have been shown to impair the ability of T cells to produce INF-γ,[169] a cytokine that drives the killing function of cytotoxic T cells (CTLs). In vivo, protection of allgrafts by IL-10 producing DCs often develops concomitantly with the expansion of Treg cells.[170-172] Treg cells restrain the proliferation and activation of CTLs.[173] Suppressive function of Treg cells are mediated by TGF-β[174] and CTLA-4.[175] In mice, Treg cells inhibit migration of CTLs from draining lymph nodes to allografts.[176] Foxp3+ cells have been found in accepted allografts[177] and in lymph nodes of animals with long-lived transplants.[178] Because of Treg cells' potential to curtail allograft rejection, the success of the *ex vivo* IL-10 gene treatment will be measured based on Foxp3 expression in recipient T cells.[118, 179-182] Because of DCs' ability to dictate the activities of naive T cells, protection of allografts can be achieved by inducing DCs to produce IL-10 to inhibit T cells activation in transplant recipients.[117, 183] IL-10-producing DCs have been tested as cellular therapy in transplant models.[183, 184] From a logistical standpoint, *ex vivo* treatment of allografts is superior to cellular therapy using the patient's own DCs.

Genetic modification of DCs to express anti-inflammatory cytokines is proposed as a strategy to mitigate transplant rejection.[185-187] A current challenge is to develop effective methods to transfer immunosuppressive cytokine genes into DCs without using viruses. Compared to chemical methods, viral vectors generally confer superior transfection efficiency, but humoral and cell-mediated immune responses triggered by viral components can interfere with the inhibitory actions of IL-10.[188] Non-viral systems are less immunogenic; but it was thought that DCs do not divide in situ and thus refractory to non-viral methods of transfection without the aid of pro-inflammatory stimuli.[189, 190] Data emerging in the past three years, however, have challenged this assumption. Using live-cell imaging techniques, it has been demonstrated that up to 5% of mouse DCs undergo division *in vivo*.[191, 192] Similarly, 2-3% of human DCs are proliferating in situ at any given time.[191] The fact that DCs undergo proliferation when residing in tissue makes it possible for in situ gene transfer in DCs using non-viral means.

Studies performed previously in our lab show that PLGA modified with the cationic peptide O10H6 ($PLGA_{O10H6}$) were effective in delivering a mouse IL-10 encoding plasmid (pIL-10) to skew bone marrow-derived DCs to downregulate T cell responses. T cells stimulated by the IL-10 gene-modified DCs exhibited characteristics of Treg cells, as evident by upregulation of Foxp3 transcription factor concomitant with an increase in TGF-β production. It can therefore be concluded that $PLGA_{O10H6}$ complexed with pIL-10 delivered an overriding suppressive signal to T cells. Physical characterization of $PLGA_{O10H6}$-pIL-10 revealed a stable colloidal dispersion. DNA molecules carried by $PLGA_{O10H6}$ were protected from serum digestion.[193] To obtain a stronger binding mechanism with O10H6, nickel ions were incorporated into the matrix of PLGA particles

using the metal chelating lipid DOGS-NTA-Ni. These particles were referred to as $PLGA_{Ni}$ particles. Binding of O10H6 raised the surface potential of $PLGA_{Ni}$ from -17mv to +13mv. This change was partially reserved by the presence of free imidazole, suggesting the binding was mediated by nickel-histidine coordination. When compared to PLGA particles without nickel (40.8%), ODN bound to O10H6 coated $PLGA_{Ni}$ particles ($PLGA_{Ni\text{-}O10H16}$) exhibited enhanced capacity (71.9%) to accumulate in DCs cultured *in vitro*. DCs exhibited cellular stress after exposure to $PLGA_{Ni\text{-}O10H16}$-DNA, but this effect can be prevented by serum and was reversed overnight.[194]

In this chapter, $PLGA_{Ni\text{-}O10H16}$ particles were used to carry pIL-10 to reduce the immunogenicity of skin allografts. The presence of DCs in skin explants was confirmed by MHC-II antibody staining. Successful transfection was evidenced by the increased IL-10 release. Reduced immunogenicity was shown by lower INF-γ production in co-culture of skin grafts with allogeneic T cells.

MATERIALS AND METHODS

Plasmid and $PLGA_{Ni\text{-}O10H6}$-pIL-10 complexation

Plasmid encoding murine IL-10 (figure 9-1, pUMVC3-mIL10; 4563 bp) was obtained from Aldevron (Fargo, ND, USA), aliquot in distilled water and stored in -80°C until use. The IL-10 gene in this vector is driven by the cytomegalovirus promoter/enhancer with trimmed intron A and a rabbit β-globin polyadenylation signal.

$PLGA_{Ni}$ particles were prepared using a double emulsion (w/o/w) solvent evaporation method, which was described in chapter 7, with metal chelating lipid DOGS-NTA-Ni incorporated in the polymer $MeCl_2$ solution. Briefly, 90mg PLGA and 0.6 mg DOGS-NTA-Ni were dissolved in 3 ml $MeCl_2$. To this organic phase 200µl ddH_2O was added and sonicated (24W) for 2 min. The resultant primary emulsion was added drop wise with energy input again (24W, 4min) to 20 ml of ddH_2O and the resulting mixture was allowed to evaporate for 4 h to remove $MeCl_2$. Particles were washed twice in ddH_2O and recovered by centrifugation. Plasmid loading was accomplished by first coating the particles (30µl from 4.5mg/ml stock) with O10H6 (60µg) followed by addition of plasmids (pIL-10, 5µg) in 300µl ddH_2O.

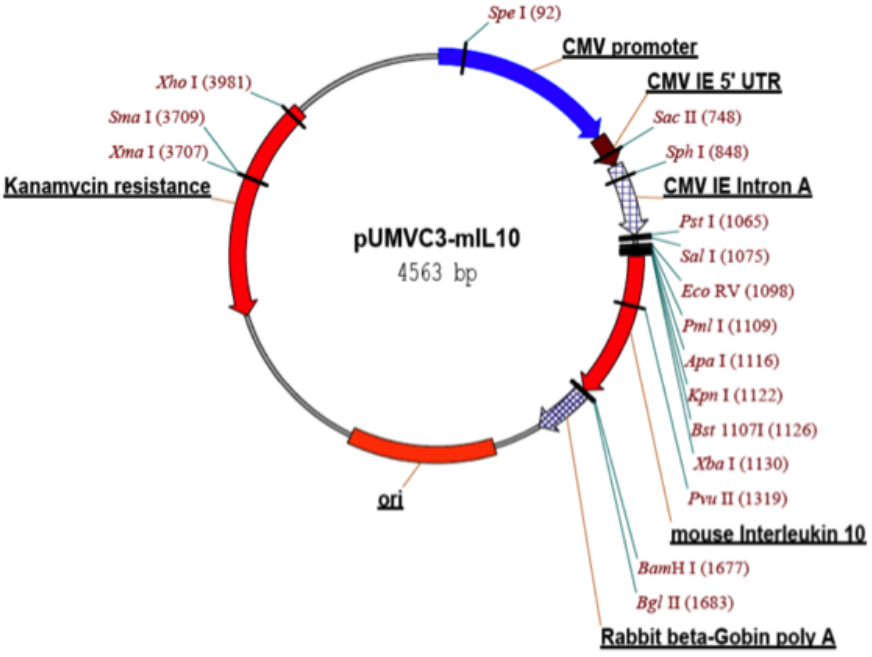

Figure 9-1: Mammalian expression vector for mouse IL-10. (obtained from Aldevron, Fargo, ND.)

Generation of skin explants and IL-10 gene transfer

Donor skin was harvested from euthanized Balb/c mouse by cutting eat off at base. Ventral and dorsal sides of tissue at base of ear were gently pulled apart. The dorsal tissue was collected with internal surface down in serum free OptiMEM media (Invitrogen, OR, USA). To visualize the DCs in dorsal sheets, PE (phycoerythrin)-conjugated I-A^d antibody was added to stain the MHC-II molecules expressed on the surface of DCs. $PLGA_{Ni\text{-}O10H6}$-pIL-10 complex was added to the cultures and incubated for 2 hours at 37°C in 5% CO_2. Media were then removed and replaced with fresh complete RPMI 1640 (Mediatech, VA, USA) containing 10% FBS and GM-CSF/ IL-4 (R&D Systems, Minneapolis, MN).

Co-culture of skin grafts with allogeneic T cells and ELISA

As the schematic shown in figure 9-2, transfected skin grafts were cultured with splenocytes of mismatched mice C57BL/6 (H-2^b). The splenocytes were depleted of red blood cells and monocytes prior to co-culture. 1×10^6 T cells were seeded with each skin graft in 1 ml complete AIM V medium (Invitrogen, OR, USA) and incubated for 24 hours in a humidified 37°C, 5% CO_2 incubator. Concentrations of IL-10 and INF-γ were determined in the culture supernatants using the ELISA DuoSet kit (R&D Systems, MN, USA) according to the manufacturer's protocol.

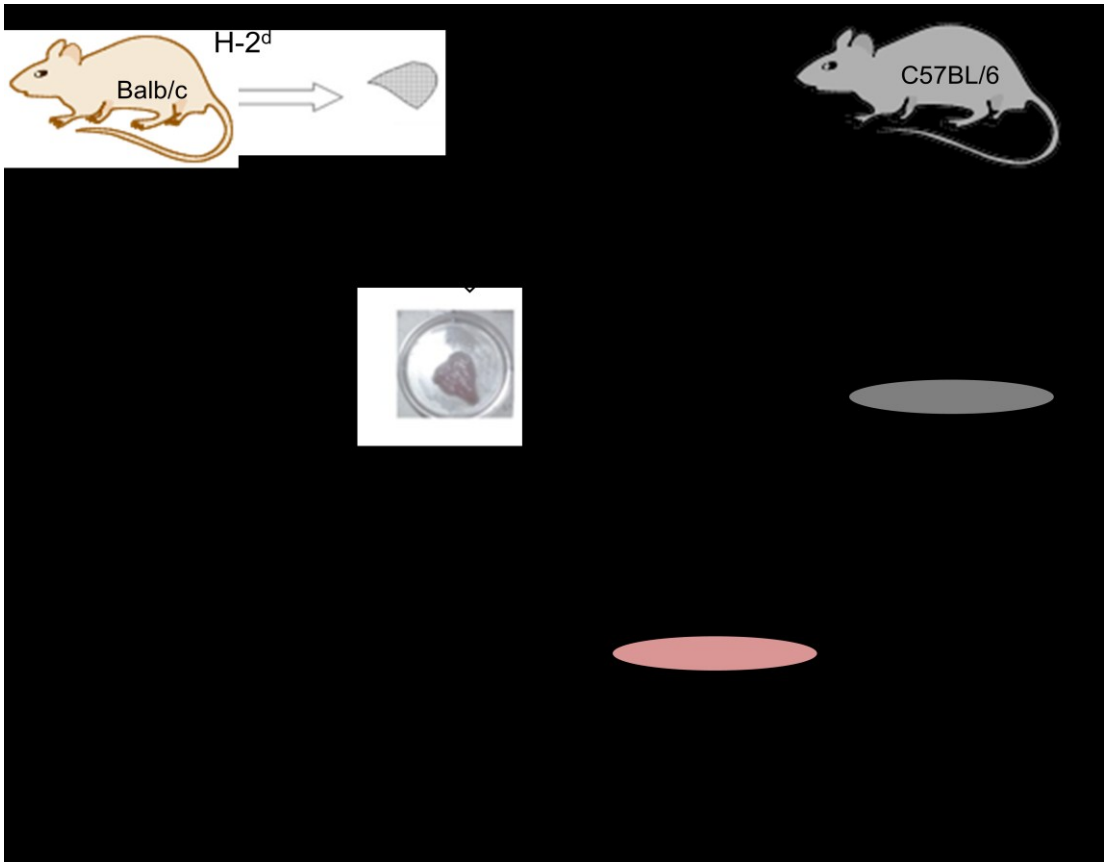

Figure 9-2: Schematic of co-culture of skin grafts and allogeneic T cells.

RESULTS AND DISCUSSION

Under confocal microscope, the presence of DCs in dorsal sheets isolated from mouse ear skins was demonstrated using red fluorescent-conjugated antibodies specific to the MHC-II molecule I-A^d expressed only on DCs and DC-like cells (figure 9-3 a). Successful transfection was evidenced in the increased IL-10 release by the explants. A 2-fold increase (p=0.0002) in IL-10 expression was found in skin cultures transfected with $PLGA_{Ni\text{-}O10H6}$-pIL-10 compared to control plasmid (figure 9-3 b). Reduced immunogenicity is shown by lower INF-γ production by allogeneic T cells mixed with skin exposed to $PLGA_{Ni\text{-}O10H6}$-pIL-10. More than 5-fold higher INF-γ (p=0.001) was found in T cells stimulated by skin explants transfected with $PLGA_{Ni\text{-}O10H6}$ complexed with control plasmid compared to those transfected with $PLGA_{Ni\text{-}O10H6}$-pIL-10 (figure 9-3 c). In the same skin-T cell cultures, higher level (2-fold difference, p=0.005) of IL-10 was produced when the IL-10 gene particles were applied compared to when a control plasmid was used (figure 9-3 d). These results show a definitive inhibitory state of donor DCs, and support that the IL-10 gene particles can reduce immunogenicity of the allograft *in vivo*.

The principle targets of the immune response to allogeneic grafts are the MHC molecules, which are highly polymorphic within species. Since laboratory mice are inbred, each strain is homozygous and has a unique halotype. For example, the MHC haplotype of Balb/c is H-2^d, and C57BL/6 is H-2^b.[4] The recognition of allograft MHC antigen is the primary event that ultimately leads to graft rejection. T cells involved in graft rejection can be sensitized against alloantigens via one of two distinct pathways: direct and indirect. In the direct pathway, organ grafts carry with them APCs of donor

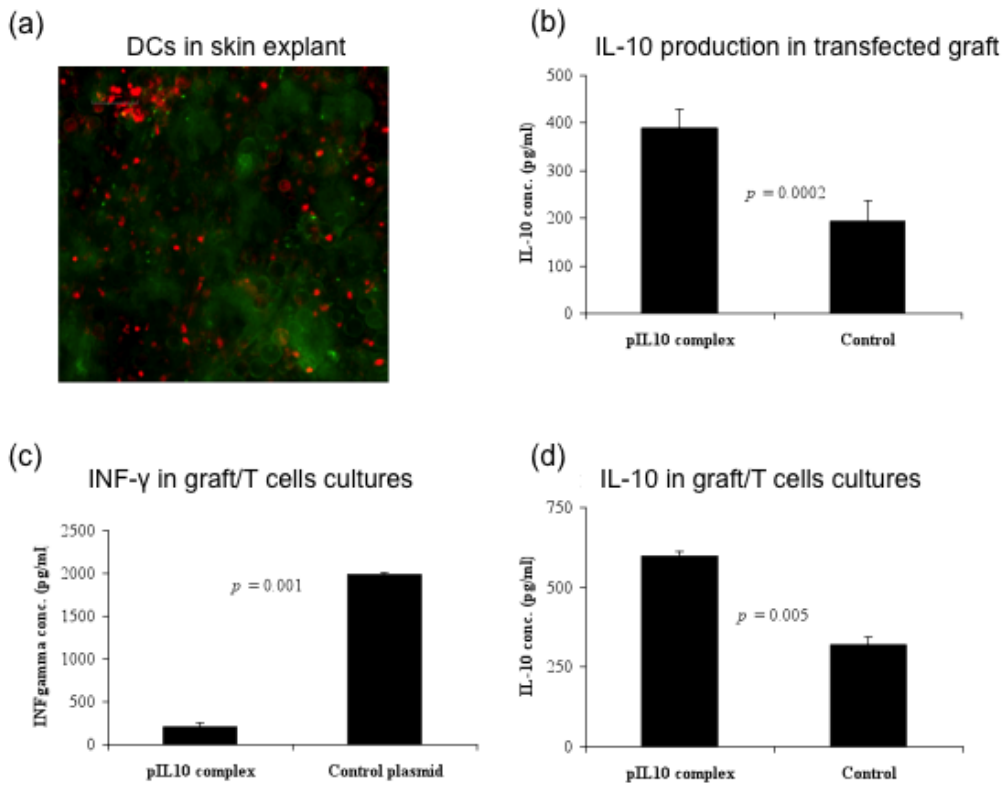

Figure 9-3: Effects of $PLGA_{Ni\text{-}O10H6}$-pIL-10 particles on the immunogenicity of intact skin explants. Excised mouse ears (BALB/c) were rinsed with 70% ethanol and split into dorsal and ventral halves. Dorsal halves were cultured in OptiMem media and subsequently exposed to $PLGA_{Ni\text{-}O10H6}$-pIL-10 particles or a control plasmid. After transfection skin, explants were incubated in culture medium for 48 h prior to mixing with T cells for an additional 24 h. The skin explants contain high density of DCs (384/mm^2; enumerated using a Zeiss AxioObserver Z1 inverted microscope), as indicated by a phycoerythrin (red) anti-BALB/c MHC-II antibody with parenchmyal cells countered stained with fluorescein (a). Supernatants from skin (b) and skin-T cell cultures (d) were analyzed for IL-10 concentration and in the latter case INF-γ release as well (c). Student's t-test was used to determine statistical significance of the ELISA results. Detection limits of IL-10 and INF-γ ELISA were 4 pg/ml and 15 pg/ml, respectively.

origin. These APCs leave the graft and migrate via the lymph to regional lymph nodes, activate those host T cells that bear the corresponding T-cell receptor. The activated alloreactive effector T cells are then carried back to the graft, which they attack directly. The ligand of the alloreactive T cell is the allogeneic MHC molecule itself. A second mechanism leading to graft rejection is the uptake of allogeneic proteins by the recipient's own APCs and their presentation to T cells by self-MHC molecules. This way is known as indirect allorecognition. Direct allorecognition is thought to be largely responsible for acute rejection, especially when MHC mismatches mean that the frequency of directly alloreactive recipient T cell is high.[195, 196] Therefore, genetic modification of donor DCs to express immunomodulatory molecules represents an effective strategy to prolong graft survival.

When the naive T cells from C57BL/6 (H-2^b) are exposed to mismatched Balb/c (H-2^d) DCs in the skin grafts, they are activated to undergo proliferation, differentiation and production of effector molecules. Among them is a main cytokine INF-γ released by CD8 effector T cells and T_H1 cells. Hence the expression level of INF-γ is a good quantitative index of the extent of host T cells can be activated. The results showed in figure 9-3 indicate a significantly decreased mixed reaction between host T cells and donor DCs by transfected with pIL-10. A possible protection regimen for skin grafts by $PLGA_{Ni\text{-}O10H6}$-pIL-10 is suggested.

REFERENCES

1. Chan, A.C. and p.J. Carter, *Therapeutic antibodies for autoimmunity and inflammation.* Nature Reviews. Immunology, 2010. **10**(5): p. 301-316.
2. Weiner, L.M., R. Surana, and S. Wang, *Monoclonal antibodies: versatile platforms for cancer immunotherapy.* Nature Reviews. Immunology, 2010. **10**(5): p. 317-327.
3. Weber, J., *Overcoming immunologic tolerance to melanoma: targeting CTLA-4 with ipilimumab (MDX-010).* The Oncologist, 2008. **13**(suppl 4): p. 16-25.
4. Janeway, C.A., et al., *Immuno Biology, the immune system in health and disease*. 6th ed: Garland Science Publishing.
5. Curiel, T.J., *Regulatory T cells and treatment of cancer.* Current Opinion in Immunology, 2008. **20**(2): p. 241-246.
6. Onizuka, S., et al., *Tumor rejection by in vivo administration of anti-CD25 (interleukin-2 receptor alpha) monoclonal antibody.* Cancer Research, 1999. **59**(13): p. 3128-3133.
7. Sutmuller, R.P.M., et al., *Synergism of cytotoxic T lymphocyte-associated antigen 4 blockade and depletion of CD25(+) regulatory T cells in antitumor therapy reveals alternative pathways for suppression of autoreactive cytotoxic T lymphocyte responses.* The Journal of Experimental Medicine, 2001. **194**(6): p. 823-832.
8. Weber, J., *Ipilimumab: controversies in its development, utility and autoimmune adverse events.* Cancer Immunology, Immunotherapy : CII, 2009. **58**(5): p. 823-830.

9. Zhang, S., et al., *Zuotin, a putative Z-DNA binding protein in Saccharomyces cerevisiae.* The EMBO Journal, 1992. **11**(10): p. 3787-3796.

10. Zhang, S., et al., *Spontaneous assembly of a self-complementary oligopeptide to form a stable macroscopic membrane.* Proceedings of the National Academy of Sciences. USA, 1993. **90**: p. 3334-3338.

11. Zhang, S., et al., *Unusually stable β-sheet formation in an ionic self-complementary oligopeptide.* Biopolymers, 1994. **34**: p. 663-672.

12. Holmes, T.C., et al., *Extensive neurite outgrowth and active synapse formation on self-assembling peptide scaffolds.* Proceedings of the National Academy of Sciences of the United States of America, 2000. **97**(12): p. 6728-6733.

13. Köhler, G. and C. Milstein, *Continuous cultures of fused cells secreting antibody of predefined specificity.* Nature 1975. **256**(5517): p. 495-497.

14. Schroeder, H.W.J. and L. Cavacini, *Structure and function of immunoglobulins.* The Journal of Allergy and Clinical Immunology, 2010. **125**(2): p. s41-s52.

15. Zola, H., et al., *CD molecules 2006 — Human cell differentiation molecules.* Journal of Immunological Methods, 2007. **319**(1-2): p. 1-5.

16. Mattes, M.J., *Binding parameters of antibodies: pseudo-affinity and other misconceptions.* Cancer Immunology, Immunotherapy : CII, 2005. **54**(6): p. 513-516.

17. Cuesta, Á.M., et al., *Multivalent antibodies: when design surpasses evolution.* Trends in Biotechnology, 2010. **28**(7): p. 355-362.

18. Plückthun, A. and P. Pack, *New protein engineering approaches to multivalent and bispecific antibody fragments.* Immunotechnology, 1997. **3**(2): p. 83-105.

19. Rudnick, S.I. and G.P. Adams, *Affinity and avidity in antibody-based tumor targeting.* Cancer Biotherapy and Radiopharmaceuticals, 2009. **24**(2): p. 155-161.

20. Todorovska, A., et al., *Design and application of diabodies, triabodies and tetrabodies for cancer targeting.* Journal of Immunological Methods, 2001. **248**(1-2): p. 47-66.

21. Hudson, P.J. and A.A. Kortt, *High avidity scFv multimers; diabodies and triabodies.* Journal of Immunological Methods, 1999. **231**(1-2): p. 177-189.

22. Bongini, L., et al., *A dynamical study of antibody-antigen encounter reactions.* Physcial Biology, 2007. **4**(3): p. 172-80.

23. Nygren, H. and M. Stenberg, *Immunochemistry at interfaces.* Immunology, 1989. **66**(3): p. 321-327.

24. Miaczynska, M. and H. Stenmark, *Mechanisms and functions of endocytosis.* The Journal of Cell Biology, 2008. **180**(1): p. 7-11.

25. Brown, W.M., *Anti-CD3 antibody MacroGenics Inc.* Current Opinion in Investigational Drugs, 2006. **7**(4): p. 381-388.

26. Weber, J., *Review: anti-CTLA-4 antibody ipilimumab: case studies of clinical response and immune-related adverse events.* The Oncologist, 2007. **12**(7): p. 864-872.

27. Mosmann, T.R., et al., *Two types of murine helper T cell clone. I. Definition according to profiles of lymphokine activities and secreted proteins.* The Journal of Immunology, 1986. **136**(7): p. 2348-2357.

28. Pardoll, D., *Metastasis-promoting immunity: when T cells turn to the dark side.* Cancer Cell, 2009. **16**(2): p. 81-82.

29. Murphy, K.M. and B. Stockinger, *Effector T cell plasticity: flexibility in the face of changing circumstances.* Nature Immunology, 2010. **11**(8): p. 674-680.

30. Zhu, J. and W.E. Paul, *Heterogeneity and plasticity of T helper cells.* Cancer Research, 2010. **20**(1): p. 4-12.

31. Harrington, L.E., et al., *Interleukin 17-producing CD4+ effector T cells develop via a lineage distinct from the T helper type 1 and 2 lineages.* Nature Immunology, 2005. **6**(11): p. 1123-1132.

32. Park, H., et al., *A distinct lineage of CD4 T cells regulates tissue inflammation by producing interleukin 17.* Nature Immunology, 2005. **6**(11): p. 1133-1141.

33. Sakaguchi, S., *Naturally arising Foxp3-expressing CD25+CD4+ regulatory T cells in immunological tolerance to self and non-self.* Nature Immunology, 2005. **6**(4): p. 345-352.

34. McCune, J.M., *The dynamics of CD4+ T-cell depletion in HIV disease.* Nature, 2001. **410**(6831): p. 974-979.

35. Veldhoen, M., *The role of T helper subsets in autoimmunity and allergy.* Current Opinion in Immunology, 2009. **21**(6): p. 606-611.

36. Dubin, P.J. and J.K. Koll, *Th17 cytokines and mucosal immunity.* Immunological Reviews, 2008. **226**(1): p. 160-171.

37. O' Quinn, D.B., et al., *Emergence of the Th17 pathway and its role in host defense.* Advance in Immunology, 2008. **99**: p. 115-163.

38. Zou, W. and N.P. Restifo, *T(H)17 cells in tumour immunity and immunotherapy.* Nature Reviews. Immunology, 2010. **10**(4): p. 248-256.

39. Bacchetta, R., E. Gambineri, and M.-G. Roncarolo, *Role of regulatory T cells and FOXP3 in human diseases.* The Journal of allergy and clinical immunology, 2007. **120**(2): p. 227-235.

40. Zou, W., *Regulatory T cells, tumor immunity and immunotherapy.* Nature Reviews. Immunology, 2006. **6**(4): p. 295-30.

41. Valzasina, B., et al., *Tumor-induced expansion of regulatory T cells by conversion of CD4+CD25- lymphocytes is thymus and proliferation independent.* Cancer Research, 2006. **66**(8): p. 4488-4495.

42. Colombo, M.P. and S. Piconese, *Regulatory-T-cell inhibition versus depletion: the right choice in cancer immunotherapy.* Nature Reviews. Cancer, 2007. **7**(11): p. 880-887.

43. Shevach, E.M., *CD4+ CD25+ suppressor T cells: more questions than answers.* Nature Reviews. Immunology, 2002. **2**(6): p. 389-400.

44. Sakaguchi, S., et al., *Immunologic self-tolerance maintained by activated T cells expressing IL-2 receptor alpha-chains (CD25). Breakdown of a single mechanism of self-tolerance causes various autoimmune diseases.* The Journal of Immunology, 1995. **155**(3): p. 1151-1164.

45. Shevach, E.M., *Mechanisms of foxp3+ T regulatory cell-mediated suppression.* Immunity, 2009. **30**(5): p. 636-645.

46. Ise, W., et al., *CTLA-4 suppresses the pathogenicity of self antigen-specific T cells by cell-intrinsic and cell-extrinsic mechanisms.* Nature Immunology, 2010. **11**(2): p. 129-135.

47. Kirkwood, J.M., et al., *Next generation of immunotherapy for melanoma.* Journal of Clinical Oncology, 2008. **26**(20): p. 3445-3455.

48. Zou, W., *Immunosuppressive networks in the tumour environment and their therapeutic relevance.* Nature Reviews. Cancer, 2005. **5**(4): p. 263-274.

49. Dunn, G.P., L.J. Old, and R.D. Schreiber, *The immunobiology of cancer immunosurveillance and immunoediting.* Immunity, 2004. **21**(2): p. 137-148.

50. Ormandy, L.A., et al., *Increased populations of regulatory T cells in peripheral blood of patients with hepatocellular carcinoma.* Cancer Research, 2005. **65**(6): p. 2457-2464.

51. Liyanage, U.K., et al., *Prevalence of regulatory T cells is increased in peripheral blood and tumor microenvironment of patients with pancreas or breast adenocarcinoma.* The Journal of Immunology, 2002. **169**(6): p. 2756-2761.

52. Schaefer, C., et al., *Characteristics of CD4+CD25+ regulatory T cells in the peripheral circulation of patients with head and neck cancer.* British Journal of Cancer, 2005. **92**(5): p. 913-920.

53. Yu, P., et al., *Intratumor depletion of CD4+ cells unmasks tumor immunogenicity leading to the rejection of late-stage tumors.* The Journal of Experimental Medicine, 2005. **201**(5): p. 779-791.

54. Coe, D., et al., *Depletion of regulatory T cells by anti-GITR mAb as a novel mechanism for cancer immunotherapy.* Cancer immunology, immunotherapy : CII, 2010. **59**(9): p. 1367-1377.

55. Jain, R.K., *Delivery of molecular and cellular medicine to solid tumors.* Journal of Controlled Release, 1998. **53**(1-3): p. 49-67.

56. Chen, P., *Self-assembly of ionic-complementary peptides: a physicochemical viewpoint.* Colloids and Surfaces A: Physicochemical and Engineering Aspects, 2005. **261**(1-3): p. 3-24.

57. Zhang, S., *Fabrication of novel biomaterials through molecular self-assembly.* Nature Biotechnology, 2003. **21**(10): p. 1171-1178.

58. Zhao, X. and S. Zhang, *Molecular designer self-assembling peptides.* Chemical Society Review, 2006. **35**(11): p. 1105-1110.

59. Gelain, F., A. Horii, and S. Zhang, *Designer self-assembling peptide scaffolds for 3-d tissue cell cultures and regenerative medicine.* Molecular Bioscience, 2007. **7**(5): p. 544-551.

60. Urry, D.W., *Five axioms for the functional design of peptide-based polymers as molecular machines and materials: Principle for macromolecular assemblies.* Biopolymers (Peptide Sciences), 1998. **47**(2): p. 167-168.

61. Zhang, S., et al., *Self-complementary oligopeptide matrices support mammalian cell attachment.* Biomaterials, 1995. **16**(18): p. 1385-1393.

62. Fung, S.Y., et al., *Concentration effect on the aggregation of a self-assembling oligopeptide.* Biophysical Journal, 2003. **85**(1): p. 537-548.

63. Hong, Y., et al., *Effect of NaCl and peptide concentratio on the self-assembly of an ionic-complementary peptide EAK-II.* Colloids and surfaces. B, Biointerfaces, 2005. **46**(3): p. 152-161.

64. Hong, Y., et al., *Effect of amino acid sequence and pH on nanofiber formation of self-assembling peptides EAK16-II and EAK16-IV.* Biomacromolecules, 2003. **4**(5): p. 1433-1442.

65. Xiong, H., et al., *Periodicity of polar and nonpolar amino acids is the major determinant of secondary structure in self-assembling oligomeric peptides.* Proceedings of the National Academy of Sciences of the United States of America, 1995. **92**(14): p. 6349-6353.

66. Gambaretto, R., et al., *Self-assembling peptides: sequence, secondary structure in solution and film formation.* Biopolymers, 2008. **89**(11): p. 906-915.

67. *BD™ PuraMatrix™ Peptide Hydrogel Guidelines for Use* Available from: http://www.bdbiosciences.com/external_files/dl/doc/manuals/live/web_enabled/354250Lpug.pdf.

68. Segers, V.F.M. and R.T. Lee, *Local delivery of proteins and the use of self-assembling peptides.* Drug Discovery Today, 2007. **12**(13-14): p. 561-568.

69. Nagai, Y., et al., *Slow release of molecules in self-assembling peptide nanofiber scaffold.* Journal of Controlled Release, 2006. **115**(1): p. 18-25.

70. Koutsopoulos, S., et al., *Controlled release of functional proteins through designer self-assembling peptide nanofiber hydrogel scaffold.* Proceedings of the National Academy of Sciences of the United States of America, 2009. **106**(12): p. 4623-4628.

71. Myers, M.W., et al., *The human mid-size neurofilament subunit: a repeated protein sequence and the relationship of its gene to the intermediate filament gene family.* The EMBO Journal, 1987. **6**(6): p. 1617-1626.

72. Hsieh, P.C.H., et al., *Local controlled intramyocardial delivery of platelet-derived growth factor improves postinfarction ventricular function without pulmonary toxicity.* Circulation, 2006. **114**(7): p. 637-644.

73. Davis, M.E., et al., *Local myocardial insulin-like growth factor 1 (IGF-1) delivery with biotinylated peptide nanofibers improves cell therapy for myocardial infarction.* Proceedings of the National Academy of Sciences. USA, 2006. **103**(21): p. 8155-8160.

74. Segers, V.F.M., et al., *Local delivery of protease-resistant stromal cell derived factor-1 for stem cell recuitment after myocardial infarction.* Circulation, 2007. **116**(15): p. 1683-1692.

75. Caplan, M., et al., *Control of self-assembling oligopeptide matrix formation through systematic variation of amino acid sequence.* Biomaterials, 2002. **23**(1): p. 219-227.

76. Kisiday, J.D., et al., *Self-assembling peptide hydrogel fosters chondrocyte extracellular matrix production and cell division: implications for cartilage tissue repair.* Proceedings of the National Academy of Sciences of the United States of America, 2002. **99**(15): p. 9996-10001.

77. Kopesky, P.W., et al., *Self-assembling Peptide hydrogels modulate in vitro chondrogenesis of bovine bone marrow stromal cells.* Tissue Engineering. Part A, 2010. **16**(2): p. 465-477.

78. Branco, M.C. and J.P. Schneider, *Self-assembling materials for therapeutic delivery.* Acta biomaterialia, 2009. **5**(3): p. 817-831.

79. Schneider, J.P., et al., *Responsive hydrogels from the intramolecular folding and self-assembly of a designed peptide.* Journal of the American Chemical Society, 2002. **124**(50): p. 15030-15037.

80. Branco, M.C., et al., *Macromolecular diffusion and release from self-assembled beta-hairpin peptide hydrogels.* Biomaterials, 2008. **30**(7): p. 1339-1347.

81. Rughani, R.V., et al., *Folding, self-assembly, and bulk material properties of a de novo designed three-stranded beta-sheet hydrogel.* Biomacromolecules, 2009. **10**(5): p. 1295-1304.

82. Branco, M.C., et al., *Fast dynamics of semiflexible chain networks of self-assembled peptides.* Biomacromolecules, 2009. **10**(6): p. 1374-1380.

83. Rajagopal, K., et al., *Tuning the pH responsiveness of beta-hairpin peptide folding, self-assembly, and hydrogel material formation.* Biomacromolecules, 2009. **10**(9): p. 2619-2625.

84. Ellis-Behnke, R.G., et al., *Nano neuro knitting: peptide nanofiber scaffold for brain repair and axon regeneration with functional return of vision.* Proceedings of the National Academy of Sciences. USA, 2006. **103**(13): p. 5054-5059.

85. Aggeli, A., et al., *pH as a trigger of peptide beta-sheet self-assembly and reversible switching between nematic and isotropic phases.* Journal of the American Chemical Society, 2003. **125**(32): p. 9619-9628.

86. Riley, J.M., et al., *Bioproduction and characterization of a pH responsive self-assembling peptide.* Biotechnology and Bioengineering, 2009. **103**(2): p. 241-251.

87. Collier, J.H. and P.B. Messersmith, *Enzymatic modification of self-assembled peptide structures with tissue transglutaminase.* Bioconjugate Chemistry, 2003. **14**(4): p. 748-755.

88. Ulijin, R.V. and A.M. Smith, *Designing peptide based nanomaterials.* Chemical Society Reviews, 2008. **37**(4): p. 664-675.

89. Glenner, G.G., E.D. Eanes, and D.L. Page, *The relation of the properties of Congo red-stained amyloid fibrils to the beta-conformation.* The Journal of Histochemistry and Cytochemistry, 1972. **20**(10): p. 821-826.

90. Kirschenbaum, D.M., *Molar absorptivity and A1%/1 cm values for proteins at selected wavelengths of the ultraviolet and visible regions. XI.* Analytical Biochemistry, 1975. **68**(2): p. 465-484.

91. Scopes, R.K., *Measurement of protein by spectrophotometry at 205 nm.* Analytical Biochemistry, 1974. **59**(1): p. 277-282.

92. Khoury, Y.E. and p. Hellwig, *Infrared spectroscopic characterization of copper-polyhistidine from 1,800 to 50 cm(-1): model systems for copper coordination.* Journal of biological inorganic chemistry, 2009. **14**(1): p. 23-34.

93. Loeffen, P.W. and R.F. Pettifer, *Vibrational force field of solid imidazole from inelastic neutron scattering.* The Journal of Chemical Physics, 1995. **103**(19): p. 8444-8455.

94. Ramani, R., et al., *Evidence of PPII-like helical conformation and glass transition in a self-assembled solid-state polypeptide-surfactant complex: poly(L-histidine)/docylbenzenesulfonic acid.* Biomacromolecules, 2008. **9**(5): p. 1390-1397.

95. Murariu, M., E.S. Dragan, and G. Drochioiu, *Model peptide-based system used for the investigation of metal ions binding to histidine-containing polypeptides.* Biopolymers, 2010.

96. Skoog, D.A., F.J. Holler, and S.R. Crouch, *Principles of Instrumental Analsis*. 6 ed. 2006.

97. Kelly, S.M. and N.C. Price, *The application of circular dichroism to studies of protein folding and unfolding.* Biochimica et Biophysica Acta, 1997. **1338**: p. 161-185.

98. Sreerama, N., S.Y. Venyaminov, and R.W. Woody, *Estimation of protein secondary structure from circular dichroism spectra: inclusion of denatured proteins with native proteins in the analysis.* Analytical Biochemistry, 2000. **287**(2): p. 243-251.

99. Sreerama, N. and R.W. Woody, *Estimation of protein secondary structure from circular dichroism spectra: comparison of CONTIN, SELCON, and CDSSTR methods with an expanded reference set.* Analytical Biochemistry, 2000. **287**(2): p. 252-260.

100. Yang, J.T., C.-S.C. Wu, and H.M. Martinez, *Calculation of protein conformation from circular dichroism.* Methods in Enzymology, 1986. **130**: p. 208-269.

101. Johnson, W.C., *Analyzing protein circular dichroism spectra for accurate secondary structures.* Proteins: Structure, Function, and Bioinformatics, 1999. **35**(3): p. 307-312.

102. Sreerama, N., S.Y. Venyaminov, and R.W. Woody, *Estimation of the number of alpha-helical and beta-strand segments in proteins using circular dichroism spectroscopy.* Protein Science : a publication of the Protein Society, 1999. **8**(2): p. 370-380.

103. Keiderling, T.A., et al., *Vibrational circular dichroism spectroscopy of selected oligopeptide conformations.* Bioorganic & medicinal chemistry, 1999. **7**(1): p. 133-141.

104. Josephy, P.D., T. Eling, and R.P. Mason, *The horseradish peroxidase-catalyzed oxidation of 3,5,3',5'-tetramethylbenzidine. Free radical and charge-transfer complex intermediates.* The Journal of Biological Chemistry, 1982. **257**(7): p. 3669-3675.

105. Patel, J.D., et al., *Preparation and characterization of nickel nanoparticles for binding to his-tag proteins and antigens.* Pharmaceutical Research, 2007. **24**(2): p. 343-352.

106. Sikkema, J.W.D., *An Fc-binding protein.* American Biotechnology laboratory, 1989. **7**(4a): p. 42.

107. Bjork, I., B.A. Petersson, and J. Sjoquist, *Some physiochemical properties of protein A from Staphylococcus aureus.* European journal of biochemistry / FEBS, 1972. **29**(3): p. 579-584.

108. Sjoquist, J., B. Meloun, and H. Hjelm, *Protein A isolated from Staphylococcus aureus after digestion with lysostaphin.* European journal of biochemistry / FEBS, 1972. **29**(3): p. 572-578.

109. Akerstrom, B., et al., *Protein G: a powerful tool for binding and detection of monoclonal and polyclonal antibodies.* Journal of Immunology, 1985. **135**(4): p. 2589-2592.

110. Akerstrom, B. and L. Bjorck, *A physicochemical study of protein G, a molecule with unique immunoglobulin G-binding properties.* The Journal of Biological Chemistry, 1986. **261**(22): p. 10240-10247.

111. Bjorck, L. and G. Kronvall, *Purification and some properties of streptococcal protein G, a novel IgG-binding reagent.* Journal of Immunology, 1984. **133**(2): p. 969-974.

112. Holliger, P. and P.J. Hudson, *Engineered antibody fragments and the rise of single domains.* Nature Biotechnology, 2005. **23**(9): p. 1126-1136.

113. Poullin, P., et al., *Protein A-immunoadsorption (Prosorba® column) in the treatment of rheumatoid arthritis.* Joint Bone Spine, 2005. **72**(2): p. 101-103.

114. Zheng, Y. and A.Y. Rudensky, *Foxp3 in control of the regulatory T cell lineage.* Nature Immunology, 2007. **8**(5): p. 457-462.

115. Kryczek, I., et al., *FOXP3 defines regulatory T cells in human tumor and autoimmune disease.* Cancer Research, 2009. **69**(9): p. 3995-4000.

116. Fontenot, J. and A.Y. Rudensky, *A well adapted regulatory contrivance: regulatory T cell development and the forkhead family transcription factor Foxp3.* Nature immunology, 2005. **6**(4): p. 331-337.

117. Steinman, R.M., *The dendritic cell system and its role in immunogenicity.* Annual Review of Immunology, 1991. **9**: p. 271-296.

118. Thomoson, A.W., *Designer dendritic cells for transplant tolerance.* Transplantation Proceedings, 2002. **34**(7): p. 2727-2728.

119. Steinman, R.M., D. Hawiger, and M.C. Nussenzweig, *Tolerogenic dendritic cells.* Annual Review of Immunology, 2003. **21**: p. 685-711.

120. Morishita, R., et al., *Molecular therapy to inhibit NF κ B activation by transcription factor decoy oligonucleotides.* Current Opinion in Pharmacology, 2004. **4**(2): p. 139-146.

121. Cui, Z. and R.J. Mumper, *Microparticles and nanoparticles as delivery systems for DNA vaccines.* Critical Reviews in Therapeutic Drug Carrier Systems, 2003. **20**(2-3): p. 103-137.

122. O'Hagan, D.T., M. Singh, and J.B. Ulmer, *Microparticles for the delivery of DNA vaccines.* Immunological Reviews, 2004. **199**(1): p. 191-200.

123. Anderson, J.M. and M. Shive, *Biodegradation and biocompatibility of PLA and PLGA microspheres.* Advanced Drug Delivery Reviews, 1997. **28**(1): p. 5-24.

124. Capan, Y., et al., *Preparation and characterization of poly (D,L-lactide-co-glycolide) microspheres for controlled release of poly(L-lysine) complexed plasmid DNA.* Pharmaceutical Research, 1999. **16**(4): p. 509-513.

125. Panyam, J. and V. Labhasetwar, *Biodegradable nanoparticles for drug and gene delivery to cells and tissue.* Advanced Drug Delivery Reviews, 2003. **55**(3): p. 329-347.

126. Hedley, M.L., *Formulations containing poly(lactide-co-glycolide) and plasmid DNA expression vectors.* Expert Opinion on Biological Therapy, 2003. **3**(6): p. 903-910.

127. Meng, W.S. and L.H. Butterfield, *Activation of antigen-presenting cells by DNA delivery vectors.* Expert Opinion on Biological Therapy, 2005. **5**(8): p. 1019-1028.

128. Capan, Y., et al., *Influence of formulation parameters on the characteristics of poly(D, L-lactide-co-glycolide) microspheres containing poly(L-lysine) complexed plasmid DNA.* Journal of Controlled Release, 1999. **60**(2-3): p. 279-286.

129. Benoit, M.A., et al., *Studies on the potential of microparticles entrapping pDNA-poly(aminoacids) complexes as vaccine delivery systems.* Journal of Drug Targeting, 2001. **9**(4): p. 253-266.

130. Kumar, M.N.V.R., U. Bakowsky, and C.M. Lehr, *Preparation and characterization of cationic PLGA nanospheres as DNA carriers.* Biomaterials, 2004. **25**(10): p. 1771-1777.

131. Li, Y., et al., *Stability and release characteristics of poly(D,L-lactide-co-glycolide) encapsulated CaPi-DNA coprecipitation.* International Journal of Pharmaceutics, 2004. **269**(1): p. 61-70.

132. Oster, C.G. and T. Kissel, *Comparative study of DNA encapsulation into PLGA microparticles using modified double emulsion methods and spray drying techniques.* Journal of Microencapsulation, 2005. **22**(3): p. 235-244.

133. Atuah, K.N., et al., *Encapsulation of plasmid DNA in PLGA-stearylamine microspheres: a comparison of solvent evaporation and spray-drying methods.* Journal of Microencapsulation, 2003. **20**(3): p. 387-399.

134. Kasturi, S.P., K. Sachaphibulkij, and K. Roy, *Covalent conjugation of polyethyleneimine on biodegradable microparticles for delivery of plasmid DNA vaccines.* Biomaterials, 2005. **26**(32): p. 6375-6385.

135. Kovacs, J.R., et al., *Polymeric microspheres as stabilizing anchors for oligonucleotide delivery to dendritic cells.* Biomaterials, 2005. **26**(33): p. 6754-6761.

136. Jia, L., et al., *Attenuated alloreactivity of dendritic cells engineered with surface-modified microspheres carrying a plasmid encoding interleukin-10.* Biomaterials, 2006. **27**(9): p. 2076-2082.

137. Putnam, D., et al., *Polymer-based gene delivery with low cytotoxicity by a unique balance of side-chain termini.* Proceedings of the National Academy of Sciences of the United States of America, 2001. **98**(3): p. 1200-1205.

138. Midoux, P., et al., *Membrane permeabilization and efficient gene transfer by a peptide containing several histidines.* Bioconjugate Chemistry, 1998. **9**(2): p. 260-267.

139. Jain, R.A., *The manufacturing techniques of various drug loaded biodegradable poly(lactide-co-glycolide) (PLGA) devices.* Biomaterials, 2000. **21**(23): p. 2475-2490.

140. Barman, S.P., et al., *Two methods for quantifying DNA extracted from poly(lactide-co-glycolide) microspheres.* Journal of Controlled Release, 2000. **69**(3): p. 337-344.

141. Inaba, k., et al., *Generation of large numbers of dendritic cells from mouse bone marrow cultures supplemented with granulocyte/macrophage colony-stimulating factor.* The Journal of Experimental Medicine, 1992. **176**(6): p. 1693-1702.

142. Ribas, A., et al., *Genetic immunization for the melanoma antigen MART-1/Melan-A using recombinant adenovirus-transduced murine dendritic cells.* Cancer Research, 1997. **57**(14): p. 2865-2869.

143. Meng, W.S., et al., *α-Fetoprotein-specific Tumor Immunity Induced by Plasmid Prime-Adenovirus Boost Genetic Vaccination.* Cancer Research, 2001. **61**(24): p. 8782-8786.

144. Chamarthy, S.P., et al., *A cationic peptide consists of ornithine and histidine repeats augments gene transfer in dendritic cells.* Molecular Immunology, 2003. **40**(8): p. 483-490.

145. Sahoo, S.K., et al., *Residual polyvinyl alcohol associated with poly (D,L-lactide-co-glycolide) nanoparticles affects their physical properties and cellular uptake.* Journal of Controlled Release, 2002. **82**(1): p. 105-114.

146. Zambaux, M.F., et al., *Influence of experimental parameters on the characteristics of poly(lactic acid) nanoparticles prepared by a double emulsion method.* Journal of Controlled Release, 1998. **50**(1-3): p. 31-40.

147. Prabha, S. and V. Labhasetwar, *Critical determinants in PLGA/PLA nanoparticle-mediated gene expression.* Pharmaceutical Research, 2004. **21**(2): p. 354-364.

148. van de Weert, M., et al., *George Posthuma, Wim E. Hennink and Daan J. A. Crommelin*

Lysozyme distribution and conformation in a biodegradable polymer matrix as determined by FTIR techniques. Journal of Controlled Release, 2000. **68**(1): p. 31-40.

149. Fu, K., et al., *FTIR characterization of the secondary structure of proteins encapsulated within PLGA microspheres.* Journal of Controlled Release, 1999. **58**(3): p. 357-366.

150. Panyam, J., et al., *Rapid endo-lysosomal escape of poly(DL-lactide-co-glycolide) nanoparticles: implications for drug and gene delivery.* The FASEB Journal: official publication of the Federation of American Societies for Experimental Biology. , 2002. **16**(10): p. 1217-1226.

151. Li, L. and S.P. Schwendeman, *Mapping neutral microclimate pH in PLGA microspheres.* Journal of Controlled Release, 2005. **101**(1-3): p. 163-173.

152. Zhu, G., S.R. Mallery, and S.P. Schwendeman, *Stabilization of proteins encapsulated in injectable poly (lactide- co-glycolide).* Nature Biotechnology, 2000. **18**(1): p. 52-57.

153. Siepmann, J., et al., *How autocatalysis accelerates drug release from PLGA-based microparticles: a quantitative treatment.* Biomacromolecules, 2005. **6**(4): p. 2312-2319.

154. Babensee, J.E. and A. Paranjpe, *Differential levels of dendritic cell maturation on different biomaterials used in combination products.* Journal of Biomedical Materials Research. Part A 2005. **74**(4): p. 503-510.

155. Yoshida, M. and J.E. Babensee, *Poly(lactic-co-glycolic acid) enhances maturation of human monocyte-derived dendritic cells.* Journal of Biomedical Materials Research. Part A, 2004. **71**(1): p. 45-54.

156. Fontenot, J., M.A. Gavin, and A.Y. Rudensky, *Foxp3 programs the development and function of CD4+CD25+ regulatory T cells.* Nature Immunology, 2003. **4**(4): p. 330-336.

157. Hori, S., T. Nomura, and S. Sakaguchi, *Control of regulatory T cell development by the transcription factor Foxp3.* Science, 2003. **299**(5609): p. 1057-1061.

158. Chapman, E.J. and J.C. Carrington, *Specialization and evolution of endogenous small RNA pathways.* Nature Reviews. Genetics, 2007. **8**(11): p. 884-896.

159. Singh, S.K. and P.B. Hajeria, *siRNAs: their potential as therapeutic agents--Part II. Methods of delivery.* Drug Discovery Today, 2009. **14**(17-18): p. 859-865.

160. Zhang, H., D. Yee, and C. Wang, *Quantum dots for cancer diagnosis and therapy: biological and clinical perspectives.* Nanomedicine, 2008. **3**(1): p. 83-91.

161. Pardridge, W.M., *Drug and gene targeting to the brain with molecular Trojan horses.* Nature Reviews. Drug Discovery, 2002. **1**(2): p. 131-139.

162. First, M.R. and W.E. Fitzsimmons, *New drugs to improve transplant outcomes.* Transplatation 2004. **77**(9): p. S88-S92.

163. Barshes, N.R., S.E. Goodpastor, and J.A. Goss, *Pharmacologic immunosuppression.* Frontiers in Bioscience 2004. **9**: p. 411-420.

164. Paczek, L., et al., *New concepts in organ transplantation.* Transplantation Proceedings, 2004. **36**(5): p. 1232-1234.

165. Moore, K.W., et al., *Interleukin-10 and the interleukin-10 receptor.* Annual Review of Immunology, 2001. **19**: p. 683-765.

166. Mahnke, K., et al., *Tolerogenic dendritic cells and regulatory T cells: a two-way relationship.* Journal of Dermatological Science 2007. **46**(3): p. 159-167.

167. Morel, A.-S., et al., *Split activity of interleukin-10 on antigen capture and antigen presentation by human dendritic cells: definition of a maturative step.* European Journal of Immunology, 1997. **27**(1): p. 26-34.

168. Enk, A.H., et al., *Inhibition of Langerhans cell antigen-presenting function by IL-10. A role for IL-10 in induction of tolerance.* Journal of Immunology 1993. **151**(5): p. 2390-2398.

169. de Smedt, T., et al., *Effect of interleukin-10 on dendritic cell maturation and function.* European Journal of Immunology, 1997. **27**(5): p. 1229-1235.

170. Steinbrink, K., et al., *CD4(+) and CD8(+) anergic T cells induced by interleukin-10-treated human dendritic cells display antigen-specific suppressor activity.* Blood, 2002. **99**(7): p. 2468-2476.

171. Bellinghausen, I., et al., *Inhibition of human allergic T-cell responses by IL-10-treated dendritic cells: differences from hydrocortisone-treated dendritic cells.* The Journal of Allergy and Clinical Immunology, 2001. **108**(2): p. 242-249.

172. Müller, G., et al., *Interleukin-10-treated dendritic cells modulate immune responses of naive and sensitized T cells in vivo.* Journal of Investigative Dermatology, 2002. **119**: p. 836-841.

173. Dai, Z., et al., *CD4+CD25+ regulatory T cells suppress allograft rejection mediated by memory CD8+ T cells via a CD30-dependent mechanism.* The Journal of Clinical Investigation, 2004. **113**(2): p. 310-317.

174. Enk, A.H., *DCs and cytokines cooperate for the induction of tregs.* Ernst Schering Research Foundation Workshop 2006(56): p. 97-106.

175. Wing, K., et al., *CTLA-4 control over Foxp3+ regulatory T cell function.* Science, 2008. **322**(5899): p. 271-275.

176. Sarween, N., et al., *CD4+CD25+ cells controlling a pathogenic CD4 response inhibit cytokine differentiation, CXCR-3 expression, and tissue invasion.* The Journal of Immunology, 2004. **173**(5): p. 2942-2951.

177. Wang, Z., et al., *Use of the inhibitory effect of apoptotic cells on dendritic cells for graft survival via T-cell deletion and regulatory T cells.* American Journal of Transplantation 2006. **6**(6): p. 1297-1311.

178. Ochando, J.C., et al., *Lymph node occupancy is required for the peripheral development of alloantigen-specific Foxp3+ regulatory T cells.* The Journal of Immunology, 2005. **174**(11): p. 6993-7005.

179. Lu, L., et al., *Genetic engineering of dendritic cells to express immunosuppressive molecules (viral IL-10, TGF-beta, and CTLA4Ig).* Journal of Leukocyte Biology 1999. **66**(2): p. 293-296.

180. Yamazaki, S., et al., *Effective expansion of alloantigen-specific Foxp3+ CD25+ CD4+ regulatory T cells by dendritic cells during the mixed leukocyte reaction.* Proceedings of the National Academy of Sciences of the United States of America 2006. **103**(8): p. 2758-2763.

181. Levings, M.K., et al., *Differentiation of Tr1 cells by immature dendritic cells requires IL-10 but not CD25+CD4+ Tr cells.* Blood, 2005. **105**(3): p. 1162-1169.

182. Cong, Y., et al., *Generation of antigen-specific, Foxp3-expressing CD4+ regulatory T cells by inhibition of APC proteosome function.* The Journal of Immunology, 2005. **174**(5): p. 2787-2795.

183. Bromberg, J.S., et al., *Gene transfer methods for transplantation.* Methods in Enzymology, 2002. **346**: p. 199-224.

184. Coates, P.T.H., et al., *Human myeloid dendritic cells transduced with an adenoviral interleukin-10 gene construct inhibit human skin graft rejection in humanized NOD-scid chimeric mice.* Gene Therapy, 2001. **8**(16): p. 1224-1233.

185. Taner, T. and A.W. Thomoson, *Fashioning regulatory dendritic cells: what is currently in vogue?* Current Opinion in Molecular Therapeutics, 2004. **6**(1): p. 78-82.

186. Kubach, J., et al., *Dendritic cells: sentinels of immunity and tolerance.* International Journal of Hematology, 2005. **81**(3): p. 197-203.

187. Slavin, A.J., et al., *Adoptive cellular gene therapy of autoimmune disease.* Autoimmunity Reviews, 2002. **1**(4): p. 213-219.

188. Sen, L., et al., *Efficiency, efficacy, and adverse effects of adenovirus vs. liposome-mediated gene therapy in cardiac allografts.* American Journal of Physiology. Heart and Circulatory Physiology, 2001. **281**(3): p. H1433-H1441.

189. Arthur, J.F., et al., *A comparison of gene transfer methods in human dendritic cells.* Cancer Gene Therapy, 1997. **4**(1): p. 17-25.

190. Philip, R., et al., *Transgene expression in dendritic cells to induce antigen-specific cytotoxic T cells in healthy donors.* Cancer Gene Therapy, 1998. **5**(4): p. 236-246.

191. Bogunovic, M., et al., *Identification of a radio-resistant and cycling dermal dendritic cell population in mice and men.* The Journal of Experimental Medicine 2006. **203**(12): p. 2627-2638.

192. Liu, K., et al., *Origin of dendritic cells in peripheral lymphoid organs of mice.* Nature Immunology, 2007. **8**(6): p. 578-583.

193. Jia, L., et al., *Expansion of Foxp3-expressing regulatory T cells in vitro by dendritic cells modified with polymeric particles carrying a plasmid encoding interleukin-10.* Biomaterials, 2008. **29**(9): p. 1250-1261.

194. Kovacs, J.R., et al., *Characterization of nickel-decorated PLGA particles anchored with a his-tagged polycation.* Journal of Biomaterials Science. Polymer edition, 2009. **20**(9): p. 1307-1320.

195. Rogers, N.J. and R.I. Lechler, *Allorecognition.* American Journal of Transplantation, 2001. **1**(2): p. 97-102.

196. Ierino, F.L., et al., *Dendritic cells expressing soluble CTLA4Ig prolong antigen-specific skin graft survival.* Immunology and Cell Biology, 2010: p. 1-5.